TO: NATIONAL AERONAUTICS AND SPACE ADMINISTRATION
WASHINGTON, D. C. 20546

ANNUAL REPORT

Crystal Growth of Device Quality GaAs in Space

(NSG-7331)

Period April 1, 1978 to March 31, 1979

Submitted by:

Professor Harry C. Gatos and Dr. Jacek Lagowski
Department of Materials Science and Engineering
Massachusetts Institute of Technology
Cambridge, Massachusetts 02139

April 1979

TABLE OF CONTENTS

SUMMARY

Our experimental and theoretical program has been focused on the growth and characterization of GaAs. In our crystal growth work we have pursued the study of quantitative relationships between growth parameters and properties. In our characterization studies we have investigated the determination of the compositional, structural and electronic properties of GaAs on a macro- and microscale. We have developed a detailed theoretical model of electroepitaxial growth and we have found it to be in excellent agreement with experimental results. The growth rate and composition of epitaxial layers can be controlled by current density. Electroepitaxial layers are structurally and electronically superior to those grown by thermal liquid phase epitaxy. The growth rates attained by electroepitaxy thus far are one to two orders of magnitude greater than those obtained by standard liquid phase epitaxy and only one order of magnitude smaller than those obtained in melt growth. In addition to electroepitaxy we have completed the design, construction and testing of apparatus for the growth of GaAs crystals from the melt. Regarding characterization, we have developed novel techniques for obtaining two-dimensional microprofiles of the carrier concentration in GaAs (scanning IR absorption) and microprofiles of the minority carrier characteristics (SEM-EBIC mode). In addition, we have developed derivative surface photovoltage spectroscopy, a new method, which permits the simultaneous determination of critical point transitions and transitions involving levels in the energy gap. At the same time we are nearing construction of standard characterization techniques such as transient deep level spectroscopy, photoluminescence and cathodoluminescence spectroscopy. Our aim is to utilize our novel and selected standard characterization techniques for investigating the electronic properties

of GaAs, such as carrier concentration, compensation ratios, minority carrier lifetime, and diffusion length on a microscale, and for relating these properties to materials parameters (compositional and structural) which in turn we will relate to growth parameters. Such relationships should permit the optimization of GaAs growth under zero-gravity conditions as well as the assessment and exploitation of the potential of GaAs in device applications.

INTRODUCTION

It is now generally accepted within the scientific and engineering community that to insure successful processing of materials (e.g., crystal growth) in space extensive work must be carried out on the ground. Ground-based work must be aimed at establishing the experimental parameters and conditions for the optimization of the unique advantages of zero gravity conditions. In addition, experimental techniques and theoretical understanding must be developed which permit the reliable characterization of the material (before and after space processing) and, thus, a detailed analysis of the implications of zero gravity environment to the advancement of basic science and to the realization of unique technological applications. Actually, the results obtained from the growth of indium antimonide in the Skylab mission and from the growth of germanium in the ASTP mission surpassed all expectations only because both systems were investigated extensively for many years prior to the design performance and analysis of those experimenta.

Accordingly, our ground-based research effort is aimed specifically at the optimization of space processing of GaAs by (a) developing an experimental and theoretical framework for the detailed compositional, structural and electronic characterization of GaAs on a macro- and microscale, (b) developing a quantitative understanding of the relationships between growth parameters and

the properties of GaAs, and (c) assessing the key GaAs parameters limiting device performance.

In this second annual report on "Crystal Growth of Device Quality GaAs in Space" we present a summary of our results on the crystal growth and on the characterization of GaAs. In addition, we present more detailed discussions of some of our results as they have recently appeared or will soon appear in the open literature.

Under "Proposed Work" we discuss our proposed research plans for a one-year period beginning April 1, 1979. Some new research areas on growth and characterization will be experimentally initiated, whereas work now in progress in solution growth and in characterization will be further pursued.

CRYSTAL GROWTH

Solution Growth

Thermodynamics predicts the solution growth, requiring lower growth temperature than melt growth, should yield single crystals of far better quality than those obtained from melt growth. Actually, in the case of GaAs, using liquid phase epitaxy (LPE) the quality of the layers and their suitability for device fabrication and device performance is essentially limited by their interactions with the substrate materal which is generally of poor quality. The standard LPE technique, because of its very low growth rates, cannot be realistically considered for the growth of bulk crystals which could replace those grown from the melt.

Electroepitaxy does not in principle have the growth rate limitations of standard LPE. In electroepitaxy crystal growth takes place by passing electric current through the growth interface while the temperature of the overall

system is maintained constant. The required supersaturation for crystal growth is brought about by electromigration of solution species to the growth interface under the applied electric field. Thus, the slow diffusion-controlled transport of solute which controls the growth rate in standard LPE is of no consequence in electroepitaxy where significantly faster transport of solute takes place through electromigration in an electric field.

We have completed the first stage of extensive experimental and theoretical studies which have resulted in the development of a comprehensive model of electroepitaxy. Thus, on the basis of mass transport principles a theoretical model of electroepitaxial growth--current-controlled LPE--was developed which defines explicitly the contribution of the Peltier effect (at the solid-solution interface) and that of solute electromigration to the overall growth process. According to the model the contribution of electromigration to growth is dominant in the absence of convection in the solution, whereas the contribution of the Peltier effect can be dominant in the presence of convection. On the basis of the model expressions were derived which relate quantitatively the growth velocity to growth parameters. The model was found to be in excellent agreement with extensive experimental data on the electroepitaxial growth of GaAs from Ga-As solution. The detailed treatment of this model and of related experimental findings is presented in the attached recent publication on "Liquid Phase Epitaxy: Growth Kinetics".

In this report we will present typical recent results illustrating the uniqueness and the potential of this technique. We have found that electroepitaxy has significant advantages over thermal epitaxy. (1) The layers grown by electroepitaxy exhibit a far superior surface morphology (Fig. 1a) than those grown by thermal epitaxy (Fig. 1b). (2) We have demonstrated that the electronic

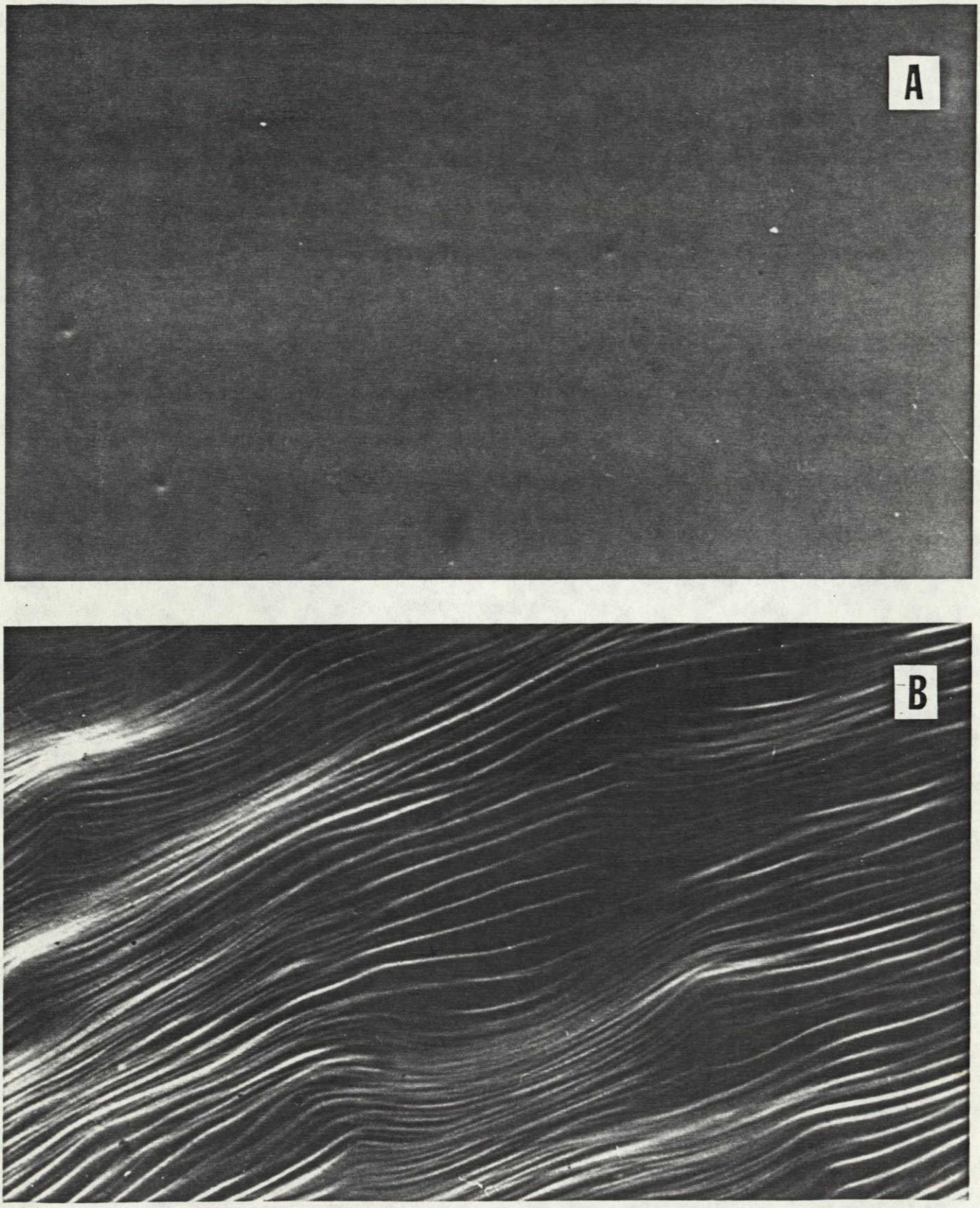

Figure 1. Surface morphology of GaAs epitaxial layer grown: (a) by electro-epitaxy; (b) by thermal epitaxy.

properties of electroepitaxial layers are superior to those grown by standard methods. (3) The distribution coefficients of dopants (k_o) and thus the carrier concentration can be readily controlled by the current density as shown in Fig. 2. (4) The growth velocity can also be controlled by the current density over a broad temperature range as shown in Fig. 3. In addition, electroepitaxy lends itself to quantitative theoretical treatment; thus, in Figs. 2 and 3 the lines were theoretically obtained and are in good agreement with the experimental points indicated on the figure. (5) The dependence of the growth rate on current density should permit the achievement of high growth rates and thus the growth of bulk GaAs material. (6) Since the current density controls the growth process, electroepitaxy lends itself uniquely to fundamental quantitative studies of crystal growth and segregation.

The conclusion that bulk GaAs crystals might be obtained by electroepitaxy is currently under investigation. Our preliminary experiments showed that by electroepitaxy GaAs growth rates of about 20 μm/min can be achieved which are 1-2 orders of magnitude greater than those achieved by standard LPE utilizing step cooling or the solution-substrate system. These growth rates are only about 1 order of magnitude smaller than those typically obtained in GaAs melt growth. It should be emphasized, however, that we have achieved the above growth rates employing our standard experimental system designed to operate in a rather limited range of temperatures and electric currents. Accordingly, in order to establish the real growth velocity limitations we have initiated the design of an electroepitaxy system for growth under extreme conditions of electric current and temperature. Furthermore, we have initiated theoretical studies on the interface mechanisms limiting the growth velocity. This work is now in progress. We believe that electroeptaxy is a simpler and better suited method for space processing of bulk GaAs crystals than melt growth, provided high growth rates can be achieved.

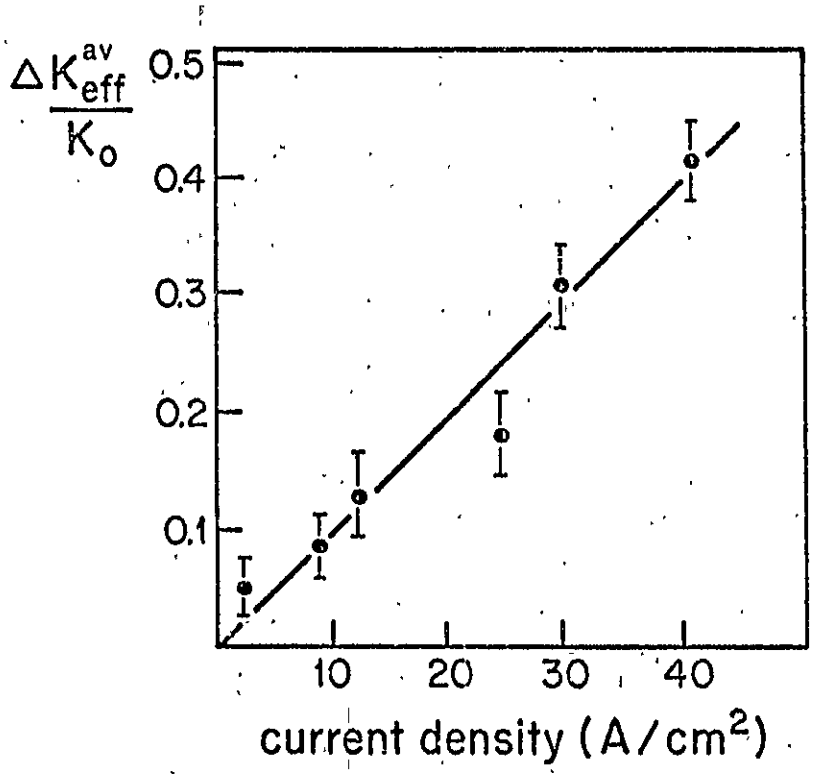

Figure 2. Current-induced change in the segregation coefficient of Sn in GaAs grown by electroepitaxy; points - experimental; line - theory

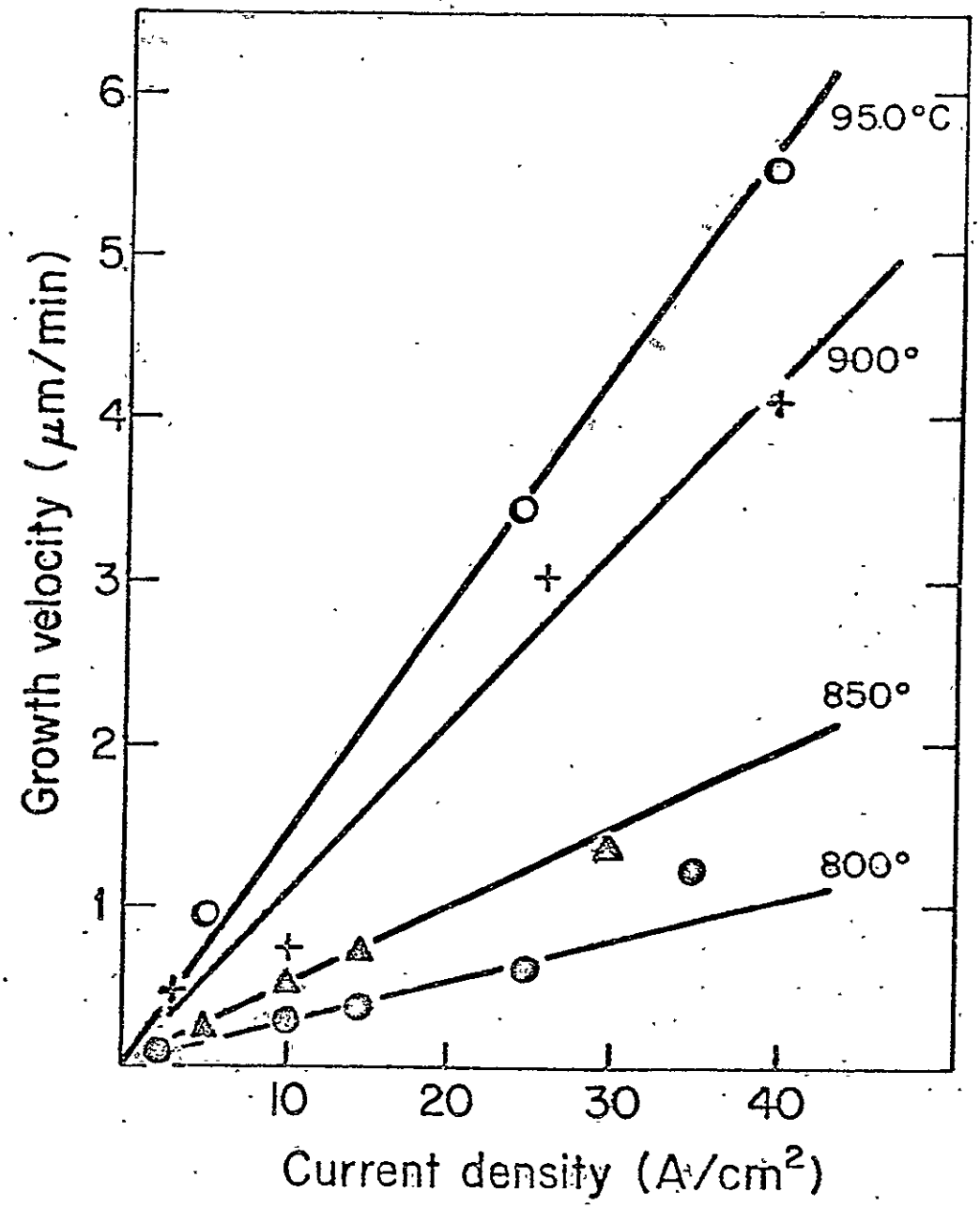

Figure 3. Electroepitaxial growth velocity of GaAs grown from Ga-As solutions as a function of current density. Points - experimental; lines - theory

Melt Growth

Growth from the melt is best suited for the growth of large single crystal within a relatively short period of time. However, as emphasized in our first annual report (April 1978), extensive studies are required before device qualit GaAs can be obtained by this method. In this respect it should be emphasized that our recently developed characterization techniques have directly supported the conclusion that the quality of the commonly available GaAs is generally poor as manifested by the measured compositional and electronic inhomogeneities and by the high degree of compensation (see below).

Presently our effort is being focused on the initiation of melt growth experiments which will enable the investigation of the effects of As vapor pressure, the effects of convection in the melt, and the effects of growth interface phenomena on characteristics of GaAs single crystals. A melt-growth apparatus has been designed and is shown schematically in Fig. 4. It consists of a three-zone furnace designed to operate in a horizontal or in a vertical position. Construction of the apparatus has been completed in a "clean" laboratory, and thermal characterization tests are now in progress. Following is a summary of equipment design, contruction and subsystem installation.

Main Furnace Assembly: A complete set of plans were drawn and submitted to the Marshall Furnace Company for construction of the main furnace. There are several unique features incorporated in this furnace design: four independently controlled platinum heating coils, an internal cooling system utilizing an alumina tube to guide the cooling gas along the heated muffle; cooling gas is supplied through a perforated inconel ring inside the furnace. This system generates increased thermal gradients without the risk of water-cooling techniques. High purity alumina tubing is used throughout the furnace to minimize

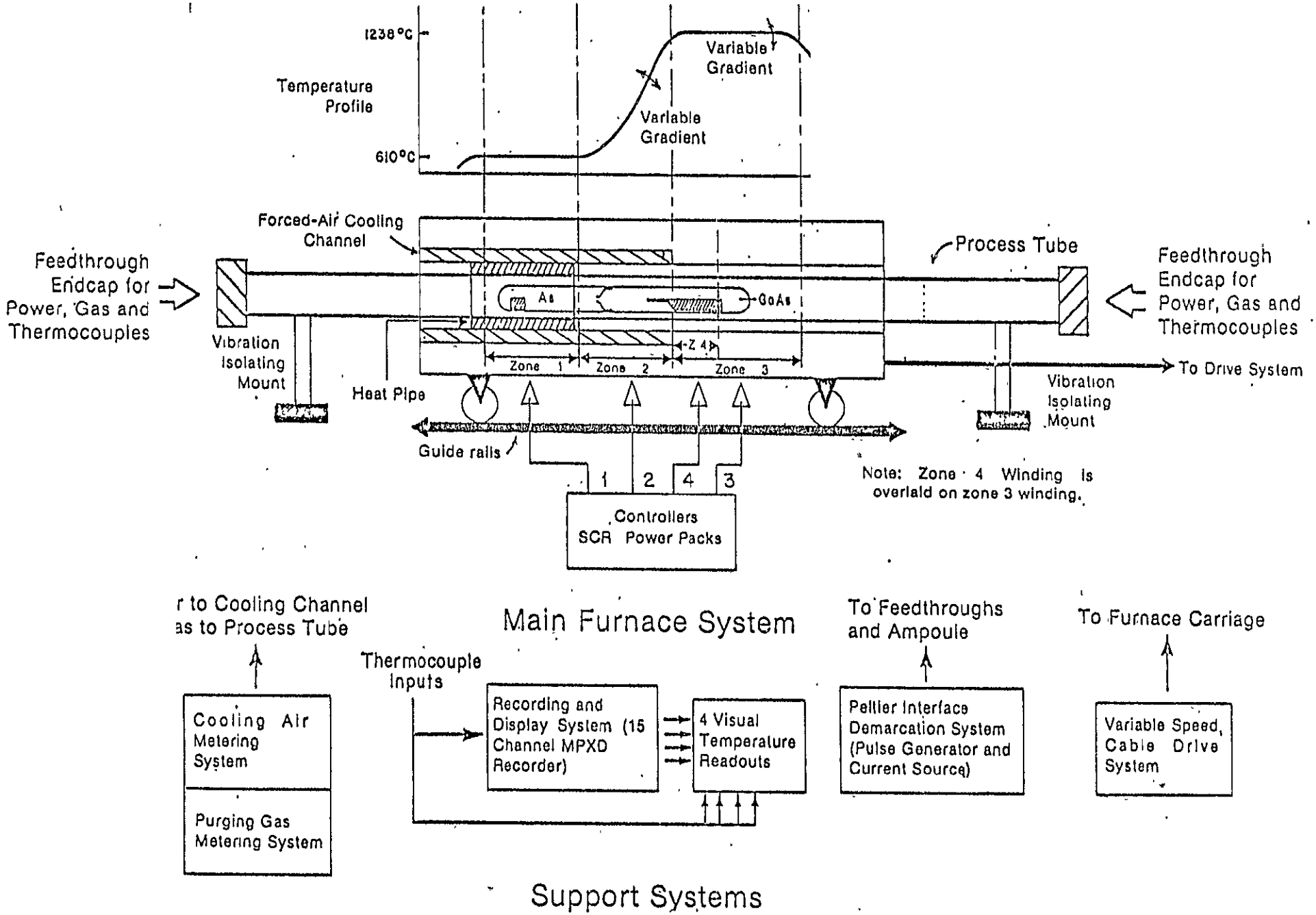

Figure 4. Schematic representation of the apparatus designed for the melt growth of GaAs

contamination and to provide fine adjustment of the thermal profile; power taps are placed in the three large windings. The furnace may be operated with or without standard size heat pipes. Installation and initial checkout above 1000°C have been completed. Stability and thermal profiling tests are forthcoming.

Carriage, Track and Bench Assembly: These systems provide physical support for the furnace, guidance during furnace movement and support for all of the furnace sub-assemblies. Design and contruction of all parts and sub-assemblies was carried out at M.I.T. Process tube mounts, drive cable guides, plumbing for gas and water, metering for process tube and cooling gases, thermocouple connection panels, furnace power connections and the cable drive unit were designed, built and installed. Plexiglas doors and shields are fitted into rails on the bench top, then fastened to the fume hood to form a protective enclosure for the entire furnace assembly. Low friction Thomson Roundway bearings support the furnace carriage on stainless steel ways. This method of guidance permits system operation in any orientation between horizontal and vertical position. Main support pivot, cable guide system and bench design permit rapid changes in system orientation with only minor alterations. Key features of the support system are: isolation of the process tube through two layers of vibration damping composite material and an asbestos pad, adjustable process tube supports to compensate for various tube diameters, tube sag or other alignment variations and flexible high pressure tubing which allows cooling gas flow to the furnace under all operating configurations without modifications. A section of the bench top may be removed to allow vertical operation. Adjustable indicators on the carriage are used to precisely position the furnace as well as measure total furnace travel.

Cable Drive Unit: This system was designed and constructed to operate under all anticipated loads generated by the furnace and carriage system. It consists of a D.C. control motor, controller, reduction gears and a threaded take-up drum. Stainless steel cable is used between the drum and carriage to minimize vibration transfer. The design of the cable guides permits the furnace track to be raised and lowered without changing the drive system or the furnace position. Speed in the drive motor is continuously variable from 0.4 mm/hr to 80 mm/hr in two overlapping ranges. Other speed ranges may be obtained by changing one gear pair.

Feedthroughs, Thermocouples and Power Wiring: Feedthrough endcaps were designed and built for two sizes of process tubes. These units are O-ring sealed and water cooled (to protect the O-ring). Overpressure of approximately 0.5 atmosphere or moderately high vacuum may be sustained in the process tube using these endcaps. Each unit can pass up to seven thermocouple tubes, gas inlets/outlets or power cables. Quick release connectors and flexible tubing permits operational simplicity and vibration isolation from the input plumbing. Thermocouple outputs are fed to two junction boxes, one at each end of the furnace. Total capacity is 20 measuring thermocouples plus 4 control thermocouples. Both type K (chromel-alumel) and type S (platinum-platinum-rhodium) thermocouples are used for the appropriate temperature ranges. Power wiring is designed for simplicity of operation: no changes are required when altering furnace configuration and the use of polarized quick connect plugs eliminates wiring errors when disassembly is required.

Monitoring and Control Systems: Hard copy recording of thermal data is provided by a 15 channel, time multiplexed chart recorder. This unit is linked directly to type K and type S thermocouple inputs and the buffered

analog outputs from the four digital thermocouple readout displays. Precision millivolt sources were designed and built to offset each of the analog outputs. This feature permits display of 1 to 50 C° full scale on the chart recorder. Furnace temperature is regulated by high sensitivity Leeds & Northrup controllers, driving SCR power packs. Each zone is independently controlled. Current metering and electronic current limiting plus a fail-safe feature in the control package prevent damage to the platinum furnace windings.

Support Systems and Materials: A single zone furnace with control system, to be used for outgassing of source materials and ampoule while under vacuum, prior to melt-growth in the main furnace has been constructed. Vacuum is provided by a cart mounted Varian diffusion pump system with ultimate pressure of 10^{-7} torr. This unit may be used for ampoule preparation or evacuation of the main furnace tube. Clean water for materials preparation is generated by the de-ionizing system. It consists of a carbon filter, demineralizer/deionizer cartridge, heater (75 C°) storage tank, an activated carbon trap for organic impurities and two ion-exchange resin beds. Water of approximately 18 megohm quality is obtained from this unit. A sterile, 22 μm filter is installed at the outlet tap to trap particulates.

Boats have been manufactured from high purity GE quartz. The boats are capable of holding approximately 35 g of material, with provision for a seed crystal, if desired. Two designs have been generated for the initial experiments. The ampoule has been modeled, with modifications in progress. Final dimensions will be determined after completion of temperature profiling tests. The ampoule is a two-piece quartz tube designed to allow independent evacuation of the source (arsenic) and boat (GaAs) regions at different temperatures. Fine diameter quartz wells protrude through the ampoule wall into the boat region. Thermocouples

placed in these wells will be used to monitor thermal conditions in the melt. (Direct contact of the melt and thermocouple is not permissible due to the corrosive nature of arsenic at elevated temperatures.) Gallium, arsenic, and gallium arsenide (polycrystalline) of greater than 6N purity have been obtained from Metron, Inc., with a spectrographic analysis of the GaAs boules included by the manufacturer.

Growth-Property Relationships

Very rapid developments in our characterization techniques made possible the initiation of direct experimental studies of growth-defect relationships earlier than originally scheduled. These studies were aimed towards the assessment of the role of the substrate as an active source of point defects in epitaxially grown layers.

Utilizing our SEM technique we have measured the distribution of minority carrier lifetime in epitaxial layers, which provides a sensitive measure of the distribution of point defects acting as recombination centers. Typical results are given in Fig. 5; they clearly illustrate the importance of defect out-diffusion from the substrate into the epitaxial layer. Thus, the value of the lifetime in the vicinity of the epilayer-substrate interface is much lower (i.e., defect concentration is much higher) than away from the interface. Furthermore, the lifetime decreases as the time during which the layers are kept at an elevated temperature increases. This time dependence is consistent with the theoretical dependence describing out-diffusion of defects from the substrate, and it was used to determine the value of defect diffusion constant, $D = 5 \times 10^{-9}$ cm^2/.

This work, initiated only recently, is still in progress. The relationship between current density and carrier concentration (segregation) pointed out in electroepitaxial growth above is also being pursued further.

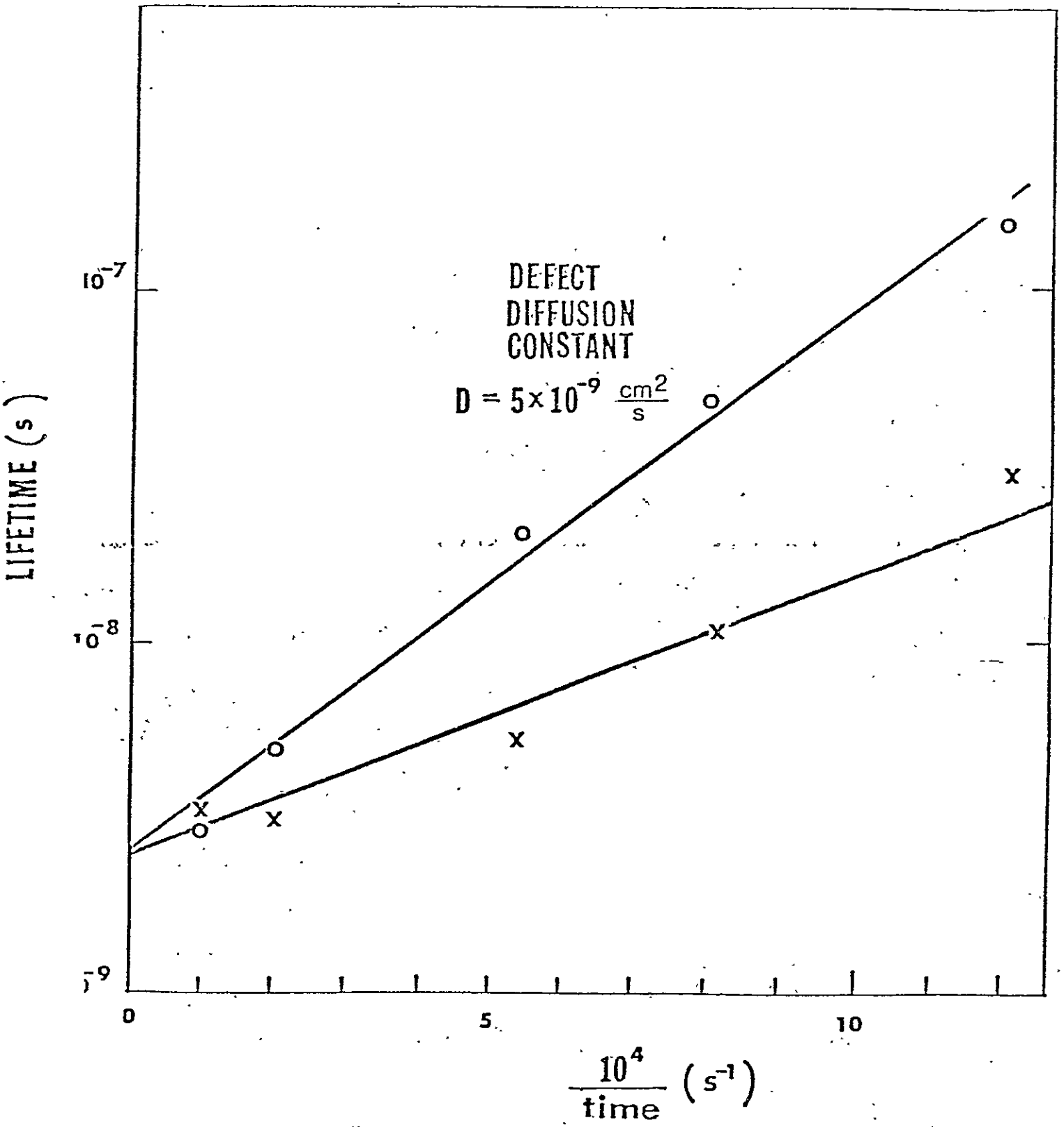

Figure 5. Lifetime as a function of time at growth temperature; crosses at substrate - epitaxial layer interface; circles away from interface. Lines correspond to out-diffusion of defects from substrate

CHARACTERIZATION OF GaAs

As shown in Table I, during the current year we have significantly advanced theoretical and experimental development of novel approaches to compositional, structural and electronic characterization of GaAs. We have also incorporated in our study standard advanced characterization methods. In the present report we will highlight the unique aspects of our novel methods.

Scanning IR Absorption

Inhomogeneities in semiconducting materials are commonly recognized as constituting a limiting major factor in microelectronic device applications. Nevertheless, the quantitative determination of inhomogeneities on a microscale have been so far possible only in elemental semiconductors (Ge and Si). The most commonly used method to obtain quantitative carrier distribution profiles is based on spreading resistance measurements. Pressure metal contacts, required for this technique, are highly irreproducible in the case of compound semiconductors, and the technique is not applicable to GaAs characterization.

Accordingly, we have developed a method and constructed an apparatus for the contactless and nondestructive determination of the spatial variation of the free carrier concentration in GaAs which is, of course, applicable to other semiconductors. The method is based on the quantitative relationship between infrared absorption and free carrier concentration, and it is applicable to any semiconductor material with free carrier concentration exceeding $10^{15} cm^{-3}$. The experimental arrangement of our system is shown in Fig. 6.

A parallel beam from a CO_2 laser (tunable between 9.16 and 11.02 μm) is transmitted through the sample positioned on a stage with x-y motion and a scanning rate ranging from 50 to 10^{13} μm/min. The light transmitted through

Table I

Methods Employed for GaAs Characterization

Method	Characterization	Present Status	Future Plans
Novel Techniques			
Scanning IR-Absorption	Profiling of carrier concentration & ionized impurities	Apparatus completed, theory developed, results obtained for n-type GaAs	p-type GaAs
SEM-Electron Beam Induced Current	Instantaneous profiling of diffusion length, lifetime & surface recombination velocity	Apparatus completed, method developed & demonstrated	Quantitative analysis, experimental extension to low & high temperatures
Derivative Surface Photovoltage Spectroscopy	Determination of optically active defect impurities & band structure transitions	Method developed, preliminary results obtained	Transient analysis yielding dynamic parameters of deep centers; extension to interface characterization
Transport Technique	Determination of compensation ratio & total amount of ionized impurities	Theory developed for n-type GaAs, results obtained	Theoretical extension to minority carriers in p-type GaAs
Standard Techniques			
Cathodoluminescence Spectroscopy	Profiling of defects & impurities active in radiative recombination	Apparatus components obtained, assembly in progress	Cross-correlation with EBIC technique
Photoluminescence Spectroscopy	Precise determination of radiative transitions, identification of residual impurities & defect complexes	Experimental arrangement designed, apparatus components being acquired	Cross-correlation with derivative surface photovoltage spectroscopy & TDLS
Transient Deep Level Spectroscopy (TDLS)	Determination of energy levels & dynamic parameters of deep centers	Apparatus components acquired, assembly in progress	Cross-correlation with derivative surface photovoltage spectroscopy

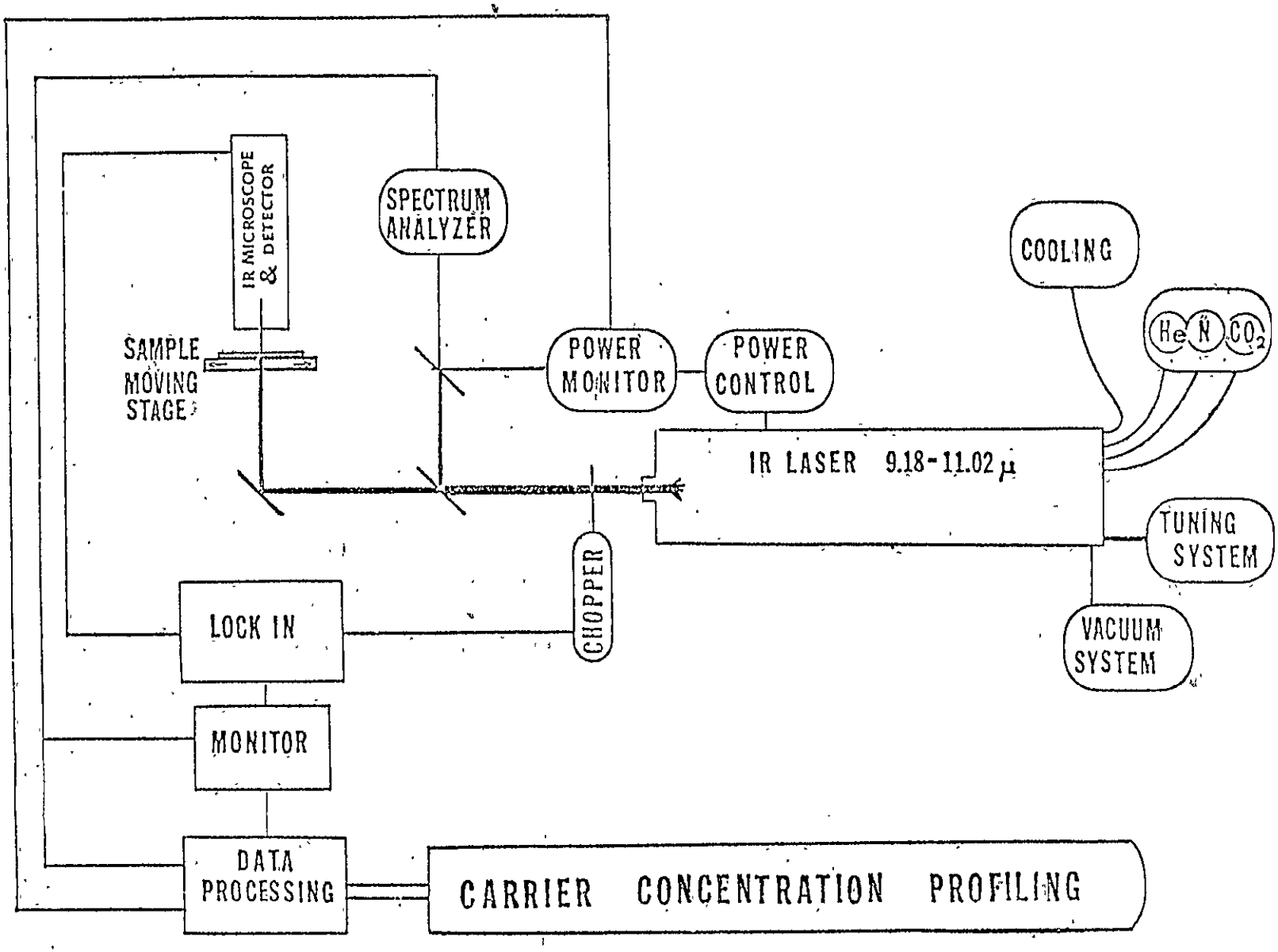

Figure 6. Schematic representation of the apparatus for IR-scanning absorption spectroscopy

the desired area of the sample is focused on a detector (bolometer) through the optics of an IR microscope; the signal from the detector, which is proportional to the intensity of radiation, is amplified and recorded.

The system permits a continuous monitoring of transmittance of the small wafer area, which is converted, through a data processing system, into variations of carrier concentration and of the compensation ratio. We have recently completed a rigorous theoretical treatment of the pertinent optical phenomena in n-type GaAs required for the quantitative processing of the data. A typical microprofiling of GaAs obtained recently is given in Fig. 7. It is seen that a two-dimensional quantitative profile of the carrier concentration in GaAs single crystals has been achieved for the first time. This profile clearly shows the pronounced inhomogeneities in the presently available melt-grown GaAs.

The spatial resoluton of our IR scanning system is about 20 μm and variations in the free carrier density in GaAs as low as $5 \times 10^{14} cm^{-3}$ in n-type and $2.5 \times 10^{14} cm^{-3}$ in p-type material can be detected.

Employing the same experimental system and a theoretical model we have developed we can determine in GaAs the average value of the compensation ratio as well as its variations.

SEM Techniques

In our approach scanning electron microscopy (SEM) is used primarily in the electron beam-induced current (EBIC) mode. Thus, the electron beam represents in essence a highly focused excitation source for excess minority carriers which are collected by a Schottky barrier or a p-n junction.

We have installed an SEM and accessory electronics especially designed for our EBIC mode approach (see Fig. 8). In parallel, we have been pursuing a theoretical and experimental study to advance our understanding of the

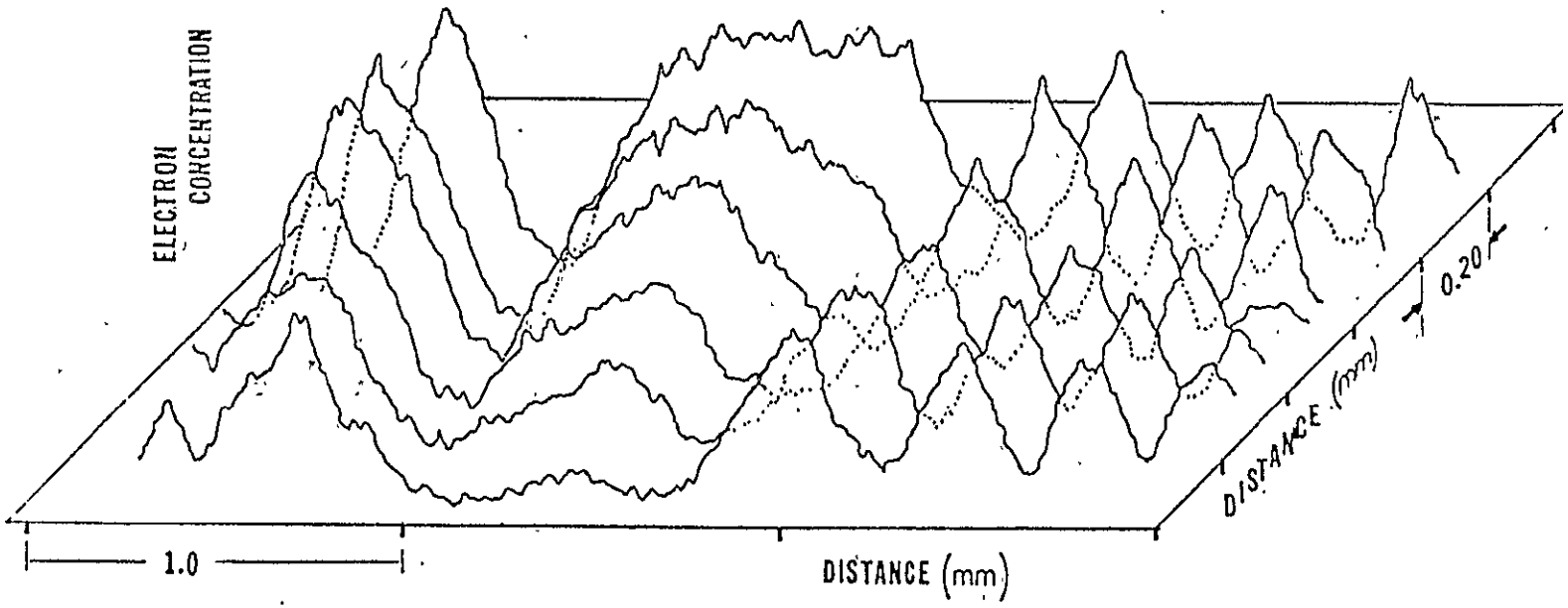

Figure 7. Typical carrier concentration microprofile of melt-grown GaAs; results obtained with IR-scanning absorption technique

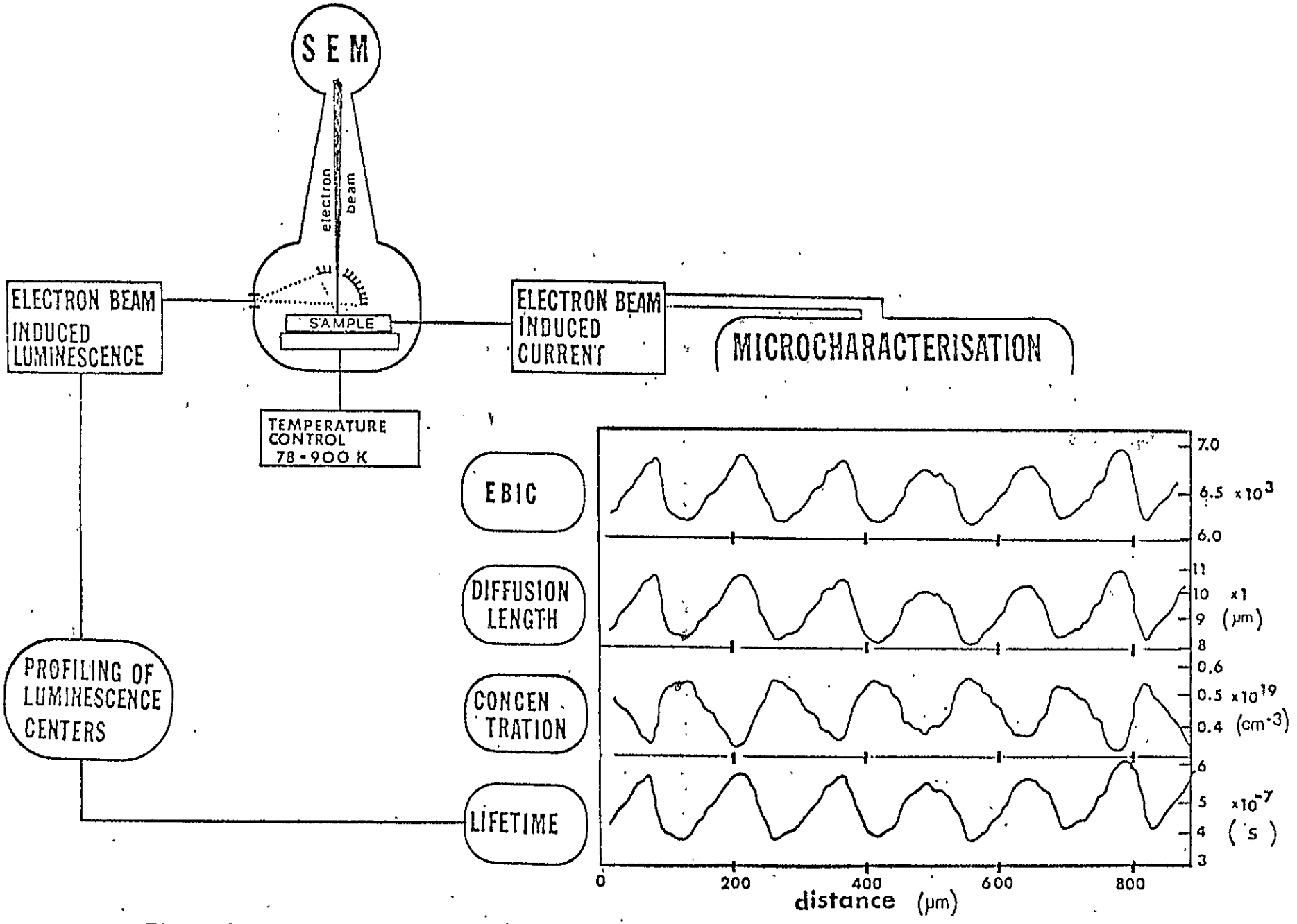

Figure 8. Schematic representation of the apparatus for semiconductor characterization using scanning electron microscopy

excitation and recombination processes associated with the EBIC mode. In these studies we have used Si as a convenient model material, and we have obtained and confirmed high resolution profiles such as the minority carrier diffusion length, the lifetime, and in certain instances, the dopant profile. Tupical results illustrating these possibilities are shown in Fig. 8 together with a schematic arrangement of the experimental system. For the first time a direct correlation has been achieved on a microscale between compositional inhomogeneities and electronics parameters such as minority carrier diffusion length and lifetime.

We have utilized this technique to analyze the lifetime distribution in epitaxially-grown GaAs. The results (shown earlier in Fig. 5) provided direct evidence of out-diffusion of defects from substrate to epitaxially grown layers.

Extensive experimental work is in progress devoted to the extension of EBIC-mode technique to temperatures well below and well above room temperatures. In spite of inherent technical difficulties, we consider such an extension of key importance in identifying the specific mechanisms of minority carrier recombination which are the controlling factors in device performance. We have also acquired apparatus and accessories for carrying out cathodoluminescence spectroscopy employing our SEM system. The assembly of this apparatus is in progress.

Derivative Surface Photovoltage Spectroscopy

Most recently we have developed a derivative form of Surface Photovoltage Spectroscopy based on the wavelength modulation of the incident light. In its standard (nonderivative) form surface photovoltage spectroscopy was successfully utilized, however, primarily for surface state studies.

Derivative photovoltage spectroscopy makes possible, in a single experiment, the quantitative characterization of optically active deep levels

(impurities and defects), of interface states and of the energy band structure above the energy gap. Preliminary results are shown in Figures 9 and 10. Figure 9 shows deep level transitions associated with impurity traps, whereas Fig. 10 shows critical point transitions. It should be emphasized that there exists hardly any other technique permitting the simultaneous characterization of these transitions.

In conjunction with these findings we have developed a data processing system (based on a theoretical quantum defect model of photoionization transitions) which permits a direct determination of such defect parameters as energy position and relative concentrations from the measured first-derivative subband-gap spectra.

Extensive studies on this technique are in progress and more detailed results will be presented in our annual report. The same experimental system employed in derivative surface spectroscopy will be complemented with apparatus for simultaneous photoluminescence and Transient Deep Level Spectroscopy measurements. The experimental arrangement has already been designed and the apparatus components are being acquired.

Transport Technique

We have completed the development of a characterization approach based on low- and high-frequency transport phenomena in n-type GaAs. Thus, utilizing an advanced theoretical treatment in conjunction with experimental studies of the electron mobility and of the free carrier absorption we succeeded in developing reliable, practical procedures for the determination of the compensation ratio and of the total concentration of ionized impurities in GaAs.

We utilized this approach in order to evaluate the quality of available melt-grown GaAs. The results are shown in Fig. 11. The $\theta = 0$ line (θ is the

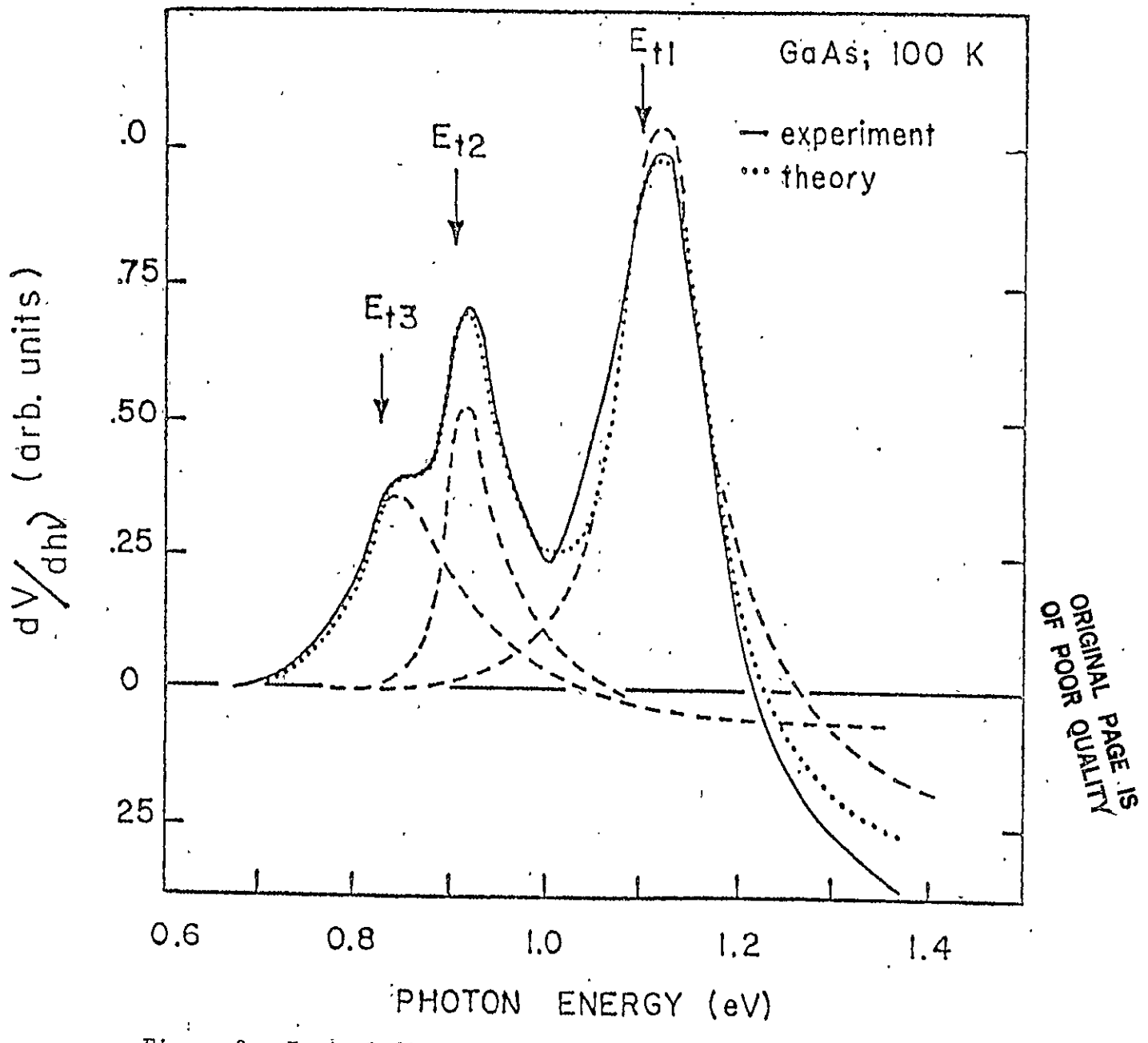

Figure 9. Typical first derivative subbandgap photovoltage spectra obt with melt-grown GaAs

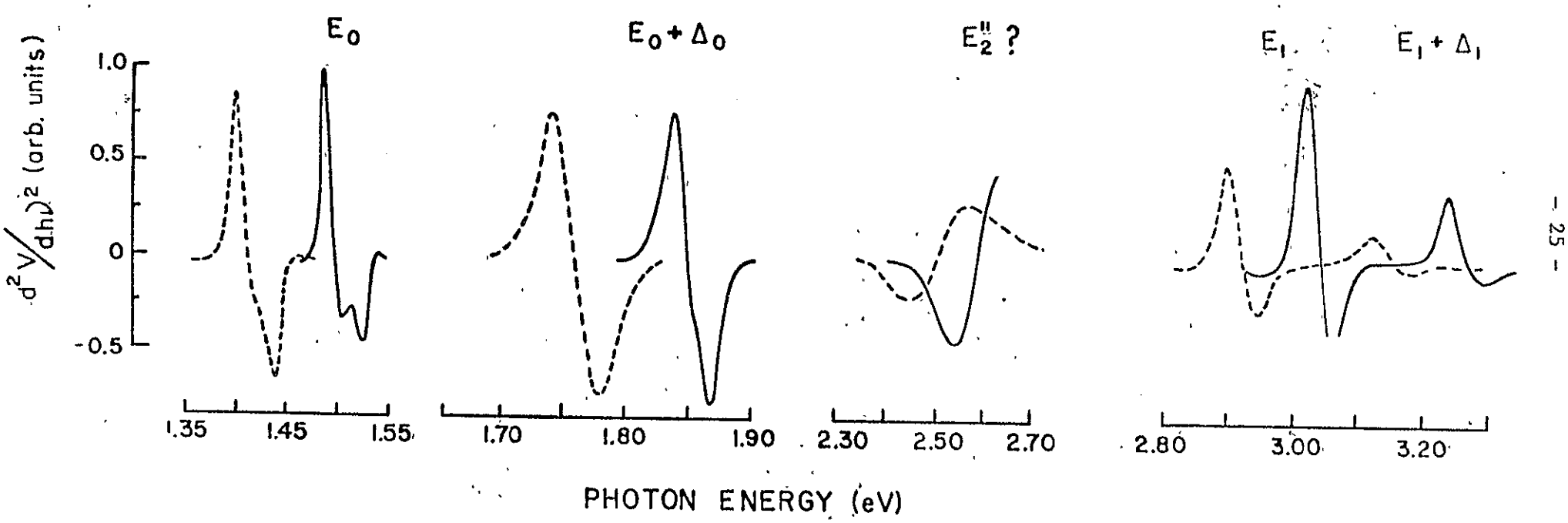

Figure 10. Band structure critical point transitions in GaAs, as revealed by second derivative surface photovoltage spectroscopy

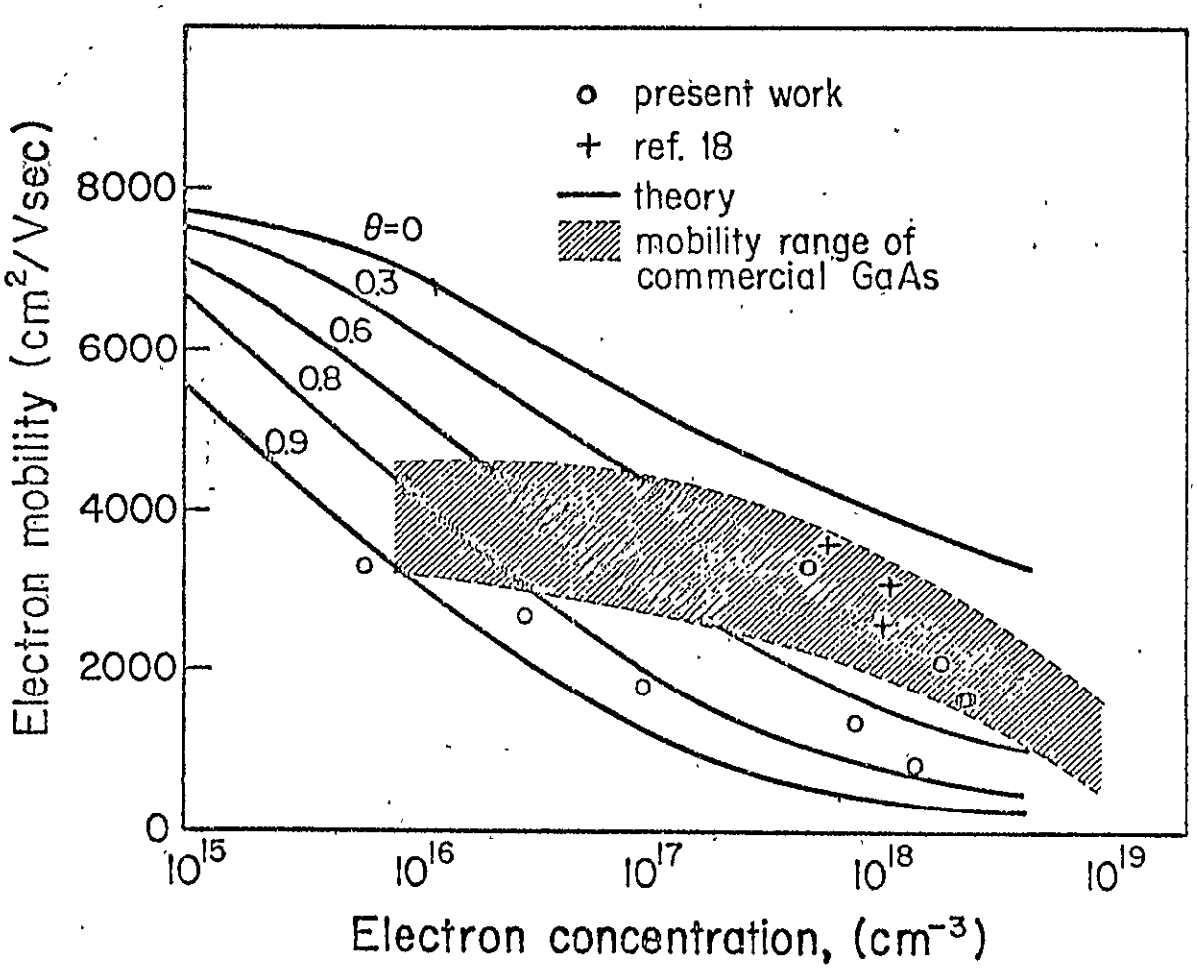

Figure 11. Electron mobility of GaAs as a function of electron concentration calculated for different values of compensation ratio. Shaded area refers to the mobility range of commercial GaAs.

compensation ratio) represents the theoretical mobility limit. The shaded area represents the mobility range of presently available bulk GaAs. It is evidence that GaAs performs below the theoretical limit and that this tendency is particularly pronounced for higher purity (lower electron concentration) material. On the basis of our theoretical and experimental results we have developed most useful tables from which the compensation ratio can be directly obtained from carrier concentration and from mobility or absorption coefficient measurements. These tables are far more accurate than those in use up to this time.

It has been recently reported that the compensating centers in GaAs are associated with point defects and defect-impurity complexes. Thus, our method for the determination of the compensation ratio will be used as a convenient means for relative determination of the overall defect density in GaAs. We plan to utilize this method in all stages of our program in direct correlation with growth experiments.

Electron mobility and free-carrier absorption in GaAs: Determination of the compensation ratio

W. Walukiewicz,[a] L. Lagowski,[a] L. Jastrzebski, M. Lichtensteiger,[b] and H. C. Gatos

Department of Materials Science and Engineering, Massachusetts Institute of Technology, Cambridge, Massachusetts 02139

(Received 19 June 1978; accepted for publication 4 August 1978)

Theoretical calculations of electron mobility and free-carrier absorption in n-type GaAs at room temperature were carried out taking into consideration all major scattering processes. It was found that satisfactory agreement between theoretical and experimental results on free-carrier absorption is obtained only when the effect of compensation is quantitatively taken into account. In conjunction with experimental studies it is shown that the electron mobility (for $n > 10^{15}$ cm^{-3}) and free-carrier absorption (for $n > 10^{16}$ cm^{-3}) are sufficiently sensitive to the ionized impurity concentration to provide a reliable means for determining the compensation ratio. Convenient procedures are presented for the determination of the compensation ratio from the free-carrier absorption coefficient and from the computed values of room-temperature electron mobility. Values of the compensation ratio obtained by these two procedures are in good agreement provided the carrier-concentration variations in the material are not appreciably greater than 10%.

PACS numbers: 72.20.Dp, 78.20.Dj, 72.20.Fr, 72.80.Ey

I. INTRODUCTION

III-V semiconductors usually exhibit an appreciable degree of compensation. Knowledge of the extent of compensation is important for the understanding of the basic electronic characteristics of these materials and their devices and for the evaluation of crystal-growth processes. The methods for determining the compensation are usually related to the fact that the compensation reduces the free-carrier concentration and it enhances free-carrier scattering by ionized impurities.

In GaAs, because of the small donor ionization energy (~ 5 meV), the accurate determination of donor and acceptor concentrations from free-carrier concentration changes must be carried out at temperatures well below 15 °K. Similarly, the determination of the compensation ratio from the amplitude of Schubnikov–de Haas oscillations, as proposed recently,[1] must be carried out at 4.2 °K. The low-temperature requirements render these methods inaccessible for routine needs. Instead, methods based on scattering of free carriers by ionized impurities are employed. The reliable determination of the compensation ratio from free-carrier scattering by ionized impurities is complicated, however, by the fact that longitudinal optical phonons contribute significantly to the overall scattering.[2] For this polar-mode scattering, the relaxation time cannot be defined except for low temperatures.[3] Accordingly, it is necessary to use variational[4] or iterative procedures[5] to combine all relevant scattering mechanisms. Earlier approaches[5,6] to the determination of the compensation ratio from electron mobility neglected these aspects. More recently, a rigorous semiempirical procedure has been formulated[7,8] for determining the compensation ratio in n-type GaAs from the Hall constant and resistivity measurements at 77 °C. This procedure takes into consideration all major scattering mechanisms but it is applicable only to nondegenerate material. Theoretical calculations of electron mobility (based on an iterative procedure for solving the Boltzmann equation) including compensation as a parameter and considering all major scattering mechanisms have also been reported.[2,9] Although the screening of polar vibrations by free carriers (which is significant at room temperature for $n > 10^{17}$ cm^{-3}) was not taken into consideration, these results represent the most reliable theoretical values of electron mobility in GaAs thus far.

Free-carrier absorption has been used also for the determination of the compensation ratio in n-type GaAs.[10–12] In this approach (in contrast to that based on the electron mobility) the ionized impurity contribution to free-carrier absorption is separable from contributions by other scattering mechanisms. This approach has not as yet been correlated with compensation-ratio values obtained by other methods. Furthermore, the values of free-carrier absorption available in the literature are not very reliable because the appropriate material parameters were not used in carrying out the computations.[13,14]

In the present study, the effect of compensation on two independently measured quantities, i.e., on the electron mobility and on the free-carrier absorption, is considered. Theoretical computations of mobility are based on a variational method in the form proposed in Ref. 4 and they include all major scattering processes and screening effects. Computations of the free-carrier absorption coefficient are based on

[a] On leave from Institute of Physics, Polish Academy of Sciences, Warsaw, Poland

[b] Present address: Coulter Systems Corporation, 35 Wiggins Avenue, Bedford, Mass. 01730.

 0021-8979/79/020899-10$01.10

the approach of Ref. 10. A comparison is made with experimental results and with data available in the literature [11,15–18]. A procedure is outlined for the convenient determination of the compensation ratio from measured values of room-temperature electron mobility and from the absorption coefficient at a wavelength of about 10 μm.

II. THEORY

A. General considerations

The present theoretical calculations are intended to provide the basis for the determination of the compensation ratio (or total density of ionized impurities) in n-type GaAs from independent room-temperature measurements of the free-carrier absorption and the electron mobility.

The electron mobility μ and the free-carrier absorption coefficient α will be defined as

$$\mu=\sigma(0)/ne, \quad \alpha(\omega)=4\pi\sigma(\omega)/cn_r, \tag{1}$$

where $\sigma(0)$ and $\sigma(\omega)$ are the dc and ac conductivity, respectively, n is the concentration of free electrons, c is the velocity of light, and n_r is the refractive index at a given irradiation frequency ω.

When the energy-band structure, the electron-phonon coupling constants, and the electron concentration are known, the value of σ can be calculated if the total concentration of ionized impurities is also known. For n-type GaAs, the available material parameters are sufficiently accurate for a quantitative calculation of μ and $\alpha(\omega)$. For a given temperature, such calculations provide two absolute quantities, i.e., μ and $\alpha|_{\omega=\text{const}}$, and one functional dependence $\alpha(\omega)$, each of which can be used to determine the concentration of ionized impurities. Accordingly, in cases where ionized impurity scattering is appreciable, experimentally measured electron mobilities, free-carrier absorption coefficients, and the frequency dependence of absorption coefficient can serve as the basis for testing the validity of the theoretical calculations and the reliability of the procedure for the determination of the compensation ratio.

In general, dc and ac conductivities can be treated in the same theoretical framework. In practice, however, it has been shown that dc conductivity is satisfactorily obtained from the solution of the semiclassical Boltzmann equation,[2,4,19] whereas ac conductivity can be conveniently obtained from second-order perturbation theory.[10,20–22] Both approaches are utilized in the present study; the computations are carried out using the material parameters given in Table I and discussed in detail in Ref. 2.

In view of the high (1.43 eV) and direct energy gap of GaAs, a single spherical and parabolic conduction band described by an effective mass m^* will be assumed. With such an approximation, the electron mobility is slightly overestimated and the free-carrier absorption is underestimated. For this reason an effective mass $m^*/m_0=0.068$ is used, which is somewhat higher than the exact value of the effective mass $m^*/m_0=0.064\pm0.002$ at the band edge of GaAs.[23]

In the theoretical approach adopted in the present study, dilute solid solutions are assumed; i.e., interactions between impurities, quantum corrections for ionized impurity scattering,[24] and differences in the short-range part of the impurity potential are not taken into consideration. This assumption sets a limit to the electron (and impurity) concentration, which for n-type GaAs at room temperature can be realistically estimated to be 3×10^{18} cm^{-3}. In this respect, it should be pointed out that differences in scattering by various impurities (Te, Se, and S) in GaAs at concentrations above 10^{18} cm^{-3} have been indicated in Refs. 25 and 16–18. However, a study of the electron mobility in about 10^3 GaAs single crystals doped with Te, Se, Sn, and Si has failed to show any consistent differences among the various dopants[26]; the only difference (slightly lower mobility) was found in Si-doped crystal (at concentrations exceeding 10^{18} cm^{-3}); this result was apparently due to the amphoteric behavior of Si.

TABLE I GaAs parameters used in present computations (300 °K) (after Refs. 2 and 9)

Low-frequency dielectric constant ϵ_0	12.91
High-frequency dielectric constant ϵ_∞	10.91
Optical-phonon energy $\hbar\omega_0$	36 meV
Deformation potential E_1	7 eV
Longitudinal elastic constant $C_l=\rho v_l^2$	14.03×10^{11} dyn/cm^2
Piezoelectric coefficient $h^2_{14}(3/C_l+4/C_t)$	2.39×10^{-2}
Effective mass m^*/m_0	0.068 (see text)

B. Free-carrier absorption

The present analysis will be confined to wavelengths greater than 4 μm, where transitions between various conduction-band minima are negligible. Thus, only the lowest conduction band with a minimum at the center of the Brillouin zone (Γ_6) needs to be considered. The absorption of free carriers in a single conduction band constitutes an indirect transition in which momentum is conserved through interactions with the lattice. Using the approximation of a parabolic conduction band, the absorption coefficient can be directly calculated from the expressions derived in Ref. 10.

The total absorption coefficient α_t is

$$\alpha_t=\alpha_{\text{op}}+\alpha_{\text{ac}}+\alpha_{\text{imp}}, \tag{2}$$

where α_{op}, α_{ac}, and α_{imp} are the absorption coefficients corresponding to electron interactions with screened optical phonons, acoustic phonons, and screened ionized impurities, respectively. Piezoelectric scattering is not taken into consideration; mobility calculations (see below) showed that for n-type GaAs, at room temperature the contribution of piezoelectric scattering to the total mobility is less than 2%; a similar contribution (which is within the accuracy of the calculations) is expected to the free-carrier absorption.

According to Ref. 10, the absorption coefficients α_ν can be written as follows, where ν designates op, ac, or imp:

$$\alpha_\nu=\frac{C}{z^3}\int_0^\infty G_\nu(x,x'_\nu)\,[f(x)-f(x'_\nu)]\,dx, \tag{3}$$

where $f(x)=1/[\exp(x-\eta)+1]$ is the electron distribution function, $x=E/k_0T$, $\eta=E_f/k_0T$, and $z=\hbar\omega/k_0T$ are the reduced electron energy, the Fermi energy, and the incident-photon energy, respectively, k_0 is the Boltzmann constant, and T is the absolute temperature. The values of C_ν, G_ν, and x'_ν are for optical phonons

$$C_{\rm op}=2.96\times10^5(m^*/m_0)\frac{z_l}{n_r}\left(\frac{1}{\epsilon_\infty}-\frac{1}{\epsilon_0}\right)\times\frac{\sinh\frac{1}{2}z}{\sinh\frac{1}{2}z_l\sinh\frac{1}{2}z'},\tag{4}$$

$$G_{\rm op}=2P_{\rm op}\left(1+\frac{a^2}{D_{\rm op}}\right)-aL_{\rm op}$$

$$x'_{\rm op}=x+z\pm z_l,$$

for ionized impurities,

$$C_{\rm imp}=2.175\times10^{-5}\frac{N_{\rm imp}}{\epsilon_0^2n_r^2T^2},$$

$$G_{\rm imp}=\tfrac{1}{4}L_{\rm imp}-a\frac{P_{\rm imp}}{D_{\rm imp}},\tag{5}$$

$$x'_{\rm imp}=x+z,$$

and for acoustic phonos,

$$C_{\rm ac}=4.79\times10^{11}\left(\frac{m^*}{m_0}\right)^2\frac{TE_1^2}{n_r\rho v_l^2},\tag{6}$$

$$G_{\rm ac}=P_{\rm ac}B_{\rm ac},$$

$$x'_{\rm ac}=x+z,$$

where

$$P_\nu=(xx'_\nu)^{1/2},\quad B_\nu=x+x'_\nu\tag{7}$$

$$L_\nu=\ln\left(\frac{B_\nu+a+2P_\nu}{B_\nu a-2P_\nu}\right),$$

$$D_\nu=(B_\nu+a)^2-4P_\nu^2.$$

The symbols in Eqs. (4)–(7) are as follows: ϵ_0 and ϵ_∞ are the static and the high-frequency dielectric constants, respectively, $N_{\rm imp}=N_D^+ +N_A^-$ is the concentration of ionized impurities, E_1 is the conduction-band deformation potential, ρ is the crystal density, v_l is the longitudinal sound velocity, $z_l=\hbar\omega_l/k_0T$ is the reduced energy of longitudinal optical phonons, m_0 is the electron mass, a is the reduced screening energy,

$$a=\hbar^2/2m^*l_D^2k_0T,\tag{8}$$

where the screening length l_D is defined as

$$\frac{1}{l_D^2}=5.80\times10^{13}\times\frac{(m^*/m_0)^{3/2}T^{1/2}}{\epsilon_0}F_{-1/2}(\eta),\tag{9}$$

and $F_n(\eta)$ is the n-th order Fermi Dirac integral.

It should be noted that $\alpha_{\rm op}$ is a sum of two terms given by Eq. (3) which correspond to $x'_{\rm op}=x+z-z_l$ and $z'=z-z_l$ and $x'_{\rm op}=x+z+z_l$ and $z'=z+z_l$, respectively. A discussion of the numerical calculations carried out on the basis of Eqs. (2)–(9) and the GaAs parameters listed in Table I will be presented below together with experimental results.

The carrier concentration $n=N_D^+-N_A^-$ (where N_D^+ and N_A^- are the concentrations of ionized donors and acceptors, respectively) enters into Eqs. (2)–(9) through the reduced Fermi level η according to

$$n=(2/\pi^{1/2})N_cF_{1/2}(\eta)\tag{10a}$$

or

$$n=5.44\times10^{15}[T(m^*/m_0)]^{3/2}F_{1/2}(\eta),\tag{10b}$$

where N_c is the effective density of states in the conduction band.

The compensation ratio θ is defined as $\theta=N_A^-/N_D^+$; accordingly, the total concentration of the ionized impurities is related to the compensation ratio as follows:

$$N_{\rm imp}=n(1+\theta)/(1-\theta).\tag{11}$$

It is apparent from Eqs. (2)–(9) that for a given frequency of the incident light and for a given electron concentration, only the term $\alpha_{\rm imp}$ depends on the compensation ratio (being proportional to $N_{\rm imp}$). thus, if $\alpha_{\rm exp}$ is the measured absorption coefficient in a material with a compensation ratio θ, and $\alpha_{\rm op}$, $\alpha_{\rm ac}$, and $\alpha_{\rm imp}$ are the absorption coefficients computed [from Eqs. (3)–(9)] for the same wavelength and the carrier concentration taking $\theta=0$ (i.e., $N_{\rm imp}=n$), the total concentration of ionized impurities can be determined by

$$N_{\rm imp}=n\frac{\alpha_{\rm exp}-(\alpha_{\rm op}+\alpha_{\rm ac})}{\alpha_{\rm imp}},\tag{12a}$$

which according to Eq. (11) leads to the following expression for the compensation ratio:

$$\theta=\frac{\alpha_{\rm exp}-(\alpha_{\rm op}+\alpha_{\rm ac}+\alpha_{\rm imp})}{\alpha_{\rm exp}+\alpha_{\rm imp}-(\alpha_{\rm op}+\alpha_{\rm ac})}.\tag{12b}$$

The values of $\alpha_{\rm imp}$, $\alpha_{\rm op}$, and $\alpha_{\rm ac}$ computed as a function of n for a wavelength of 10 μm are given in Table II.

A direct comparison between the experimental values of absorption coefficient and the theoretical dependence of the total free-carrier absorption [computed from Eqs. (2)–(7)] on electron concentration is not possible since samples with varying electron concentration can be characterized by a different degree of compensation. To provide a means for such comparison, a reduced experimental absorption coefficient, $\alpha^*_{\rm exp}$ will be introduced representing $\alpha_{\rm exp}$ for zero compensation.

$$\alpha^*_{\rm exp}\equiv\alpha_{\rm exp}-(N_{\rm imp}/n)\alpha_{\rm imp},\tag{13a}$$

which according to Eq. (11) becomes

$$\alpha^*_{\rm exp}=\alpha_{\rm exp}-\alpha_{\rm imp}2\theta/(1-\theta).\tag{13b}$$

The theoretically obtained data in Table II can be used for relating $\alpha^*_{\rm exp}$ to the compensation ratio as determined by other means (e.g., by electron-mobility measurements). This

TABLE II Computed values of electron mobility and ir absorption in n-type GaAs

Electron Conc. (cm^{-3})	Compensation ratio θ =	Electron mobility (cm^2/V sec)										Absorption at 10 μm (cm^{-1})		
		0.0	0.1	0.2	0.3	0.4	0.5	0.6	0.7	0.8	0.9	α_{imp}	α_{ac}	α_{op}
	1×10^{15}	7810	7760	7700	7620	7530	7400	7220	6940	6490	5590			
	1.5×10^{15}	7740	7680	7590	7490	7360	7200	6970	6640	6120	5150			
	2×10^{15}	7600	7510	7410	7290	7140	6950	6690	6330	5770	4780			
	3×10^{15}	7540	7430	7300	7150	6960	6730	6420	6000	5400	4370			
	4×10^{15}	7450	7320	7170	6990	6780	6510	6180	5730	5100	4070			
	5×10^{15}	7370	7230	7060	6870	6640	6350	6000	5540	4850	3870			
	6×10^{15}	7280	7130	6950	6730	6490	6190	5820	5340	4700	3670			
	7×10^{15}	7230	7060	6860	6640	6380	6060	5680	5200	4540	3510			
	8×10^{15}	7150	6970	6760	6530	6260	5930	5540	5050	4390	3370			
	9×10^{15}	7050	6860	6650	6400	6120	5790	5390	4900	4250	3232			
	1×10^{16}	6980	6790	6560	6310	6020	5680	5280	4790	4140	3120	0.0036	0.025	0.341
	1.5×10^{16}	6710	6480	6230	5950	5640	5280	4870	4370	3720	2710	0.0080	0.038	0.510
	2×10^{16}	6500	6250	5980	5680	5360	5000	4580	4080	3430	2440	0.0142	0.050	0.679
	3×10^{16}	6190	5920	5630	5320	4980	4610	4180	3680	3030	2060	0.032	0.075	1.10
	4×10^{16}	5970	5690	5380	5060	4720	4340	3910	3410	2760	1820	0.056	0.100	1.35
	5×10^{16}	5810	5510	5200	4870	4520	4140	3710	3200	2560	1640	0.087	0.126	1.68
	6×10^{16}	5680	5370	5050	4720	4370	3980	3550	3040	2400	1510	0.125	0.152	2.00
	7×10^{16}	5570	5260	4940	4600	4250	3860	3420	2910	2270	1400	0.169	0.178	2.32
	8×10^{16}	5480	5160	4840	4490	4140	3740	3300	2790	2160	1320	0.220	0.203	2.65
	9×10^{16}	5400	5080	4750	4400	4040	3640	3200	2690	2060	1240	0.277	0.229	2.97
	1×10^{17}	5330	5010	4670	4320	3960	3560	3120	2600	1980	1180	0.340	0.255	3.28
	1.5×10^{17}	5090	4750	4400	4030	3650	3240	2790	2280	1690	960	0.746	0.387	4.84
	2×10^{17}	4910	4540	4160	3780	3390	2970	2520	2030	1470	820	1.29	0.521	6.35
	3×10^{17}	4730	4350	3960	3560	3160	2730	2280	1790	1270	680	2.79	0.796	9.26
	4×10^{17}	4530	4130	3730	3320	2920	2490	2050	1590	1100	580	4.82	1.08	12.1
	5×10^{17}	4470	4060	3640	3220	2800	2380	1940	1490	1020	530	7.26	1.34	14.8
	6×10^{17}	4370	3950	3520	3100	2680	2260	1830	1390	950	480	10.2	1.68	17.5
	7×10^{17}	4290	3860	3420	3000	2580	2160	1740	1320	890	450	13.5	1.99	20.1
	8×10^{17}	4220	3780	3340	2910	2500	2080	1670	1260	840	420	17.2	2.32	22.7
	9×10^{17}	4160	3710	3270	2840	2430	2010	1610	1200	800	400	21.3	2.65	25.3
	1×10^{18}	4100	3640	3200	2770	2360	1950	1550	1160	770	380	25.8	3.00	27.9
	1.5×10^{18}	3860	3400	2950	2520	2130	1740	1370	1010	660	330	53.4	4.85	40.5
	2×10^{18}	3690	3220	2780	2360	1980	1600	1250	920	600	290	88.8	6.91	52.8
	3×10^{18}	3460	3000	2560	2160	1790	1440	1120	810	530	260	178	11.6	76.6
	4×10^{18}	3300	2840	2410	2020	1670	1340	1040	750	480	230	284	16.9	98.6
	5×10^{18}	3200	2750	2330	1950	1600	1280	990	710	460	220	400	22.8	120

procedure will be discussed below in conjunction with experimental results. At this time, an analytical extension of the above procedure to other wavelengths will be considered without resorting to additional numerical calculations. In previous treatments,[11, 20–22] approximate analytical expressions have been obtained on the frequency dependence of the absorption coefficient assuming a nondegenerate electron gas. They were found to be in fairly good agreement with experiment even in the case of highly doped materials for which the assumption of nondegeneracy is not satisfied. It can be shown, however, that these results are not inconsistent since similar analytical expressions can be obtained from Eqs. (2)–(9).

Thus, in a spectral region, where $\hbar\omega$ is much greater than $\hbar\omega_0$, E_F, k_0T, and ak_0T, Eqs. (3)–(7) reduce to

$$\alpha_{op}\simeq\frac{4C_{op}}{z^{2.5}}F_{1/2}(\eta)$$

or

$$\frac{\alpha_{op}}{n}\simeq=\frac{2\pi^{1/2}}{N_c}\left(\frac{k_0T}{hc}\right)^{2.5}C_{op}\lambda^{2.5},\qquad(14a)$$

$$\alpha_{imp}\simeq\frac{C_{imp}}{z^{3.5}}F_{1/2}(\eta)$$

or

$$\frac{\alpha_{imp}}{n}\simeq\frac{\pi^{1/2}}{2N_c}\left(\frac{k_0T}{hc}\right)^{3.5}C_{imp}\lambda^{3.5},\qquad(14b)$$

$$\alpha_{ac}\simeq\frac{C_{ac}}{z^{1.5}}F_{1/2}(\eta)$$

or

$$\frac{\alpha_{ac}}{n}\simeq\frac{\pi^{1/2}}{2N_c}\left(\frac{k_0T}{hc}\right)^{1.5}C_{ac}\lambda^{1.5}.\qquad(14c)$$

These expressions give the same frequency (or wavelength) dependence of the absorption coefficient as the expressions in Ref. 11 and 20–22. For GaAs at room temperature and in

the spectral region of 4–10 μm unequality $\hbar\omega \gg \hbar\omega_0, E_F, \kappa_0 l$, and ak_0T is fairly well satisfied up to an electron concentration of about 10^{18} cm^{-3}. For higher electron concentration Eqs. (14a)–(14b) still constitute a reasonable approximation for shorter wavelengths (e.g., 4–7 μm), in agreement with previously reported experimental results.[11,14]

According to Eqs (14a)–(14c), the procedure for determining the compensation ratio, from Eq. (12), and the numerical values in Table II for $\lambda_0 = 10\,\mu$m, can be simply extended to other wavelengths λ by calculating the absorption coefficient according to the approximate relationships

$$\alpha_{\mathrm{op},\lambda_1} = \alpha_{\mathrm{op},\lambda_0}(\lambda_1/\lambda_0)^{2.5}, \tag{15}$$
$$\alpha_{\mathrm{imp},\lambda_1} = \alpha_{\mathrm{imp},\lambda_0}(\lambda_1/\lambda_0)^{3.5},$$
$$\alpha_{\mathrm{ac},\lambda_1} = \alpha_{\mathrm{ac},\lambda_0}(\lambda_1/\lambda_0)^{1.5}.$$

For an electron concentration $n = 10^{18}$ cm^{-3} and for $8 \leqslant \lambda \leqslant 12$ μm the error in absorption coefficients calculated according to Eq. (15) [rather than from more exact numerical calculation based on Eqs. (3)–(7)] does not exceed 9% for α_{imp} and 4% for $\alpha_{\mathrm{op}} + \alpha_{\mathrm{ac}}$. These errors decrease rapidly with decreasing electron concentration.

C. Electron mobility

The present computations of electron mobility are based on a variational principle method in the form proposed in Ref. 4 and 19. This method allows the combination of all scattering mechanisms without invoking Matthiessen's rule, and it has been successfully applied to the calculation of mobilities in a number of semiconductor compounds.[3,19,27–30]

The following scattering mechanisms are considered: screened optical-phonon scattering;[31] screened ionized-impurity scattering,[19,32] acoustic-phonon scattering through the deformation potential,[33] and piezoelectric interactions.[34] The final expression used (see the Appendix) is

$$\mu = 308.6\left[\left(\frac{1}{\epsilon^\infty} - \frac{1}{\epsilon_0}\right)\left(\frac{m^*}{m_0}\right)^{3/2} T^{1/2} \times z_i F_{1/2}(\eta)\right]^{-1} \frac{D_{3/2,3/2}}{D}, \tag{16}$$

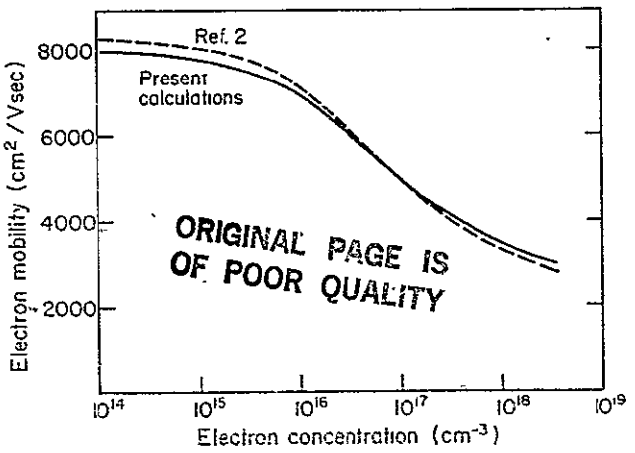

FIG. 1. Comparison of electron mobilities calculated by a variational method (present calculations) and by an iterative procedure (Ref. 2) for n-type GaAs at room temperature, screening of polar scattering is not included (see text).

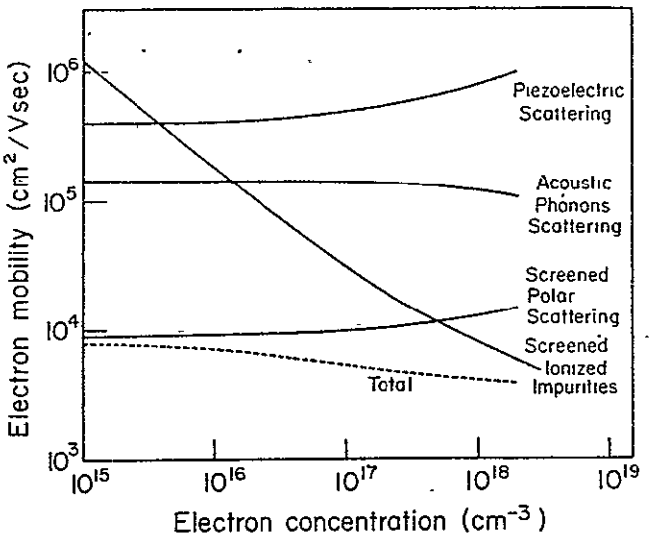

FIG. 2. Calculated component and total electron mobility as a function of electron concentration in n-type GaAs at room temperature.

where $D_{3/2,3/2}$ and D are the determinants defined in the Appendix.

Mobility values as a function of electron concentration obtained in the present study are shown in Fig. 1 together with results reported in Ref. 2 where an iterative procedure was used for solving the Boltzmann equation; screening of polar scattering intentionally is not included in the calculations shown in Fig. 1 since this type of screening was not included in the calculations of Ref. 2. It is seen that the two methods are in very good agreement; the observed discrepancy at low and high electron concentration is primarily due to the assumption of a parabolic conduction band used in the present study; in Ref. 2 a nonparabolic conduction band was used with a slightly smaller band-edge effective mass (0.066).

The component electron mobilities [i.e., electron mobilities calculated from Eq. (16) for each scattering mechanism acting alone] are shown as a function of electron concentration in Fig. 2. It is seen that the maximum contribution to the total mobility from piezoelectric scattering does not exceed 2%, consistent with the assumption made above in the case of free-carrier absorption. It is also seen that screening effects become pronounced for an electron concentration exceeding 10^{17} cm^{-3}.

In Fig. 3 the total electron mobility calculated from Eq. (16) is shown together with the electron mobility obtained by summarizing the component mobilities according to Matthiessen's rule (i.e., $1/\mu = \Sigma_i 1/\mu_i$). It is seen that for an electron concentration of 10^{17} cm^{-3} Matthiessen's rule leads to an error of about 30%. Thus, in determining the compensation ratio one must rely on the results of numerical calculations of mobility as a function of carrier concentration and compensation ratio. The results obtained in the present study are summarized in Table II.

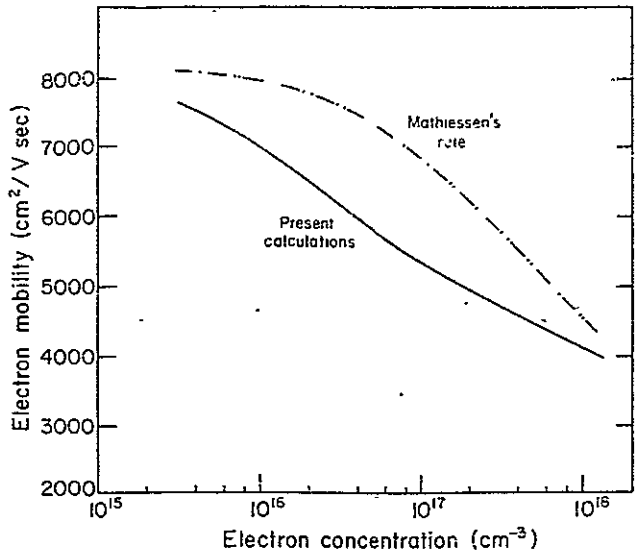

FIG 3. Comparison of electron mobilities in n-type GaAs calculated by a variational method and by Matthiessen's role employing the component mobilities.

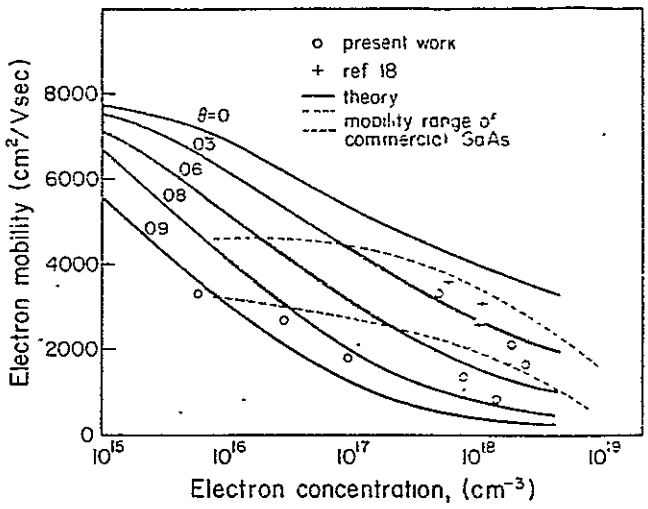

FIG 4 Theoretical (solid lines) and experimental values of mobility as a function of electron concentration in n-type GaAs for various compensation ratios: the mobility range for commercially available GaAs is also indicated.

III. COMPARISON WITH EXPERIMENT

A. Experimental procedure and sample homogeneity

Hall effect, dc conductivity, and infrared absorption measurements were carried out on n-type GaAs samples with electron concentrations ranging from 6×10^{15} to 2.6×10^{18} cm^{-3}.

Melt-grown GaAs single crystals obtained from commercial suppliers and two epitaxially grown Te-doped layers (intentionally compensated with Ge) were used in this study. In order to obtain consistent and meaningful results, it was found necessary to assess the homogeneity of the samples. The carrier concentration distribution on a macroscale and microscale was determined employing a recently reported ir scanning technique.[35] In the melt-grown commercial crystals, the spatial variation of the absorption coefficient at $\lambda=10.6\,\mu$m was found to be of the order of its average value (or Δn of the order of n_{av}). In such samples the measured mobility can be higher[36] and the infrared absorption lower than theoretical limits. Accordingly, only samples with carrier-concentration inhomogeneities not exceeding approximately 10% are considered in this study. The parameters of these samples are listed in Table III.

The experimental values of the electron mobility and electron concentration were obtained from Hall-effect and conductivity measurements. In order to avoid ambiguities associated with the value of the Hall factor r the Hall constant was determined as a function of magnetic field up to a value of 100 kG; the saturation value (which corresponds to $r=1$) was used to determine the electron concentration.

The results obtained are shown in Fig. 4 together with the theoretical dependence of electron mobility on electron concentration for different compensation ratios. The results of Ref. 18 which will be discussed in conjunction with free-carrier absorption are also shown. It is seen that all mobility values are well below the theoretical values at zero compensation. From the electron concentration and the electron mobility, the compensation ratio for each sample was deter-

TABLE III. Compensation ratios derived from mobility and ir absorption measurements

Sample No.	Electron Conc. (cm^{-3})	Growth	Dopant	Homogeneity $\Delta n/n_{av}$	Mobility (cm^2/V sec)	Compensation ratio θ Mobility	Absorption
1	3×10^{16}	Melt	Te	<10%	2700	0.83 ± 0.03	0.89 ± 0.05
2	1.1×10^{17}	Melt	?	<10%	1800	0.83 ± 0.03	0.85 ± 0.03
3	5.5×10^{17}	Melt	Te	<10%	3300	0.25 ± 0.06	0.23 ± 0.08
4[a]	8.5×10^{17}	LPE	Te	<3%	1350	0.67 ± 0.03	0.65 ± 0.04
5[a]	1.5×10^{18}	LPE	Te	<3%	800	0.76 ± 0.02	0.77 ± 0.03
6	2.0×10^{16}	Melt	?	<15%	2100	0.37 ± 0.08	0.29 ± 0.08
7	6×10^{15}	Melt	...	<20%	3300	>0.9	>0.9
8	2.6×10^{18}	Melt	...	<20%	1650	0.40 ± 0.1	0.3 ± 0.1
Ref. 18	6×10^{17}	...	Te	...	3600	0.18	0.18
Ref. 18	1.15×10^{18}	...	S	...	2600	0.31	0.25
Ref. 18	1.2×10^{16}	...	Te	...	3100	0.22	0.22

[a]Intentionally compensated with Ge (see text).

mined directly from Table II, the values of θ are given in Table III. The normal range of mobility in commercially available high-quality GaAs single crystals is indicated in Fig 4 by the striped area; in the low-electron-concentration region, the available GaAs is significantly compensated and typically the total concentration of ionized impurities exceeds by an order of magnitude the electron concentration.

The absorption coefficient was determined from the transmittance T (measured with a Fourier spectrometer) using

$$T=\frac{(1-R)^2\exp(-\alpha d)}{1-R^2\exp(-2\alpha d)}, \tag{17}$$

where d is the thickness of the sample and R is the reflectance of GaAs (e.g., for $\lambda=10\,\mu$m $R=0.28$). Tabulated values of $R(\lambda)$ are given in Ref. 37 For sufficiently thin samples ($\alpha d<1$) the transmittance measured as a function of the thickness of the sample can also be used to determine $R(\lambda)$. Measurements carried out in this study showed that for electron concentrations exceeding 10^{18} cm^{-3} and for $\lambda>10\,\mu$m the reflectance decreases with increasing electron concentration (see also Refs. 12 and 15). However, for lower electron concentrations, R was found to be essentially independent of n.

The transmission measurements, intended to provide a basis for determining the absorption coefficient, were carried out on thick samples and, with the exception of sample 7, the condition $\alpha d>1$ was satisfied for wavelengths in the vicinity of $10\,\mu$m.

The experimental results on the absorption coefficient for $\lambda=10\,\mu$m are given in Fig. 5 together with those available in the literature. For comparison, the theoretical values of the total absorption coefficient α_t and the absorption components α_{op}, α_{imp}, and α_{ac} are also given in Fig. 5. As it has been discussed above, these absorption coefficients were computed assuming no compensation. Thus, it is understandable that experimental values of α are greater than the theoretical ones Some of the experimental values of Ref 11 are smaller than those computed theoretically. Although the reason for this discrepancy is not clear, it should be noted that in the present study absorption coefficients smaller than those obtained theoretically were observed in samples exhibiting signigicant carrier-concentration inhomogeneities.

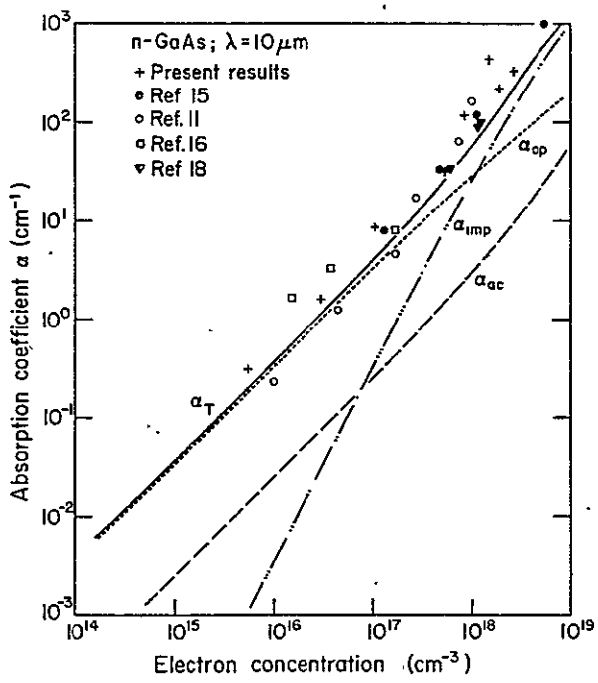

FIG 5 Theoretical and experimental values of the absorption coefficient as a function of electron concentration in GaAs at room temperature

B. Characteristics of free-carrier absorption

As pointed out above, a comparison between the experimental and theoretical dependence of free-carrier absorption on the electron concentration for samples of different degrees of compensation can be achieved by reducing the experimental absorption coefficient to zero compensation[Eq. (13b)]. Such a reduction of the experimental results of Fig. 5 was carried out using the values of compensation ratio determined for each sample from electron mobility (Table III), and the computed values of α_{imp} as given in Table II. The results of α^*_{exp} versus electron concentration are given in Fig. 6 together with the theoretical dependence of $\alpha_t(n)$. The obtained agreement is very good, and it is worth emphasizing that no adjustable parameters were used in the calculation of the mobility, which provides the basis for the determination of θ and of the free-carrier absorption coefficient.

The values of the compensation ratio determined from electron mobilities (Table III) have also been used to compare the experimental and theoretical dependence of the absorption coefficient on the wavelength λ. Typical results are given in Fig. 7. It is seen that very good agreement is ob-

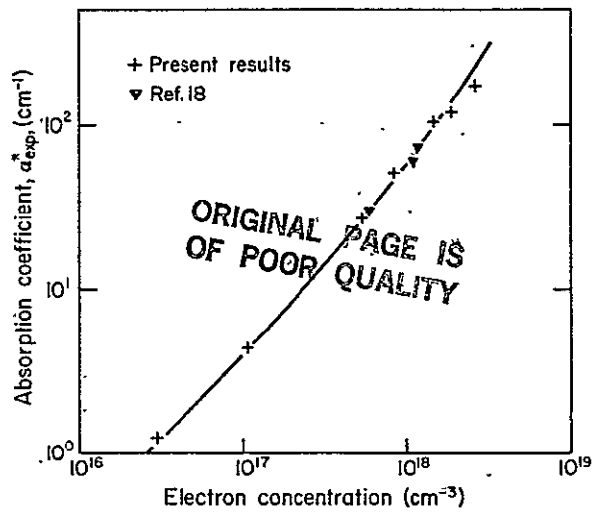

FIG. 6. Theoretical (solid line) and experimental values of the absorption coefficient reduced to zero compensation (see text) as a function of electron concentration in GaAs at room temperature; wavelength of radiation $\lambda=10$ μm.

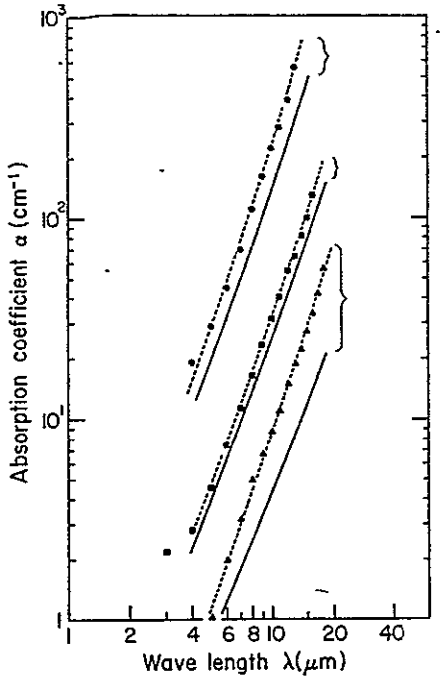

FIG. 7. The absorption coefficient as a function of wavelength Solid and dotted lines correspond to theoretical values, neglecting compensation, and dotted lines correspond to theoretical values obtained by taking into account compensation as determined from electron mobility; ●, ▩, and ▲ are experimental values obtained with samples 6, 3, and 2, respectively, of GaAs as in Table III.

tained when the effect of compensation is quantitatively taken into account. It is also seen that for the lower electron concentration ($n = 1.1 \times 10^{17}$ cm^{-3}) the compensation affects noticeably both the absolute value of α and its wavelength dependence (i.e., the slope $d \ln\alpha / d \ln\lambda$). This behavior is not surprising since with increasing compensation the dominant role of polar scattering is superseded by ionized-impurity scattering. These two scattering modes lead to different wavelength dependences of the absorption coefficient.

C. Compensation ratio

The present results have shown that the measured values of electron mobility (Table III) and the experimental characteristics of the free-carrier absorption (concentration and wavelength dependences) are satisfactorily explained by theory taking into account compensation.

As discussed above, the value of the compensation ratio can be determined independently from the electron mobility and the electron concentration (utilizing Table II) and from the free-carrier absorption coefficient [utilizing Eq. (12b) and the values of absorption components given in Table II]. The values of θ obtained by these methods are in very good agreement as shown in Table III. The differences in values of θ are within experimental error which is primarily due to inhomogeneity of the material. In the case of intentionally compensated epitaxial layers (samples 4 and 5 in Table III), the values of θ determined (0.67 and 0.76, respectively) here are in good agreement with the nominal compensation ratio estimated from the concentration of impurities introduced during the growth (i.e., 0.7 and 0.75, respectively). Thus, it must be concluded that both procedures for determining the compensation ratio lead to reliable and consistent results.

As pointed out above, the upper limit to which the present approach is applicable corresponds to electron (and impurity) concentrations of about 3×10^{18} cm^{-3}. The lower concentration limit is determined by the sensitivity of the room-temperature electron mobility and of the free-carrier absorption to ionized impurites. These limits are apparent from Table II (and/or Figs. 4 and 5). Thus, for a reliable determination of the compensation ratio from electron mobility, the electron concentration should be greater than 10^{15} cm^{-3} and in the case of free-carrier absorption the electron concentration should be greater than 10^{16} cm^{-3}. It should also be emphasized that, for the reliable application of the present procedures, GaAs should be reasonably homogeneous. Thus, it is desirable to supplement measurements of mobility and/or free-carrier absorption with measurements of the carrier concentration distribution on a microscale. Employing scanning ir absorption[35] for this purpose, it also becomes possible (on the basis of the present study) to obtain a compensation ratio profile with a spatial resolution of about 20 μm.

IV. SUMMARY

Theoretical and experimental studies of room-temperature electron mobility and the free-carrier absorption coefficient have been carried out on n-type GaAs. It was shown that for a total concentration of ionized impurities smaller than 10^{15} cm^{-3}, the room-temperature electron mobility is dominated by polar scattering (with about 10% contribution from acoustic-phonon and piezoelectric scattering) and it approaches a value of about 8000 cm^2/V sec, in agreement with previous experimental and theoretical results. For impurity concentrations exceeding 10^{15} cm^{-3}, the mobility becomes sensitive to ionized-impurity scattering, permitting the determination of the compensation ratio in the material. It was found, however, that the contribution from ionized impurity cannot be analytically separated from other scattering mechanisms since the application of Matthiessen's rule leads to significant errors. Thus, in determining the compensation ratio, one must rely on the results of numerical calculations. The calculated values of electron mobility as a function of compensation ratio given in Table II can be readily used for the determination of the compensation ratio in n-type GaAs with electron concentrations ranging from 10^{15} to 3×10^{15} cm^{-3}.

It was also shown that the free-carrier absorption coefficient is sensitive to compensation in GaAs for electron concentrations exceeding 10^{16} cm^{-3}. An analysis of the present experimental results and those available in the literature showed that the characteristics of free-carrier absorption (concentration and wavelength dependences) can be satisfactorily explained only when compensation is quantitatively accounted for.

A procedure for the determination of the compensation ratio from the value of the free-carrier absorption coefficient for $\lambda_0 = 10\,\mu$m (or other wavelengths $8 < \lambda \leq 12\,\mu$m), and the

calculated values of the component absorption coefficients was outlined. For reasonably homogeneous materials, a good agreement was obtained between the values of compensation ratios obtained from electron mobility and from free-carrier absorption. It should be pointed out that no fitting parameters other than the compensation ratio were used in comparing the experimental and theoretical results.

It was thus concluded that both the room-temperature electron mobility and the free-carrier absorption coefficient provide a reliable and consistent means for determining the degree of compensation (or the total concentration of ionized impurities) in n-type GaAs. In the form presented here, these methods can be used as practical procedures requiring relatively simple instrumentation. The electron concentration and mobility can be determined by means of standard conductivity and Hall-effect measurements, taking the Hall factor r as unity; the error due to this assumption is estimated to be about 10% for $n \approx 10^{15}$ cm^{-3} and decreases with increasing carrier concentration.

The free-carrier absorption method outlined here requires the determination of the absorption coefficient for one arbitrarily chosen wavelength in the spectral region $8 \leqslant \lambda \leqslant 12$ μm. Accordingly, relatively simple ir spectrometric instrumentation is required (e.g., a CO_2 laser and suitable ir detector). For sufficiently thick samples (satisfying the condition $\alpha d \geqslant 1$) the error associated with minor changes in reflectance due to electron-concentration changes can be neglected (for $n \leqslant 3 \times 10^{18}$ cm^{-3}) and one can utilize the values of $R(\lambda)$ given in Ref. 36. When the electron concentration, the electron mobility, and/or the free-carrier absorption coefficient are experimentally determined, the compensation ratio and the total number of ionized impurities can be determined from Table II and Eqs. (11) or (12).

ACKNOWLEDGMENTS

The authors are grateful to the National Aeronautics and Space Administration and the Department of the Air Force, Electronic Systems Division, for financial support. They would also like to express their appreciation to the technical staff of the Francis Bitter National Magnet Laboratory for the use of their high-field facilities.

APPENDIX

Equation (16) describing low-field electron mobility has been obtained with the aid of the variational principle method[4] adapted to the case of the screened electron–optical-phonon interaction.[27] The change of the electron-distribution function f can be written in the form

$$\left(\frac{\partial f}{\partial t}\right)_{\text{coll}} = -Ak\cos\vartheta \frac{\partial f_0}{\partial x} L(C), \tag{A1}$$

where $x = E/k_0T$, E is the electron energy, $k\cos\vartheta$ is the projection of the electron-wave vector on the electric field direction, and

$$A = A(x, T, m^*)$$

$$= 4.768\times 10^{25} \frac{z_l}{x^{3/2}} \frac{(m^*/m_0)^{1/2}}{T^{1/2}} \left(\frac{1}{\epsilon_\infty} - \frac{1}{\epsilon_0}\right). \tag{A2}$$

The operator $L(C)$ consists of four terms describing the different scattering mechanisms considered at present

$$L(C) = L_{\text{opt}}(C) + \frac{C(E)}{A}\left(\frac{1}{\tau_{\text{imp}}} + \frac{1}{\tau_{\text{ac}}} + \frac{1}{\tau_{\text{pel}}}\right). \tag{A3}$$

The relaxation times τ for elastic scattering processes are given by the following:

Screened ionized impurities,[32]

$$\frac{1}{\tau_{\text{imp}}} = 2.415 \frac{N_{\text{imp}}}{\epsilon_0^2}\left(\frac{m^*}{m_0}\right)^{-1/2}(xT)^{-3/2} \times\left[\ln\left(1+\frac{4x}{a}\right) - \frac{4x/a}{1+4x/a}\right], \tag{A4}$$

Acoustic-phonon scattering through deformation potential,[33]

$$\frac{1}{\tau_{\text{ac}}} = 4.167\times 10^{19} \frac{E_1^2}{\rho v_l^2}\left(\frac{m^*}{m_0} T\right)^{3/2} x^{1/2}, \tag{A5}$$

and piezoelectric (acoustic-mode) scattering,[34]

$$\frac{1}{\tau_{\text{pel}}} = 1.052\times 10^7 \times h_{14}^2 \left(\frac{3}{C_l} + \frac{4}{C_t}\right)\left(\frac{T}{x}\frac{m^*}{m_0}\right)^{1/2}. \tag{A6}$$

For screened optical-phonon (polar) scattering[27]

$$L_{\text{opt}}(C) = (f_+/f)(N+1)C_+[(R_+ + a)S_+ - aR_+T_+ - 4U_+] - 2x(f_+/f)(N+1)C_+(S_+ - aT_+) + h(x - z_l) \times\{(Nf_-/f)C_-[(R_- + a)S_- - aR_-T_- - 4U_-] - 2\times NC_-(f_-/f)(S_- - aT_-)\}, \tag{A7}$$

where

$$f_\pm = f_0(x \pm z_l), \quad C_\pm = C(E \pm \hbar\omega_l),$$
$$R_\pm = 2x + a \pm z_l, \quad U_\pm = [x(x \pm z_l)]^{1/2},$$
$$T_\pm = \frac{4U_\pm}{R_\pm^2 - 4U_\pm^2},$$
$$S_\pm = \ln\left(\frac{R_\pm + 2U_\pm}{R_\pm - 2U_\pm}\right),$$

and $N = 1/[\exp(z_l) - 1]$ is the optical-phonon occupation number. Following the procedure developed in Ref. 4 one obtains the following expression for electron mobility:

$$\mu = 308.6\left[\left(\frac{1}{\epsilon_\infty} - \frac{1}{\epsilon_0}\right)\left(\frac{m^*}{m_0}\right)^{3/2} T^{1/2}\right.$$

$$\times z_i F_{1/2}(\eta)\Big]^{-1}\left(\frac{D_{3/2\,3/2}}{D}\right), \tag{A8}$$

where the determinants have forms

$$D_{3/2,3/2}=\begin{vmatrix} 0 & \beta_0^{(3/2)} & \beta_1^{(3/2)} & \cdots \\ \beta_0^{(3/2)} & d_{00} & d_{01} & \cdots \\ \beta_1^{(3/2)} & d_{10} & d_{11} & \cdots \\ \cdot & \cdot & \cdot & \\ \cdot & \cdot & \cdot & \\ \cdot & \cdot & \cdot & \end{vmatrix}, \tag{A9}$$

$$D=\begin{vmatrix} d_{00} & d_{01} & \cdots \\ d_{10} & d_{11} & \cdots \\ \cdot & \cdot & \\ \cdot & \cdot & \\ \cdot & \cdot & \end{vmatrix}. \tag{A10}$$

The elements of the determinants are given by the integrals

$$\beta_r^{(3/2)}=\int_0^\infty E^{3/2}\Phi_r\frac{\partial f_0}{\partial E}\,dE, \tag{A11}$$

$$d_{r,s}=\int_0^\infty \Phi_r L(\Phi_s)\frac{\partial f_0}{\partial E}\,dE \tag{A12}$$

The functions Φ_r should represent a complete set of functions of electron energy E. In the present computations, the set $\Phi_{r(s)}=E^{r(s)}$ was chosen with values of r and s equal to 0, 1, and 2, which at room temperature assure an accuracy of the mobility calculations within a few percent.[4,38]

[1]A. Raymond, J.L. Robert, and B. Pistoulet, *Proc. VI Int. Symp. on GaAs and Related Compounds, Edinburgh, Sept.* 1976, edited by C. Hilsum (The Institute of Phys., London, 1976), p. 105

[2]For a recent review see D.L. Rode in *Semiconductors and Semimetals*, edited by R.K. Willardson and A.C. Beer (Academic, New York, 1975), Vol. 10, Chap. 1.

[3]H. Ehrenreich, J. Appl Phys 32, 2155 (1961)

[4]D. Howarth and E.H Sonheimer, Proc. Phys. Soc London A 219, 53

[5]F J Reid, in *Compound Semiconductors, Vol. I*, edited by R K. Willardson and H L. Goering (Reinhold, New York, 1962), p 158

[6]H. Kressel and H. Nelson, J. Appl Phys 40, 3720 (1969).

[7]C M. Wolfe, G.E Stillman, and J O Dimmock, J. Appl Phys 11 504 (1970)

[8]G.E. Stillman and C M Wolfe, Thin Solid Films 31, 69 (1976). D L Rode, Phys Rev B 2, 1012 (1970)

[9]D.L Rode and S Knight, Phys Rev. B 3, 2543 (1971)

[10]E Haga and H Kimura, J. Phys Soc Jpn 19, 658 (1964)

[11]K. Osamura and Y. Murakami: Jpn J Appl. Phys 11, 365 (1972).

[12]J K. Kung and W.G. Spitzer, J. Electrochem. Soc. 121, 1482. (1974).

[13]Compare the values of GaAs parameters used in Ref. 10 and 11 with those of Table I of Ref. 2 For a recent discussion of GaAs parameters, see Ref 14.

[14]G.E. Stillman, C M. Wolfe, and J.O Dimmock, in Ref. 2, Vol. 12, Chap 4.

[15]W G Spitzer and J.M. Whelan, Phys Rev. 114, 59 (1959).

[16]M G. Milvidskii, V.B Osvenskii, E P. Rashevskaya, and T G. Yugova Sov. Phys –Solid State 7, 2784 (1966).

[17]E P. Rashevskaya and V.I. Fistul, Sov. Phys –Solid State 9, 1443 (1976)

[18]E P. Rashevskaya and V.I. Fistul, Sov. Phys –Solid State 9, 2849 (1968)

[19]H. Ehrenreich, Phys Rev. 120, 1951 (1960).

[20]H.Y. Fan, W. Spitzer, and R J. Collins, Phys. Rev. 101, 566 (1956)

[21]R.Rosenberg and M. Lax, Phys Rev 112, 843 (1958)

[22]S. Visvanathan, Phys Rev. 120, 376 (1960)

[23]For a recent discussion of GaAs effective mass, see Ref 14, p 180–186.

[24]E.J. Moore, Phys. Rev. 160, 607 (1967); 160, 618 (1967).

[25]V.I. Fistul, E.M. Omelyanovskii, O.V. Pelevin, and V.B. Ufimtsev, Izv Akad. Nauk SSSR Neorg. 2, 657 (1966).

[26]S M Sze and J.C. Irvin, Solid-State Electron. 11, 599 (1968).

[27]H. Ehrenreich, J. Phys. Chem Solid 2, 131 (1957); 9, 129 (1959)

[28]S.L. Lehoczky, J.G Broerman, D.A. Nelson, and C.R. Whitsett, Phys. Rev. B 9, 1598 (1974).

[29]W. Walukiewicz, J. Phys. C. 9, 1945 (1976)

[30]S.S. Devlin, in *Physics and Chemistry of II-VI Compounds*. edited by M Aven and J.S. Prener (North-Holland, Amsterdam, 1967), Chap 11.

[31]H. Ehrenreich, J. Phys Chem Solids 8, 130 (1959).

[32]R.B. Dingle, Philos .Mag. 46, 831 (1955).

[33]W. Shockley, *Electrons and Holes in Semiconductors* (Van Nostrand–Reinhold, Princeton, N.J , 1950).

[34]J.D. Zook, Phys. Rev. 136, 869 (1964).

[35]L. Jastrzebski, J. Lagowski, and H.C. Gatos, Electrochemical Society Meeting, Seattle, 1978, extended abstracts, Vol. 78-1, p. 551 (unpublished).

[36]C.M. Wolfe and G.E. Stillman, in Ref. 2, Chap. 3.

[37]B.O. Seraphin and H.E Bennett, in Ref. 2, Vol. 3, Chap. 12.

[38]The accuracy of the variational principle method increases with decreasing $z_i=\hbar\omega_0/kT$. For GaAs at room temperature $z_i\simeq 1.4$. A comparison of results in Ref. 4 and recent calculations [C. Hammer and B. Magnusson. Phys Scr. 6, 206 (1972)] show that the accuracy of variational calculations in the form presented here can be expected to be better than 5%.

Quantitative Determination of the Carrier Concentration Distribution in Semiconductors by Scanning *IR* Absorption: Si

L. Jastrzebski, J. Lagowski,[1] and H. C. Gatos*

Department of Materials Science and Engineering, Massachusetts Institute of Technology, Cambridge, Massachusetts 02139

ABSTRACT

A contactless method is reported for the quantitative measurement of spatial variations of the free carrier concentration in semiconductors with a resolution of about 20 μm and a sensitivity better than 1%. The method is based on free carrier absorption in the infrared region where other absorption processes are negligible. In the experimental arrangement a CO_2 laser beam passes through a semiconductor wafer mounted on a stage with a calibrated x-y motion; detection of the transmitted light through the desired area of the wafer about 20 μm in diameter is achieved by employing an *IR* microscope in conjunction with an *IR* detector. The principles and applications of the method are discussed using n- and p-type silicon. Carrier concentration profiles obtained by scanning *IR* absorption were found to be in good agreement with those obtained by standard spreading resistance measurements.

The determination of spatial variations of the carrier concentration in semiconductor materials continues to be of fundamental importance in device studies and applications and in studies of crystal growth and segregation. A number of methods have been developed for carrier concentration profiling utilizing the Schottky barrier (1), ESM (2), electroreflectance (3), electroluminescence (4), *IR* topography (5, 6), and spreading resistance (7). Most of these methods are qualitative in nature and their application is limited to specific concentration ranges. The most commonly used method to obtain quantitative carrier distribution profiles is based on spreading resistance measurements. This method, however, is applicable only to elemental semiconductors (pressure metal contacts with compound semiconductors are irreproducible); it introduces indentations on the surface and is very sensitive to surface preparation conditions (7). Optical methods are most desirable, as they require no electrical contacts (5, 6). Thus far, striations in Ge (5), Si, and GaAs (6) have been observed through free-carrier *IR* absorption (8). Infrared topography is limited to a narrow carrier concentration range and is of a qualitative nature.

In the present study *IR* absorption by free carriers in a scanning mode is employed for the quantitative determination of free-carrier concentration profiles in Si over a wide concentration range.

Experimental Approach and Results

Procedure:—Silicon samples of n- and p-type carrier concentrations ranging 10^{15}-10^{19} cm^{-3} were cut from Czochralski-grown crystals. They were mechanically lapped to thicknesses ranging from 1 cm to 50 μm (depending on the carrier concentration) and Syton polished. In order to assess the effect of surface preparation on the reflection coefficient, final polishing was also carried out with 0.3 or 0.03 μm particle diameter abrasive.

Measurements of infrared transmission in the spectral region of 2.5-25 μm were performed in a Fourier spectrometer. The values of the absorption coefficient, α, were obtained from the measured transmittance T using the expression

$$T = \frac{I}{I_0} = \frac{(1-R)^2 e^{-\alpha z}}{1 - R^2 e^{-2\alpha z}} \qquad [1]$$

where I is the intensity of the transmitted light, I_0 is the intensity of the incident light, R is the reflection coefficient, and z is the thickness of the sample; the spectral dependence and values of R employed in this study were taken from Ref. (9). Equation [1] was also used in some instances to obtain the value of R by measuring the transmittance as a function of sample thickness (10). With this procedure the reflection coefficient at 10 μm was obtained for sample with different carrier concentrations and different surface preparations.

Dependence of absorption coefficient on wavelength and carrier concentration.—The measured absorption coefficient of n- and p-type Si as a function of wavelength is presented in Fig. 1 and 2 for various concentrations. It is seen that, in general, the absorption coefficient increases with increasing wavelength. This increase is primarily due to free-carrier absorption (8); infrared radiation is absorbed by free carriers in the valence or in the conduction band when scattering mechanisms (by phonons or ionized impurities) provide conservation of momentum. For small carrier concentrations, other absorption processes leading to strong absorption peaks are superimposed on free carrier absorption.

In the vicinity of 10 μm (outside of the oxygen absorption band) even for small-carrier concentrations, the free-carrier absorption dominates all other absorption processes. The absorption coefficient of n- and p-type Si taken from Fig. 1 and 2 for radiation with a wavelength of 10 μm is shown in Fig. 3 and 4, respectively, as a function of free-carrier concentration,

* Electrochemical Society Active Member.
[1] Permanent address: Institute of Physics, Polish Academy of Sciences, Warsaw, Poland.
Key words: absorption, *IR*, semiconductor.

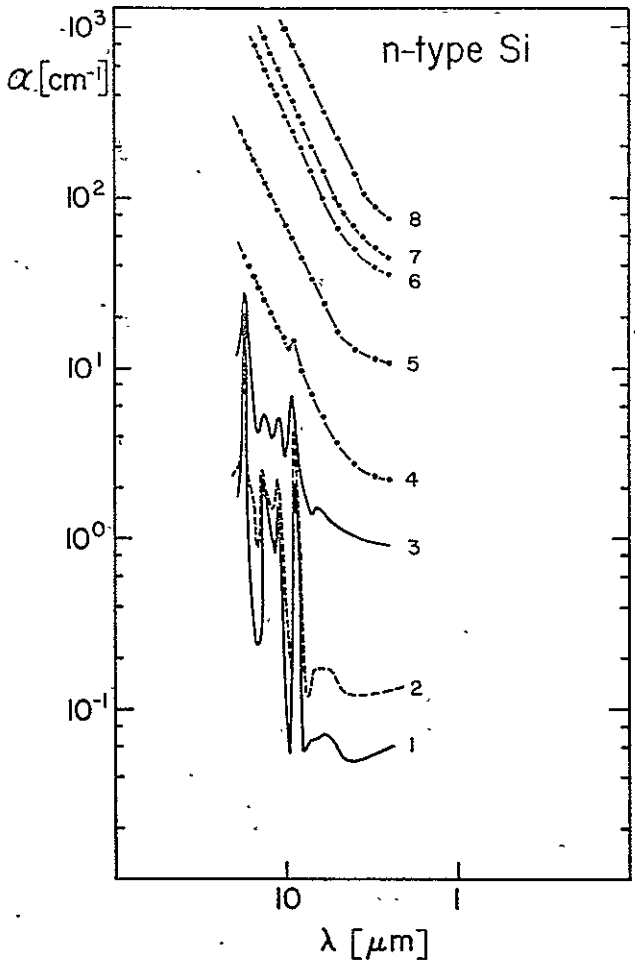

Fig. 1. Dependence of absorption coefficient, α, on wavelength of radiation for Si samples with different electron concentrations: 1, 1.1×10^{15}; 2, 7.6×10^{15}; 3, 5.1×10^{16}; 4, 2×10^{17}; 5, 7.2×10^{17}; 6, 2.9×10^{18}; 7, 3.6×10^{18}; and 8, 7.1×10^{18} cm^{-3}.

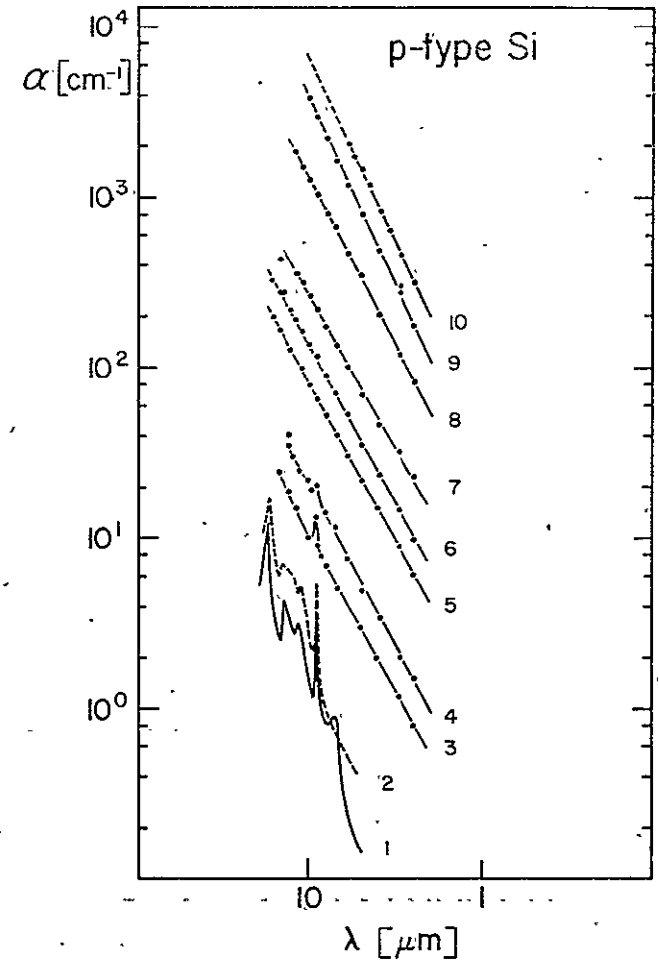

Fig. 2. Dependence of absorption coefficient on wavelength of radiation, α, for Si samples with different hole concentrations: 1, 7.4×10^{15}; 2, 3.3×10^{16}; 3, 9.1×10^{16}; 4, 1.7×10^{17}; 5, 5.2×10^{17}; 6, 7.4×10^{17}; 7, 1.4×10^{18}; 8, 5.0×10^{18}; 9, 1.2×10^{19}; and 10, 1.7×10^{19} cm^{-3}.

together with the data reported in the literature (11-14). In n-type Si, the absorption coefficient increases linearly with increasing electron concentration ranging from 10^{15} to about 5×10^{17} cm^{-3}; for higher electron concentrations the absorption coefficient exhibits a slightly overlinear dependence on the carrier concentration. This behavior is associated with an increased contribution of impurity scattering (8) to free-carrier absorption.

In p-type Si (Fig. 4) the absorption coefficient exhibits a linear dependence on hole concentration in the range of 3×10^{16}-2×10^{19} cm^{-3}. For smaller concentrations the absorption coefficient decreases, but less than expected for free-carrier absorption.

Dependence of transmittance on carrier concentration.—The dependence of the absorption coefficient on the carrier concentration (for $\lambda = 10$ μm) can be employed for the determination of the absolute value of the carrier concentration and carrier concentration fluctuations. It is convenient to introduce a cross section of absorption, $K_{n,p}$, describing the sensitivity of the absorption coefficient changes to carrier concentration changes, as follows

$$K_{n,p} = \frac{\alpha_{n,p}}{n,p} \qquad [2]$$

For n-type Si, $K_n = 1 \times 10^{-16}$ cm^{-3} (for electron concentrations up to 5×10^{17} cm^{-3}) and increases to 2×10^{-16} cm^{-3} as the concentration increases to 2×10^{19} cm^{-3} (Fig. 3). For p-type Si, $K_p = 2 \times 10^{-16}$ cm^{-3} for concentrations higher than 3×10^{16} cm^3; for small changes in carrier concentration ($\Delta n, \Delta p$), $\Delta\alpha = K_{n,p}\Delta n$,

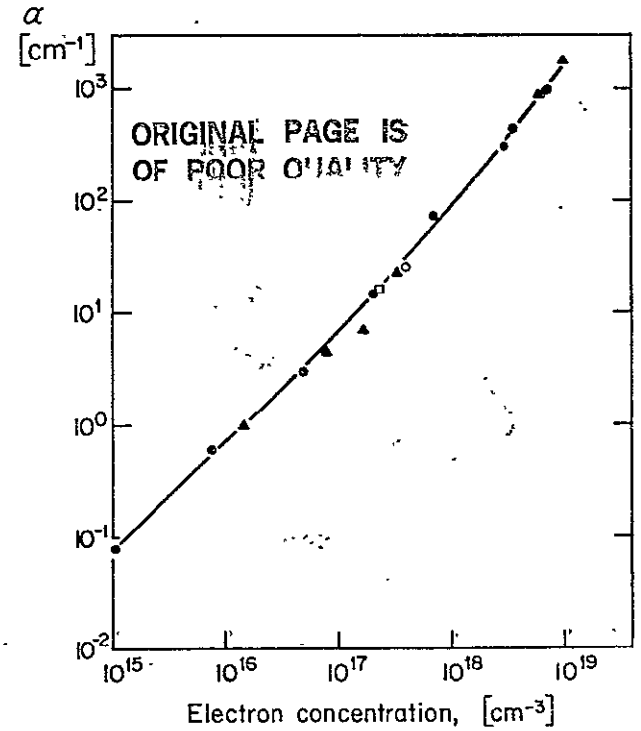

Fig. 3. Dependence of the absorption coefficient on electron concentration for radiation with 10 μm wavelength: ● present work; ▲ Ref. (11), ○ Ref (12), ■ Ref. (13).

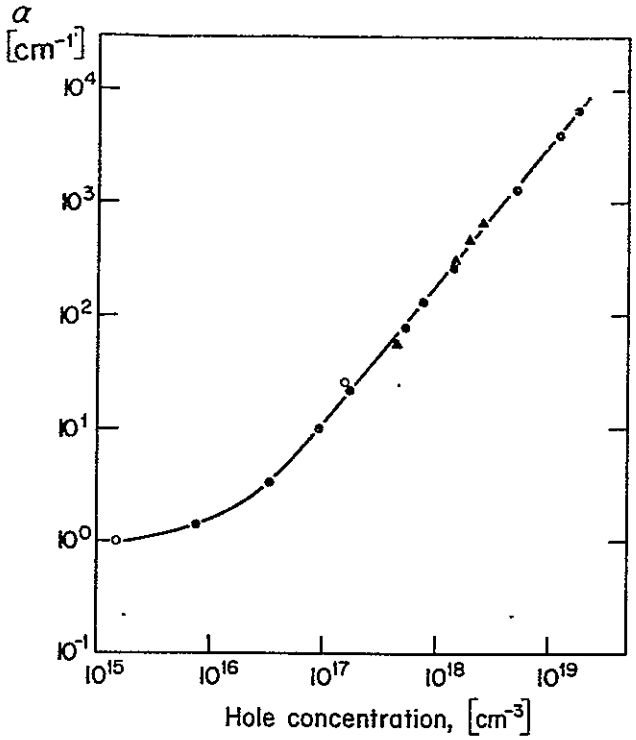

Fig. 4. Dependence of absorption coefficient on hole concentration for radiation with 10 μm wavelength: ● present work; ▲ Ref. (14), ○ Ref. (12).

Δp. Changes in concentration should lead to relative changes in transmittance, and if changes in R are negligible, then according to Eq. [1], for $\Delta n, \Delta p \ll n,p$, one obtains

$$\frac{1}{z}\frac{\Delta T}{T_{av}} = K_{n,p} \times \Delta n, \Delta p \qquad [3]$$

where T_{av} is the average value of transmittance along the wafer. Thus, variations in carrier concentration can be determined from variations in transmittance, providing corresponding variations in R are insignificant.

Reflection coefficient.—The reflection coefficient becomes sensitive to carrier concentration variations only when the wavelength of the radiation is near the wavelength at which the minimum in reflection due to plasma absorption occurs (9). For Si with moderate carrier concentrations the minimum in reflection occurs at far longer wavelengths than that of the radiation analyzed in this study (10 μm). For n-type silicon this minimum begins to shift appreciably at carrier concentrations above 10^{18} cm^{-3}, and reaches a wavelength of 22 μm at 5×10^{18} cm^{-3}; in p-type Si the minimum shifts to 16 μm at a carrier concentration of 1.2×10^{19} cm^{-3} (15).

Values of R were determined as a function of carrier concentration employing Eq. [1], as outlined above. It was found that R remained constant (0.29) for concentrations up to 1×10^{18} cm^{-3} in the case of n-type Si and for concentrations up to 2×10^{18} cm^{-3} in the case of p-type Si; for higher concentrations R decreased to 0.26 in going to $n = 5 \times 10^{18}$ cm^{-3} and to 0.19 for $p = 1.2 \times 10^{19}$ cm^{-3}. However, these changes of R were found to be orders of magnitude smaller than for corresponding changes in the absorption coefficient. Thus, in going from $p = 0.9 \times 10^{19}$ cm^{-3} to $p = 1 \times 10^{19}$ cm^{-3}, the contribution of the change of R to the change of transmittance was found to be an order of magnitude smaller than the contribution of the absorption coefficient for samples where $\alpha z = 2$. Accordingly, for samples where $\alpha z > 2$, variations of R are not taken into account in analyzing variations in transmittance.

The effects of variations in surface preparation on R were assessed by determining R for samples having the same carrier concentration but having been polished with an 0.3 and 0.03 μm particle diam abrasive and by Syton. The value of R was found to be the same, within experimental error (about 5%), for samples polished with 0.03 μm particle abrasive and for those polished with Syton. For samples polished with 0.3 μm particle diam abrasive the value of R was about 10% greater than that for samples polished with Syton. This variation of R for samples where $\alpha z = 2$ contributes about 3% error to the values obtained for α and for carrier concentration. Accordingly, variations in R due to surface preparation variations need not be taken into account in analyzing variations in transmittance.

Scanning IR absorption measurements.—Scanning *IR* absorption measurements were carried out employing an experimental arrangement shown schematically in Fig. 5. A paraliel beam 1 cm in diam from a CO_2 laser (tunable between 9.16 and 11.02 μm) is transmitted through the sample positioned on a stage with x-y motion and scanning rate ranging from 50 to 10^3 μm/min. The light transmitted through the desired area of the sample is focused on a detector (bolometer) through the optics of an *IR* microscope, and the signal from the detector, which is proportional to the intensity of radiation, is amplified and recorded. Using a 74× objective, the image of an area of about 20 μm diam is obtained.

In the present study a radiation power of about 0.2W was used to prevent heating of the sample. The average transmittance (T_{av}) was determined from the recorded intensity of the laser beam with and without the sample on the microscope stage. Changes in transmittance (ΔT) were recorded as the stage moved at a constant rate in the x or y direction. In the present arrangement changes in transmittance $\Delta T/T_{av}$, with an accuracy of about 0.1%, and a spatial resolution of about 20 μm were determined. On the basis of Eq. [3] (taking the value of $K_{n,p}$ from Fig. 3 or 4), transmittance changes of 0.1% correspond to fluctuations in carrier concentration of $\Delta n = 10^{13}/z$ cm^{-3} and $\Delta p = 5 \times 10^{13}/z$ cm^{-3}; thus, for a typical wafer with a thickness of 200 μm, $\Delta n = 5 \times 10^{14}$ and $\Delta p = 2.5 \times 10^{14}$ cm^{-3}.

A typical example of carrier concentration fluctuations obtained by scanning *IR* absorption for an n-type Si sample, 100 μm thick, with an average carrier concentration of 3×10^{18} cm^{-3} (cut from Czochralski-grown crystal along the growth direction) is shown in Fig. 6. The observed carrier fluctuations of about 15% are typical for the commercially grown single crystals by the Czochralski method; these carrier concentration fluctuations reflect turbulent convection-controlled segregation.

Comparison of scanning IR absorption with spreading resistance measurements.—Scanning *IR* absorption was directly compared with spreading resistance measurements by obtaining carrier concentration profiles on the same Si sample (average electron concen-

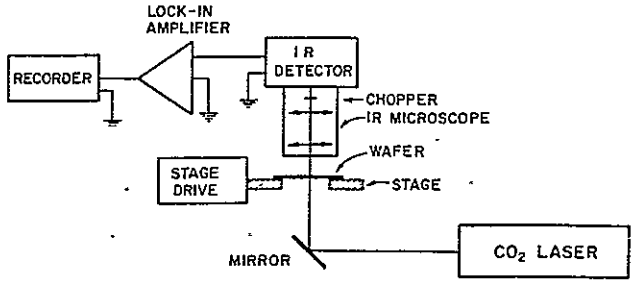

Fig. 5. Experimental arrangements for scanning absorption measurements.

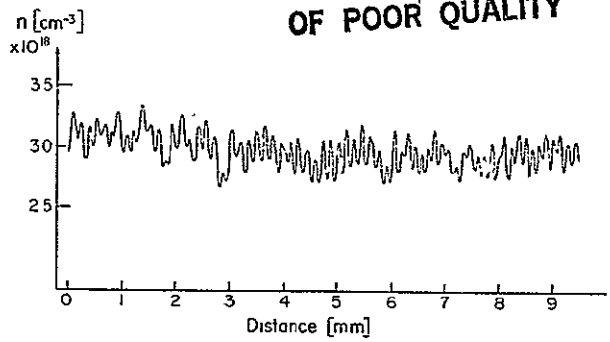

Fig. 6. Carrier concentration fluctuation along the growth direction in Czochralski-grown n-type Si.

tration 2×10^{18} cm^{-3}) employing both methods. To carry out spreading resistance measurements (one-point probe) a uniform ohmic back contact was made to the sample with an indium layer and a scan was performed at 10 μm intervals; the ohmic contact was lapped off and the sample polished; subsequently, scanning *IR* absorption measurements were carried out 50 μm from either side of the spreading resistance scan. The results are shown in Fig. 7. It is seen that the results obtained by the two methods are in very good qualitative agreement. The observed differences such as changes in the shape and position of carrier concentration maxima are attributed to the fact that the scans are 50 μm apart and, thus, reflect radial variations in carrier concentration. In addition, the volume probed by the two methods is somewhat different; thus, in spreading resistance measurements the volume probed is semispherical with a diameter of about 20 μm in the immediate vicinity of the pressure contact, whereas in *IR* absorption the volume probed is cylindrical with a diameter of about 15 μm and a length equal to the sample thickness.

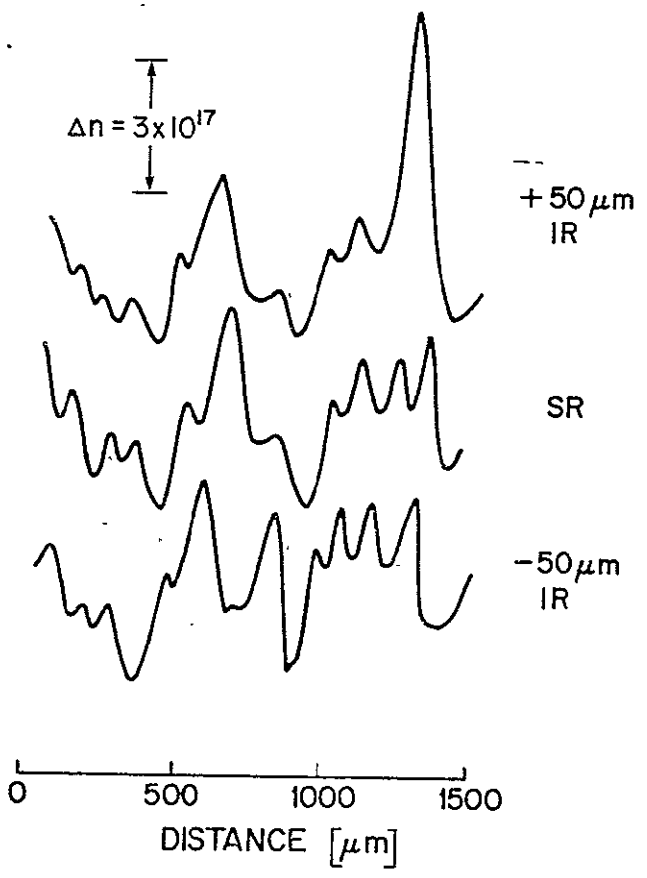

Fig. 7. Comparison of carrier concentration fluctuations in n-type Czochralski-grown Si (average concentration 3×10^{18} cm^{-3}) by spreading resistance measurements (SR) and by scanning absorption, 50 μm from either side of the spreading resistance scan.

Summary and Conclusions

Infrared absorption by free carriers was employed for the quantitative determination of the carrier concentration on the microscale in n and p Si. Employing radiation with a wavelength of 10 μm, the method was found to be applicable to concentrations ranging from 10^{16} to 10^{19} cm^{-3} with a sensitivity of about 5×10^{14} cm^{-3} and a spatial resolution of about 15 μm.

Carrier concentration profiles obtained with this method and with spreading resistance measurements were found to be in very good agreement. Thus, scanning *IR* absorption provides a fast, sensitive, contactless, and reliable method for the determination of carrier concentration on a microscale in Si over a wide range of carrier concentrations. The application of this method for obtaining carrier concentration profiles in compound semiconductors is currently being studied.

Acknowledgment

The authors are indebted to the National Aeronautics and Space Administration for financial support, to Mr. M. Lichensteiger for carrying out the spreading resistance measurements, and to Mr. C. J. Herman for his competent assistance with the experimental arrangement.

Manuscript submitted June 19, 1978; revised manuscript received Aug. 21, 1978.

Any discussion of this paper will appear in a Discussion Section to be published in the December 1979 JOURNAL. All discussions for the December 1979 Discussion Section should be submitted by Aug. 1, 1979.

Publication costs of this article were assisted by the Massachusetts Institute of Technology.

REFERENCES

1. H. F. Matare, *Solid State Technol.*, **20**, 56 (1977).
2. A. J. R. deKock, S. D. Ferris, L. C. Kimerling, and H. J. Leamy, *Appl. Phys. Lett.*, **27**, 313 (1975).
3. R. Sittig and W. Zimmerman, *Phys. Status Solidi A*, **12**, 663 (1972).
4. H. C. Casey, Jr., *This Journal*, **114**, 153 (1967).
5. F. E. Roberts, *Solid-State Electron.*, **1**, 93 (1960).
6. B. Sherman and J. F. Black, *Appl. Opt.*, **9**, 802 (1970).
7. See for example, J. R. Ehrstein, in "Semiconductor Silicon 1977," H. R. Huff and E. Sirtl, Editors, p. 327, The Electrochemical Society Softbound Symposium Series, Princeton, N.J. (1977).
8. H. Y. Fan, "Semiconductor and Semimetals," Vol. 3, Chap. 9, Academic Press, New York (1967).
9. P. A. Schumann, Jr., W. A. Keenan, A. H. Tong, H. H. Gegenworth, and C. P. Schneider, *This Journal*, **118**, 145 (1971).
10. H. Y. Fan and M. Becker, "Semiconductor Materials," Proc. Conf. Univ. Reading 1950, H. K. Henisch, Editor, p. 132, Academic Press, New York (1951).
11. W. Spitzer and H. Fan, *Phys. Rev.*, **108**, 268 (1966).
12. V. Vavilov, *Sov. Phys.-Solid State (Engl. Transl)*, **2**, 340 (1960).
13. Y. Ukhanov, *ibid.*, **4**, 2010 (1963).
14. H. Hara and Y. Nishi, *J. Phys. Soc. Jpn.*, **21**, 1222 (1966).
15. H. F. Wolf, in "Silicon Semiconductor Data," p. 117, Pergamon Press, New York (1969).
16. See for example, A. Murgai. H. C. Gatos, and A. F. Witt, in "Semiconductor Silicon 1977," H. R. Huff and E. Sirtl, Editors, p. 72, The Electrochemical Society Softbound Symposium Series, Princeton, N.J. (1977).

Liquid-phase electroepitaxy: Growth kinetics

L. Jastrzebski, J. Lagowski,[a] H. C. Gatos, and A. F. Witt

Department of Materials Science and Engineering, Massachusetts Institute of Technology, Cambridge, Massachusetts 02139

(Received 27 March 1978; accepted for publication 6 June 1978)

On the basis of mass-transport principles, a theoretical model of electroepitaxial growth—current-controlled liquid-phase epitaxy—was developed which defines the contribution of the Peltier effect (at the solid-solution interface) and that of solute electromigration to the overall growth process. According to the model, the contribution of electromigration to growth is dominant in the absence of convection in the solution, whereas the contribution of the Peltier effect can be dominant in the presence of convection. On the basis of the model, expressions were derived which relate quantitatively the growth velocity to growth parameters. The model was found to be in excellent agreement with extensive experimental data on the electroepitaxial growth of GaAs from a Ga-As solution.

PACS numbers: 68.55.+b, 81.10.Dn, 68.45.−v, 61.50.Cj

INTRODUCTION

The electronic-device structures of GaAs and of all other III-V compounds are based totally on epitaxial layers grown on bulk single-crystal substrates. For most types of devices, epitaxial layers are presently grown from liquid solutions. In liquid-phase epitaxy (LPE) the substrate (e.g., GaAs) is thermally equilibrated with the solution [e.g., Ga(rich)-As solution] and growth takes place upon supersaturation of the solution brought about by a temperature decrease.

While LPE has been highly developed in recent years, precise control of the microscopic growth velocity (and thus control of segregation and defect structure) is still a problem. It has been recognized for many years that control of the growth velocity and of segregation could be achieved through passage of electric current across the growth interface since it induces Peltier cooling (or heating) in the immediate vicinity of the interface[1,2] and also causes electromigration of the solute to the growth interface.[3–8] Although approaches to the growth of bulk single crystal from the melt have been proposed,[1,2,4] they have not been reduced to practice because of convective instabilities in the melt and other complexities introduced by Joule heating.[7]

Current-controlled growth has been successfully carried out in recent years[9] in an LPE configuration where Joule heating presents no significant difficulties because the dimensions of the substrate and the solution are relatively small. Electroepitaxial layers were first obtained using the InSb system[9]; growth was initiated and sustained by passing electric current through the substrate-solution interface while the temperature of the overall growth system was maintained constant. Electroepitaxy has since been employed for the growth of GaAs,[10–17] InP,[18] GaAlAs,[19–23] and garnet layers.[24]

Electroepitaxy is still in the early stages of development. However, its advantages in achieving controlled doping,[10,11,13,14] improved surface morphology and defect structure,[16,17] improved electronic structures,[20,13] and in studying growth and segregation[14] have already been demonstrated.

Attempts to explain the electroepitaxial process have been, thus far, qualitative in nature and limited in scope. It was originally proposed[9] that Peltier cooling at the growth interface was responsible for supersaturation and electroepitaxial growth. Subsequently, it was demonstrated that under certain conditions electromigration constitutes the dominant contribution to supersaturation,[12] while in other studies it was shown that Peltier cooling dominates electroepitaxy.[21]

In the present study a comprehensive theoretical model of electroepitaxy is developed which relates, on a quantitative basis, the contribution of Peltier cooling and electromigration to the growth kinetics; the model also relates quantitatively the growth velocity to growth parameters and it is successfully used for the analysis of extensive experimental results. In part II of this investigation a theoretical model of segregation in electroepitaxy will be developed.

PROCESS AND PHENOMENA

The process

Electroepitaxy utilizes the standard LPE configuration modified to permit passage of electric current through the solution-substrate interface.[15] A schematic representation of a typical growth cell is shown schematically in Fig. 1. After

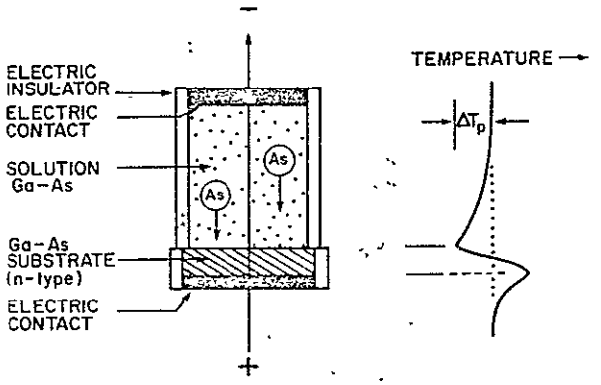

FIG. 1. Schematic representation of growth cell used for electroepitaxial growth of GaAs from Ga-As solution and of the temperature profile resulting from Peltier cooling at the substrate-solution interface and from Peltier heating at the substrate-electric contact interface.

[a]On leave from the Institute of Physics, Polish Academy of Sciences, Warsaw, Poland

 0021-8979/78/4912-5909$01.10

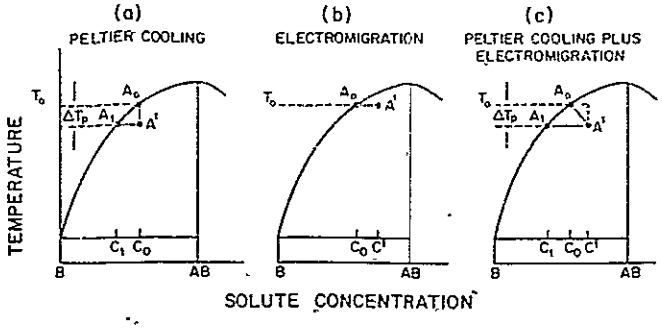

FIG 2. Schematic representation of the pertinent part of the phase diagram of an A^{III}-B^{V} system and transition involved in electroepitaxial growth.

thermal equilibration, growth is initiated and sustained by passing electric current through the substrate-solution interface in the appropriate direction (see below), while the overall temperature of the system is maintained constant.

Peltier cooling

The substrate and solution, being different electrical conductors, have different thermoelectric coefficients. Thus, flow of electric current across their interface is accompanied by absorption of heat or evolution of heat, depending on the current direction. The magnitude of this heat, Q, is proportional to the difference in Peltier coefficients, π_p, and the current density J: $Q=\pi_p J$. For $A^{III}B^{V}$ semiconductor compounds and the temperature range used in electroepitaxy, Q is of the order of 1 W/cm^2 at a current density of about 10 A/cm^2. In an equilibrated isothermal LPE system the absorption of this heat decreases the interface temperature by ΔT_p, which is typically of the order of 0.1 or 1 °C and, thus, induces supersaturation leading to epitaxial growth.

Using the pertinent part of a schematic-phase diagram of the compound $A^{III}B^{V}$ [Fig. 2(a)], Peltier-induced LPE can be illustrated by the vertical transition $A_0 \rightarrow A^1$, i.e., supercooling, and the subsequent horizontal transition $A^1 \rightarrow A_1$, which leads to precipitation (solidification of compound $A^{III}B^{V}$). Using temperature-composition coordinates (T,C), the process can be expressed as $(T_0,C_0) \rightarrow (T_0-\Delta T_p,C_0) \rightarrow (T_0-\Delta T_p,C_1)$. Accordingly, in the following treatment of growth induced by Peltier cooling, the supersaturation C_1-C_0 will be approximated as

$$C_1-C_0 = \Delta T_p \left.\frac{\partial C}{\partial T}\right|_L^{T_0}, \qquad (1)$$

where L designates liquidus.

Electromigration

The solutions of elements from groups III-V used in electroepitaxy are metallic conductors; essentially they exhibit no ionic contribution to the current. However, in these solutions, as in other liquid metals, electromigration takes place due to electron-momentum exchange and/or electrostatic field forces.[8] Under the electric field E induced by the current flow, species in solution migrate with a velocity $v=\mu E$, where μ is the mobility.

In Ga-As solutions, electromigration of As species is anode directed; thus, when the substrate has a positive polarity, the solution becomes supersaturated with As at the substrate-solution interface leading to epitaxial growth.[25] As shown schematically in Fig. 2(b), electromigration causes (in a thermally equilibrated solution) transition $A_0 \rightarrow A^1$, i.e., supersaturation, which in turn leads to transition $A^1 \rightarrow A_0$, i.e., precipitation (solidification) of GaAs; in T,C coordinates, these transitions can be expressed as $(T_0,C_0) \rightarrow (T_0,C_0+\Delta C^1) \rightarrow (T_0,C_0)$.

Simultaneous Peltier cooling and electromigration

When both Peltier cooling and electromigration are significant, the following transitions are involved in the growth process [Fig. 2(c)]: the diagonal supersaturation transition $A_0 \rightarrow A^1$, i.e., $(T_0,C_0) \rightarrow (T_0-\Delta T_p,C_0+\Delta C^1)$ and the horizontal precipitation (solidification) transition $A^1 \rightarrow A_1$, i.e., $(T_0-\Delta T_p,C_0+\Delta C^1) \rightarrow (T_0-\Delta T_p,C_1)$.

In treating the solidification (precipitation) transitions as strictly isothermal, it must be assumed that the contribution of the heat of solidification is negligible. This assumption is justified for the commonly encountered rates of solidification in LPE which are of the order of 1 μm/min.

MODEL OF ELECTROEPITAXY

Growth kinetics

In the model of electroepitaxy presented in this paper it is assumed, as in LPE,[26,27] that the solute transported to the advancing growth interface is removed from the solution only through epitaxial growth on the substrate. Transport of solute due to temperature gradients in the solution is neglected but solute transport due to convective flow in the solution is taken into consideration. In certain approximations and in calculations used in the present treatment, electroepitaxy of GaAs from Ga-As solutions is used as a specific case.

The widely adopted isothermal diffusion treatment of LPE[26,27] is here extended to include solute transport by electromigration which is controlled by the mobility μ of the migrating solute and the electric field E in the solution: thus,

$$D\frac{\partial^2 C}{\partial x^2} - v\frac{\partial C}{\partial x} - \mu E\frac{\partial C}{\partial x} = \frac{\partial C}{\partial t}, \qquad (2)$$

where D is the diffusion coefficient of the solute in the solution, C is the solute concentration, x is the distance from the advancing growth interface, v is the growth velocity, and t is the time. (The sign of the electromigration term $\mu E\,\partial C/\partial x$ is determined by the direction of the current flow.)

The following boundary conditions are considered applicable in the present case (the notation is as in Fig. 2; the concentration in the solid is C_s and the thickness of the solute boundary layer is δ).

$$D\left.\frac{\partial C}{\partial x}\right|_0 - \mu E C_1 = v(C_1 - C_s), \qquad (2a)$$

at $t=0$, $C=C_0$ for all x, (2b)

at $t>0$, $C=C_0$ for $x=\infty$ (absence of convection), (2c)

or

at $t>0$; $C=C_0$ for $x>\delta$ (presence of convection), (2d)

at $t>0$ and $x=0$, $C=C_1$ (growth follows the liquidus line). (2e)

In solving the transport equation (2), the term $v(\partial C/\partial x)$ is neglected as being very small compared with the diffusion and the electromigration terms; for example, in electroepitaxy of GaAs, μE is usually one order of magnitude greater than v; in addition, it is assumed that the concentration of the solute for either $x=\infty$ or $x=\delta$ remains constant during growth; this assumption is considered valid when feed material (on top of the solution) is present or when the thickness of the grown layer is very small; in the latter case the maximum time of growth is limited and in common LPE is of the order of h^2/D, where h is the height of the solution.[28]

The procedure for solving Eq. (2) is presented in Appendix A. The expressions obtained for the growth velocity of electroepitaxy are given below:

In the absence of convection ($\delta=\infty$):

$$v=\frac{\Delta T_p}{C_s-C_1}\frac{dC}{dT}\bigg|_L\left(\frac{D}{\pi t}\right)^{1/2}\times\frac{\exp[-(\mu Et)^2/4Dt]}{\operatorname{erfc}[-\mu Et/2(Dt)^{1/2}]}-\mu E\frac{C_1}{C_s-C_1}, \quad (3)$$

in the presence of convection (finite boundary layer thickness)

$$v=\frac{\Delta T_p}{C_s-C_1}\frac{dC}{dT}\bigg|_L\left(\frac{D}{\pi t}\right)^{1/2}\times\frac{\exp[-(\mu Et)^2/4Dt]}{\operatorname{erfc}[-\mu Et/2(Dt)^{1/2}]-\operatorname{erfc}[(\delta-\mu Et)/2(Dt)^{1/2}]}-\mu E\frac{C_1}{C_s-C_1}, \quad (4)$$

where ΔT_p is the temperature decrease at the interface due to Peltier cooling.

Equations (3) and (4) can be rewritten in a simplified general form where the contribution to the growth velocity by the temperature decrease at the interface (Peltier cooling) and by electromigration are designated as v_T and v_E, respectively:

$$v=v_T f_k(E,\delta,t)+v_E, \quad (5)$$

where

$$v_T=\frac{\Delta T_p}{C_s-C_1}\frac{dC}{dT}\bigg|_L\left(\frac{D}{\pi t}\right)^{1/2}, \quad (6a)$$

$$v_E=\mu E\frac{C_1}{C_s-C_1}; \quad (6b)$$

in the absence of convection:

$$f_k\equiv f_1(E,t)=\frac{\exp[-(\mu Et)^2/4Dt]}{\operatorname{erfc}[-\mu Et/2(Dt)^{1/2}]}; \quad (6c)$$

and in the presence of convection

$$f_k\equiv f_2(E,\delta,t)=\frac{\exp[-(\mu Et)^2/4Dt]}{\operatorname{erfc}[-\mu Et/2(Dt)^{1/2}]-\operatorname{erfc}[(\delta-\mu Et)/2(Dt)^{1/2}]}. \quad (6d)$$

Note that for $\delta\to\infty$, $f_2(E,\delta,t)\to f_1(E,t)$.

The asymptotic behavior of f is as follows:

$$f_1(E,t)\simeq\tfrac{1}{2}(\pi t/D)^{1/2}\mu E \quad \text{for } \mu E(t)^{1/2}\ll 2(D)^{1/2}, \quad (7a)$$

$$f_1(E,t)\simeq 1 \text{ for } \mu E(t)^{1/2}\ll 2(D)^{1/2}, \quad (7b)$$

$$f_2(E,t,\delta)\simeq(\pi Dt)^{1/2}/\delta \text{ for } \delta^2/4D\ll t\ll 4D/\mu^2E^2. \quad (7c)$$

It is of interest to point out that in view of the above asymptotic behavior of f, Eqs. (3) and (4) derived here, reduce for $E\to 0$ and $\Delta T_p\equiv\Delta T$ to the standard expressions for diffusion-controlled growth[26,27]:

$$v=\frac{\Delta T}{C_s-C_1}\frac{dC}{dT}\bigg|_L\left(\frac{D}{\pi t}\right)^{1/2}, \quad (8a)$$

$$v=\frac{\Delta T}{C_s-C_1}\frac{dC}{dT}\bigg|_L\frac{D}{\delta}. \quad (8b)$$

Absence of convection

In electroepitaxy from nonmetallic solutions—e.g., electroepitaxial growth of garnets[24]—the electric field can be of the order of V/cm so that after a time period of a few seconds the inequality $\mu E(t)^{1/2}\gg 2(D)^{1/2}$ is satisfied. Accordingly, approximation (7a) is valid and the time dependence of v in Eq. (5) cancels out through v_T [Eq. (6b)] and $f(E,t)$; thus, Eq. (3) reduces to

$$v=\frac{\mu E}{C_s-C_1}\left(\frac{\Delta T_p}{2}\frac{dC}{dT}\bigg|_L+C_1\right). \quad (9)$$

In such a case, electroepitaxy proceeds at a constant growth velocity for a constant current density; actually, the growth velocity can be proportional to J^2, since both E and ΔT_p are proportional to J; diffusion plays no role in the growth process.

On the other hand, in metallic-type Ga-As solutions a typical value of μE for 10 A/cm^2 is of the order of 10^{-5} cm/sec [12,29] and the diffusion constant of As (at 800 °C) is about 6×10^{-5} cm^2/sec[30]; thus, for time periods less than about 10 h ($t\ll 2\times10^6$ sec) approximation (7b) is valid. Accordingly, Eq. (5) reduces to

$$v=v_T+v_E,$$

i.e.,

$$v=\frac{\Delta T_p}{C_s-C_1}\frac{dC}{dT}\bigg|_L\left(\frac{D}{\pi t}\right)^{1/2}+\mu E\frac{C_1}{C_s-C_1}. \quad (10)$$

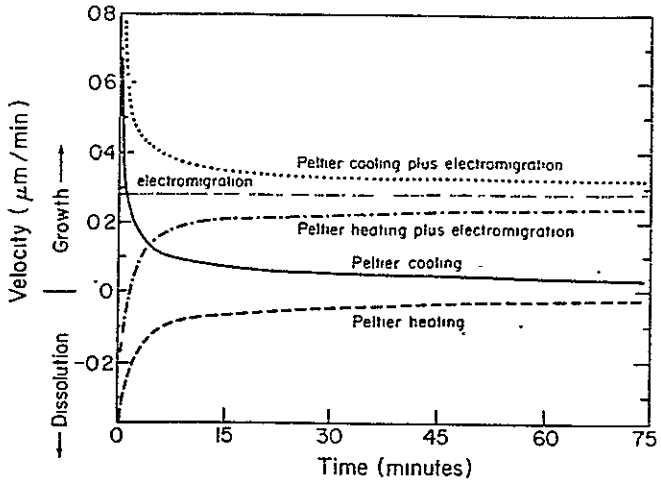

FIG. 3. Growth (or dissolution) velocity transients of GaAs calculated from Eq. (10) from a Ga-As solution taking $T_0=800$ °C, $D=6\times10^{-5}$ cm²/sec, $\mu E=10^{-5}$ cm/sec, and $\Delta T_p=-3$ °C for Peltier cooling and $\Delta T_p=+3$ °C for Peltier heating at the substrate-solution interface. The contribution of the Peltier effect and of electromigration to the overall growth (or dissolution) are indicated.

The first term in Eq. (10) represents the contribution of the Peltier effect, whereas the second term represents the contribution of electromigration to the growth velocity; both terms depend linearly on the current density, through ΔT_p and E, respectively. The relative contribution of these terms to electroepitaxy of GaAs from a Ga-As solution at 800 °C is shown in Fig. 3; a ΔT_p value of -3 °C is assumed and μE is taken equal to 10^{-5} cm/sec for a current density of 10 A/cm². It is seen that after 1 h of growth the contribution of Peltier cooling to the growth rate reduces to about 15%; it is also seen that even in the presence of Peltier heating at the interface, electroepitaxial growth does take place, i.e., the contribution of electromigration to growth dominates over dissolution of the substrate due to Peltier heating.

On the basis of the present model the salient features of electroepitaxial growth in the absence of convection can be summarized as follows: (a) In an isothermal substrate-solution system electroepitaxial growth can be initiated and sustained through solute electromigration to the interface; the contribution of Peltier cooling at the interface to growth is relatively small. (b) In metallic-type solutions, as in those of $A^{III}B^{V}$ compounds, the growth velocity is proportional to the current density since the electric field in the solution and the Peltier cooling are proportional to the current density (Eq. 10). (c) The contribution of the Peltier effect to the growth velocity decreases with time as $1/(t)^{1/2}$, which is a typical behavior of diffusion-controlled processes; the contribution of solute electromigration to the growth velocity is time independent. (d) The temperature dependence of the growth velocity is primarily dictated by the phase diagram of the system (e.g., Fig. 2). The Peltier-effect contribution is also enhanced to some extent by temperature through D. The dependence of π_p and μ on temperature is relatively weak.

Presence of convection

Convection in the solution leads to the formation of a solute boundary layer of thickness δ. Approximation (7c) is readily satisfied after a few minutes of growth; accordingly, Eq. (3) reduces to

$$v=\frac{\Delta T_p}{C_s-C_l}\frac{dC}{dT}\bigg|_L\frac{D}{\delta}+\mu E\frac{C_l}{C_s-C_l}. \tag{11}$$

The presence of a boundary layer significantly increases the contribution of the Peltier effect to electroepitaxial growth, as illustrated in Fig. 4(a), where the growth velocity,

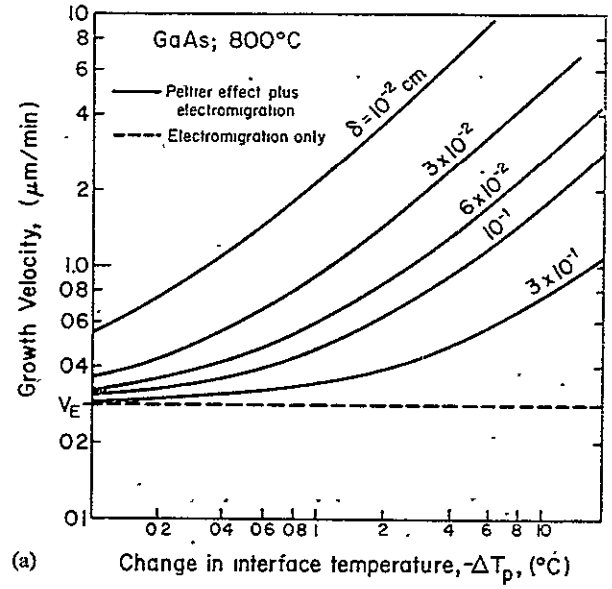

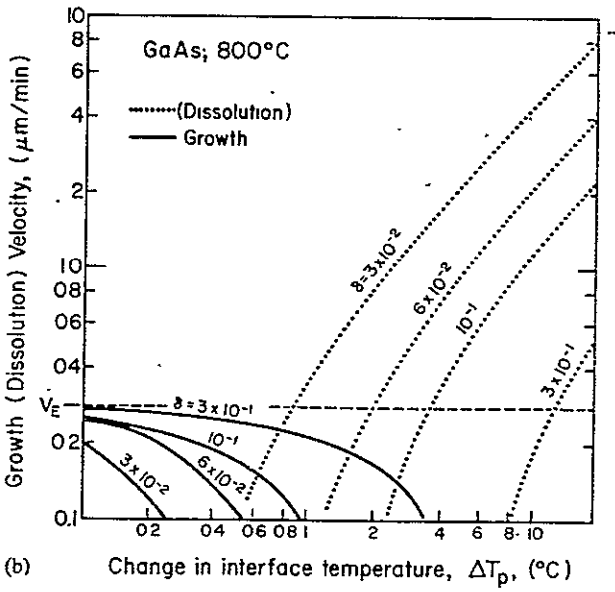

FIG. 4(a). Growth velocity of GaAs from a Ga-As solution calculated from Eq. (11) for various values of the solute-boundary layer δ, taking $T_0=800$ °C, $D=6\times10^{-5}$ cm²/sec, and $\mu E=10^{-5}$ cm/sec. Peltier cooling results when an n-type substrate has positive polarity; v_E is the contribution of electromigration to growth velocity. (b) Growth velocity (solid curves) or dissolution velocity (dashed curves) of GaAs calculated from Eq. (11) for different values of boundary-layer thickness δ, as a function of Peltier heating (p-type substrate with positive polarity) taking T_0, D, and μE as in (a). v_E is the contribution of electromigration to the growth velocity.

as calculated from Eq. (11), is plotted as a function of $-\Delta T_p$ (Peltier cooling) for various values of δ. The parameters used in these calculations are the same as those used for Fig. 3, i.e., they correspond to GaAs growth from a Ga-As solution at 800 °C under 10 A/cm^2. The contribution of electromigration (which is independent of ΔT_p) to the growth velocity is about 0.3 μm/min (as in Fig. 3). For a given (small) value of δ the growth velocity increases rapidly with increasing Peltier cooling (ΔT_p) at the interface, and for a given amount of Peltier cooling the rate increases rapidly with decreasing δ (increasing convective flow). However, for large values of δ ($> 10^{-1}$ cm) and ΔT_p values of the order of -0.1 °C, the growth rate is controlled by electromigration.

In Fig. 4(b) the growth (or dissolution) velocity calculated from Eq. (11) [as in Fig. 4(a)] is plotted as a function of Peltier heating for various values of δ. It is seen that growth does take place for relatively small amounts of Peltier heating and/or large values of δ. Dissolution of the substrate is pronounced for small values of δ and particularly as ΔT_p exceeds about 0.15 °C.

Thus, in the presence of convection the salient features of electroepitaxial growth are the following: (a) The contribution of the Peltier effect can dominate that of electromigration, particularly for small values of δ and larger values of T_p. (b) After a period of growth $t \gg \delta^2/4D$, the growth is independent of time. (c) The dependence of the growth velocity on temperature is as outlined in the absence of convection.

Maximum thickness of epitaxial layer

When no feed material is used in the growth system, electroepitaxial growth proceeds up to a certain thickness and then stops due to the gradual depletion of the solute in the solution. The maximum thickness of the epitaxial layers, Z_{max}, is related to fundamental growth parameters; since it can be readily measured experimentally, it contitutes an important means for the characterization of the growth process.

The amount of solute incorporated in the epitaxial layer represents the decrease of solute concentration in the solution; it is, thus, apparent that

$$Z_{max} C_s = C_0 h - \int_0^h C(x)\, dx, \tag{12}$$

where $x=0$ at the growing interface, h is the height of the solution, and $C(x)$ is the solute concentration in the solution when the growth process stops; it is assumed that $Z_{max} \ll h$.

Electroepitaxial growth stops when the net solute flow in the solution equals zero; thus, Eq. (1) reduces to a steady-state expression

$$D \frac{dC}{dx} - \mu E C = 0. \tag{13}$$

the boundary conditions are

$C = C_1$, for $x = 0$ (at the interface),

$C = C_d$, for $x > \delta$.

The value of C_d is obtained from Eq. (11) taking $v = 0$:

$$C_d = C_1 - (\mu E/D)\delta C_1. \tag{14}$$

Thus, the solution of Eq. (13) becomes

$$C(x) - C_1 = (C_1 - C_d) \times \frac{\exp(\mu E x/D) - 1}{1 - \exp(\mu E \delta/D)},$$

for $x \leqslant \delta$ (15)

and $C(x) = C_d$, for $x \geqslant \delta$

For GaAs, $h\mu E/D \ll 1$, for $h < 1$ cm. Thus, for solution heights not significantly more than 1 cm, Eq. (15) reduces to

$$C(x) - C_1 = (C_d - C_1)(x/\delta) \quad \text{for } x \leqslant \delta \tag{16}$$

and

$C(s) = C_d$, for $x \geqslant \delta$.

From Eqs. (12), (14), and (16), Z_{max} is readily obtained: thus, for $\delta = h$ (absence of convection)

$$Z_{max} \simeq \frac{C_0 - C_1}{C_s} h + \frac{\mu E C_1}{2D C_s} h^2, \tag{17a}$$

and for $\delta \ll h$ (presence of convection)

$$Z_{max} \simeq \frac{C_0 - C_1}{C_s} h + \frac{\mu E C_1}{D C_s} \delta \left(h - \frac{\delta}{2}\right). \tag{17b}$$

It is apparent that in Eqs. (17a) and (17b) the first term represents the contribution of the Peltier effect and the second term the contribution of electromigration.

In Fig. 5 the Z_{max} values obtained from Eq. (17b) are plotted as a function of $-\Delta T_p$ for various values of δ. The calculations were carried out for GaAs growth from a Ga-As solution at 800 °C, for $h = 1$ cm, $\mu E = 10^{-5}$ cm/sec, and $D = 6 \times 10^{-5}$ cm^2/sec (C_0 and C_1 values are taken from the GaAs phase diagram).[32] Here again, for small values of

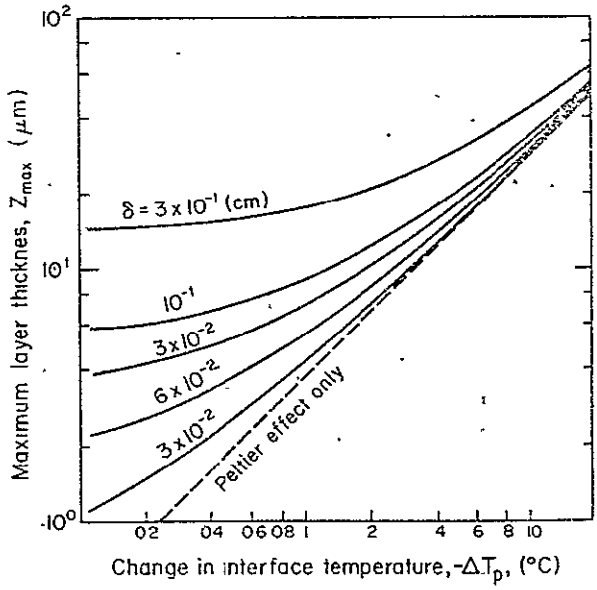

FIG. 5. Maximum layer thickness of GaAs grown from a Ga-As solution calculated from Eq. (17b) as a function of Peltier cooling at the growth interface for various values of solute-boundary-layer thickness δ, taking T, D, and μE as in Fig. 4(a)

Peltier cooling and large values of δ (absence of appreciable convection), the contribution of the Peltier effect to the maximum thickness of the epitaxial layer is very small; the contribution of the Peltier effect becomes dominant in the presence of convection (small value of δ).

Criteria for the contribution of Peltier cooling and of electromigration: critical Peltier cooling and critical substrate thickness

According to the model developed and discussed above, there are two effects operating in electroepitaxy, Peltier cooling at the growth interface and electromigration of solute species to the interface (or solution species away from the interface). The relative contribution of these effects depends on the experimental conditions.

On the basis of the present model, quantitative criteria can be established for the determination of the relative contribution of the Peltier effect and electromigration to electroepitaxy.

It is convenient to introduce a critical value of temperature decrease at the interface, ΔT_c, for which the contribution of the Peltier effect and electromigration to the growth velocity are equal; i.e., considering Eq. (5)

$$|v_T f_k| = |v_E|. \tag{18}$$

On the basis of Eqs. (6a) and (6b)

$$\Delta T_c = \frac{\mu E C_1}{f_k} \frac{dT}{dc}\bigg|_L \left(\frac{\pi t}{D}\right)^{1/2}. \tag{19a}$$

In the presence of convection and for $t \gg \delta^2/D$, Eq. (19a) reduces to

$$\Delta T_c = \mu E C_1 \frac{dT}{dC}\bigg|_L \frac{\delta}{D} \tag{19b}$$

Thus, for small amounts of Peltier cooling, $\Delta T_p \ll \Delta T_c$, electromigration dominates, whereas, for large amounts of cooling, $\Delta T_p \gg \Delta T_c$, the Peltier effect dominates the growth process.

Considering a typical configuration for epitaxial growth, as shown in Fig. 1, Peltier cooling at the substrate-solution interface is accompanied by Peltier heating at the substrate-electrical (back) contact interface. Thus, heat transport across the substrate affects the amount of cooling at the growth interface; indeed ΔT_p at the growth interface increases with increasing substrate thickness.[33]

For most practical cases, ΔT_p can be approximated as follows:

$$\Delta T_p \simeq J \pi_p d/2\kappa, \tag{20}$$

where J is the current density, π_p is the differential Peltier coefficient, and κ is the thermal conductivity of the substrate (see also Appendix B). On the basis of Eq. (20) and taking into account the fact that in the solution $E/J = \rho$ (where ρ is the resistivity of the solution), then Eq. (17a) can be rewritten to define a critical substrate thickness d_c for which the contributions of the Peltier effect and electromigration to the growth velocity are equal:

$$d_c = \frac{2\mu\rho\kappa C_1}{\pi_p f_1} \frac{dT}{dC}\bigg|_L \left(\frac{\pi t}{D}\right)^{1/2}. \tag{21a}$$

In the presence of convection Eq. (21a) reduces to

$$d_c = \frac{2\mu\rho\kappa C_1}{\pi_p} \frac{dT}{dC}\bigg|_L \frac{\delta}{D}, \tag{21b}$$

where for $d > d_c$ the Peltier effect dominates and for $d < d_c$ electromigration dominates the growth process.

Thus, with thick substrates and in the presence of significant convective flow, electroepitaxial growth is dominated by Peltier cooling; on the other hand, with thin substrates and in the absence of significant convective flow, electromigration dominates electroepitaxial growth.

APPLICATION OF THEORY TO EXPERIMENT

Electroepitaxial-growth experiments were carried out from Ga-As solutions in a standard LPE apparatus modified to permit passage of electric current through the solution-substrate interface as described elsewhere.[15] Semi-insulating (Cr doped), n and p type substrates (with a room-temperature free-carrier concentration of about 2×10^{15} /cm^3) were used; their thickness ranged from 250 to 1500 μm.

In the thermally equilibrated growth cell, upon passage of current, Joule heating introduced horizontal thermal gradients (as discussed in detail elsewhere[15]) and the electroepitaxial growth velocity was found to depend on the solution height; this behavior is typical for the presence of convection in the solution. The effects of Joule heating were compensated by modifying the the thermal configuration of the growth system; as the horizontal gradients were drastically reduced it was found that the electroepitaxial-growth velocity was essentially independent of the solution height, indicating the absence of convective interference. The present model will be applied to the analysis of the experimental results ob-

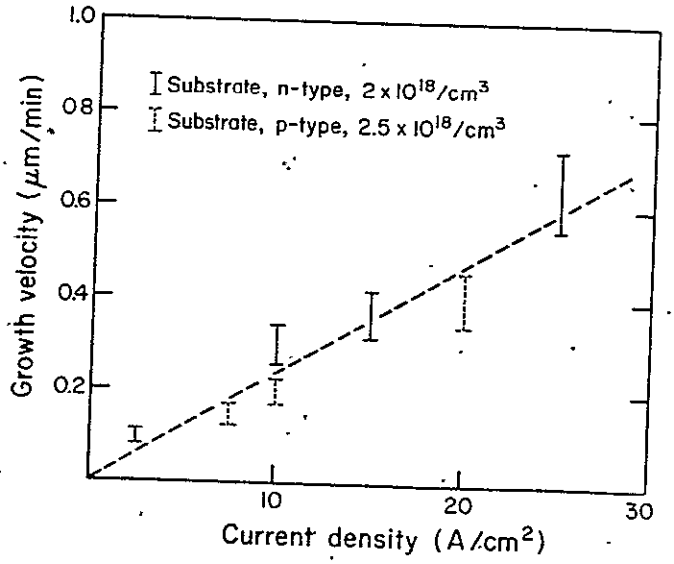

FIG. 6 Growth velocity of GaAs from Ga-As solutions at 800 °C as a function of current density; substrate thickness was 300 μm.

tained both in the absence and in the presence of convective interference

Absence of convection

The magnitude of the temperature change in the vicinity of the interface induced by the Peltier effect was determined by positioning a thermocouple near the substrate-solution interface (0.3 mm from the interface). It was found that for a given current polarity and at a current density of 10 A/cm² the temperature change ranged from −0.3 to 0.5 °C, depending on the thickness and conductivity type of the substrate (see Appendix B). Approximate calculations show that under the present experimental conditions $\Delta T_p < \Delta T_c$, where ΔT_c is given in Eq. (19a). Thus, electroepitaxial growth in this case is expected to be dominated by electromigration.

Typical experimental results are shown in Fig. 6, where the electroepitaxial-growth velocity (as determined by interface demarcation[23]) on substrates with a starting thickness of 300 μm is plotted against current density; the polarity of both the n- and p-type substrate was positive. It is seen that the growth velocity on the p-type substrates (Peltier heating at the interface) is only somewhat smaller than on n-type substrates (Peltier cooling at the interface). Actually these results indicate a Peltier-effect contribution to the growth velocity not exceeding about 15%, which is comparable in magnitude to the experimental error associated with the determination of the growth velocity.

The linear relationship between the growth velocity and current density in Fig. 6 is consistent with the present theory, e.g., Eq. (6b), since E is proportional to J. Taking $C_l(C_s - C_l)$ at 800 °C $\simeq 4.5\times10^{-2}$ [32] and using Eq. (6b) a value of 1.3×10^{-5} cm/sec is obtained for the electromigration velocity of As species, μE, at 10 A/cm²; this value is in agreement with those reported earlier,[12,29]

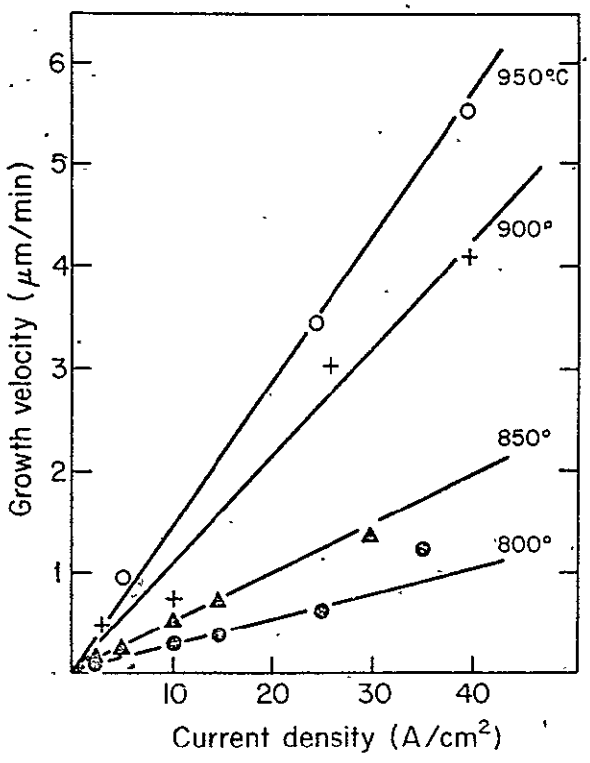

FIG. 7. Electroepitaxial-growth velocity of GaAs from Ga-As solutions as a function of current density; substrates were n-type 2×10^{18}/cm³ and 300 μm thick.

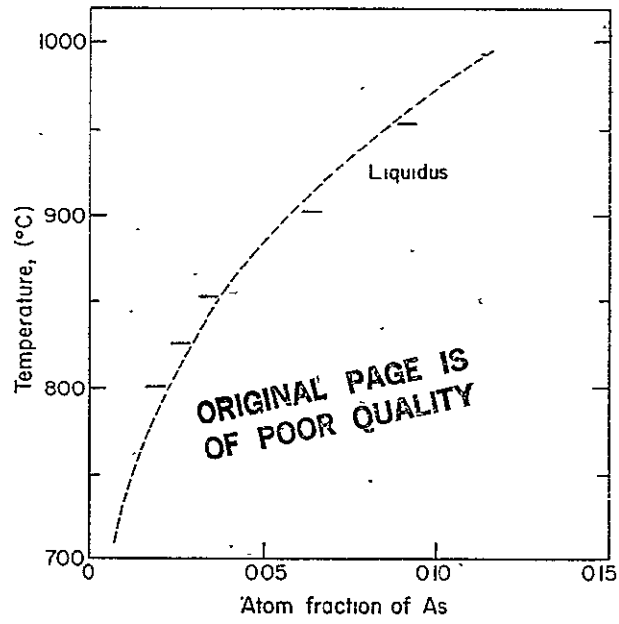

FIG. 8. Atom fraction of As in Ga-As solutions calculated from the results of Fig. 7 and Eq. (6b). Dashed line is the Ga-As liquidus (Ref. 32).

Typical results of experiments carried out at various temperatures as a function of current density with 350-μm-thick n-type substrates ($n = 2\times10^{18}$/cm³) are shown in Fig. 7. It is seen that, consistent with the present model, the growth velocity is linearly dependent on current density for all temperatures and that, for a given current density, the growth velocity increases with temperature.

From the growth-velocity data of Fig. 7 and Eq. (6b), the values of the As concentrations C_l (at the growth interface) were calculated at the various temperatures. These values are plotted in Fig. 8, together with those obtained directly from the Ga-As diagram[32] (liquidus line). It is seen that the experimental results as reduced through Eq. (6b) are in good agreement with the Ga-As phase diagram. Thus, within experimental error, electroepitaxial growth takes place under nearly equilibrium conditions.

Maximum thickness of epitaxial layer

The maximum thickness of electroepitaxial GaAs layers was determined for a solution height h ranging from 0.3 to 1.2 cm at 800 °C using n-type substrates ($n = 2\times10^{18}$/cm³) 300 μm thick. The time necessary for achieving Z_{max} ranged from 1 to 5 h. The results are shown in Fig. 9, where Z_{max}/h is plotted against h. The observed linear relationship is in agreement with Eq. (17a) of the present theoretical treatment.

From the slope $d(Z_{max}h^{-1})/dh$ (Fig. 8) the value of $\mu E/D$ at 10 A/cm² is found to be 0.22 cm⁻¹. Since

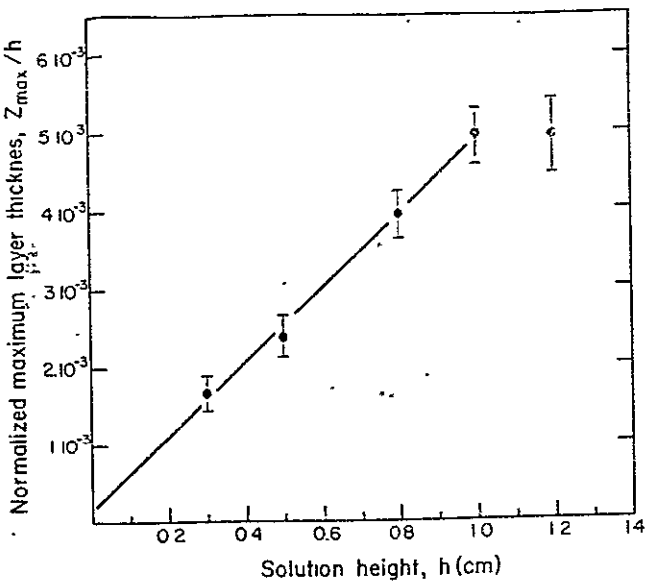

FIG. 9. Normalized maximum GaAs layer thickness as a function of solution height. Experiments carried out at 800 °C, substrates were n type 2×10^{18}/cm³, 300 μm thick (see text)

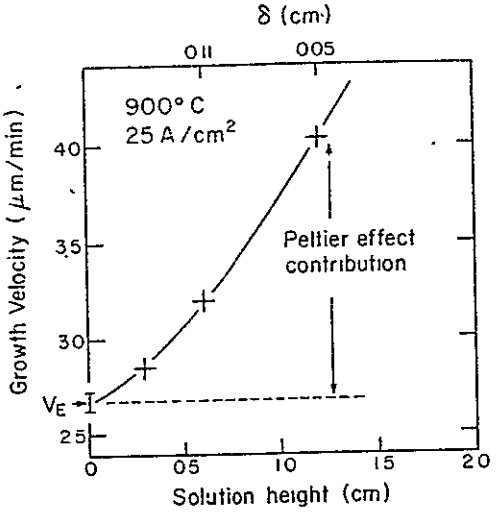

FIG. 10 Growth velocity of GaAs from a Ga-As solution (900 °C, 25 A/cm²) as a function of solution height. Substrates were Cr doped and 300 μm thick v_E represents the contribution of electromigration to the growth velocity. Estimated values of the solute-boundary-layer thickness δ are indicated.

$\mu E = 1.3\times10^{-5}$/sec (as determined above), the value of the diffusion constant is found to be $D = 6\times10^{-5}$ cm/sec. This value determined on the basis of the present electroepitaxial model is in good agreement with the diffusion constant of As in an equilibrated Ga-As solution at 800 °C reported in the literature.[30]

Presence of convection

Assuming that no thermal gradients are present in the growth cell prior to electroepitaxy, they can be introduced by passage of electric current causing convection in the solution. Thus, horizontal thermal gradients are introduced from Joule heating at the asymmetrically located current electrodes[15]; vertical thermal gradients can result from Joule heating at the substrate; finally horizontal and vertical thermal gradients can be introduced at the interface by the Peltier effect.

According to the present model of electroepitaxial growth, the contribution of electromigration to the growth velocity [second term in Eq. (11)] is independent of convective flow; however, the contribution of the Peltier effect does depend on the presence of convection [first term in Eq. (11)] since the solute boundary layer thickness δ is a function of the convective flow in the solution.

Electroepitaxial growth of GaAs has been carried out under conditions leading to pronounced convection[15] employing Cr-doped substrates with a thickness of 300 μm and a current density of 25 A/cm² at 900 °C. The current-induced temperature decrease at the growth interface ΔT_p was 1.8 °C. Under these conditions the growth velocity was found to be dependent on convective flow[15]; the results are shown in Fig. 10. For very small values of solution height convection becomes negligible and the growth velocity approaches the theoretical limit corresponding to the growth velocity v_E due to electromigration alone. The value of v_E indicated in Fig. 10 was calculated for the present condition from Eq. (10), taking $\mu E \approx 3.2\times10^{-5}$ cm/sec for 25 A/cm² (since μE for 10 A/cm² was determined to be 1.3×10^{-5} cm/sec). Equation (11) can be rewritten as

$$\delta = \frac{D}{v_T}\frac{\Delta T_p}{C_s - C_l}\left.\frac{dC}{dT}\right|_L^{T_0} \qquad (22)$$

Thus, knowing v_T and ΔT_p the solute-boundary thickness can be estimated. Values of δ, estimated from Eq. (22) for the results shown in Fig. 10. are indicated in the figure.

Thus, the growth behavior presented in Fig. 10 demonstrates, in excellent agreement with Eq. (11), the enhancement of the Peltier-effect contribution to the growth velocity by convection.

The contribution of the Peltier effect to the growth velocity shown in Fig. 10 (for 300-μm-thick substrates) increases with increasing substrate thickness. According to Eq. (21b), when the thickness of the substrate exceeds a critical thickness d_c, the contribution of the Peltier effect to the growth velocity becomes greater than that of electromigration. Consequently, electroepitaxial growth can take place, while electromigration of solute proceeds away from the growth interface, i.e., when a negative substrate polarity and a thick p-type substrate (Peltier cooling) are used (opposite to that illustrated in Fig. 1). Accordingly, the behavior encountered in Ref. 21 where growth does take place on thick (2 mm) p-type substrates with negative polarity (opposite to that required for solute electromigration towards the substrate) can now be readily explained.

SUMMARY AND CONCLUSIONS

The model of electroepitaxial growth presented here relates quantitatively the growth behavior to Peltier cooling

and electromigration in terms of fundamental growth parameters. The validity of the model was tested with experimental results on electroepitaxial growth of GaAs from Ga-As solutions. According to the model, in the absence of convection in the solution, the growth velocity is controlled by electromigration and the contribution of the Peltier effect is negligible. The dependence of the growth velocity on time, current density, and temperature, and the dependence of the maximum thickness of the epitaxial layer on the solution height, given by the model under such conditions, were found to be in quantitative agreement with experimental results obtained in the absence of appreciable convection. In addition, the values of the diffusion coefficient of As in Ga-As solutions, of the electromigration velocity, and of the equilibrium concentrations of As in Ga-As solutions as a function of temperature, calculated from the experimental results on the basis of the model, were found to be in good agreement with the reported values obtained by other means.

The contribution of the Peltier effect to the growth rate, according to the model, can become dominant in the presence of convection and is a function of the thickness of the solute-boundary layer. In agreement with the model, the growth velocity of GaAs in the presence of convection was found to increase with solution height (in the presence of thermal gradients convective flow increases and, thus, δ decreases with increasing solution height). At very small values of solution height the growth velocity approached a value which was equal to that calculated from the model taking into account electromigration alone. Thus, on the basis of the model it is possible to determine the relative contributions of the Peltier effect and of electromigration to the growth velocity. It is also possible to estimate the thickness of the boundary layer. In addition to the influence of the boundary-layer thickness on the contribution of the Peltier effect to the growth velocity, the model predicts that the Peltier-effect contribution becomes dominant for thick substrates, consistent with experimental results.

Electroepitaxy controlled by electromigration (i.e., using relatively thin substrates in the absence of appreciable convective flow) takes place under essentially isothermal conditions. As expected, under such conditions, epitaxial layers exhibit improved surface morphology and decreased defect density, and should lead to improved device structures.

ACKNOWLEDGMENTS

The authors are grateful to the National Science Foundation and the National Aeronautics and Space Administration for financial support.

APPENDIX A: SOLUTION OF EQ. (2)

The solution of Eq. (2) for $C(x,t)$ with boundary conditions (2a)–(2c) can be obtained as a superposition of solution $C(\zeta,t)$, corresponding to the case where all the diffusing solute is initially contained in a plane at a distance ζ from plane

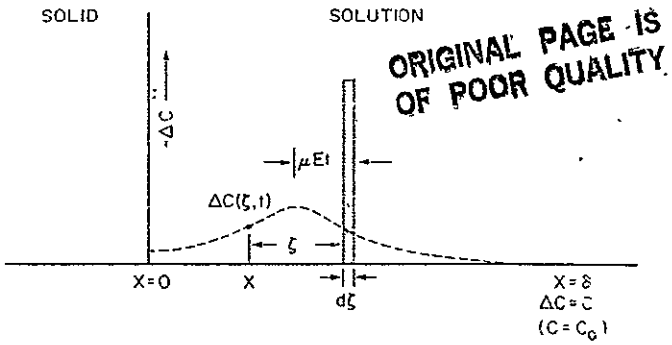

FIG. 11. Schematic representation of the change in solute distribution by diffusion and by the presence of an electric field; the solute was originally confined in plane $d\zeta$ (see text)

x[24] (Fig. 11):

$$C=\frac{A}{t^{1/2}}\exp\left(-\frac{(x-\mu Et)^2}{2(Dt)^{1/2}}\right), \tag{A1}$$

where A is an arbitrary constant.

Accordingly, $C(\zeta,t)$ can be expressed as

$$C(\zeta,t)=\frac{A}{t^{1/2}}\exp\left(-\frac{(\zeta-\mu Et)^2}{2(Dt)^{1/2}}\right) \tag{A2}$$

and, thus, $C(x,t)$ can be obtained as

$$C(x,t)-C_0=A(t)\int_x^\infty C(\zeta,t)\,d\zeta+B(t). \tag{A3}$$

Substituting in Eq. (A3) $C(\zeta,t)$ from Eq. (A2), one obtains

$$C(x,t)-C_0=A'(t)\operatorname{erfc}\left(\frac{x-\mu Et}{2(Dt)^{1/2}}\right)+B'(t), \tag{A4}$$

where erf is

$$\operatorname{erf} z\equiv(2/\pi^{1/2})\int_0^z\exp(-y^2\,dy),\ \operatorname{erfc} z\equiv 1-\operatorname{erf} z. \tag{A5}$$

From Eq. (A4) and boundary conditions (2d) and (2e),

$$A'(t)=\frac{C_1-C_0}{\operatorname{erf}[(\delta-\mu Et)/2(Dt)^{1/2}]-\operatorname{erf}[-\mu Et/2(Dt)^{1/2}]}, \tag{A6a}$$

$$B'(t)=-A'(t)\operatorname{erfc}[(\delta-\mu Et)/2(Dt)^{1/2}], \tag{A6b}$$

and thus, Eq. (A4) can be rewritten as

$$\frac{C(x,t)-C_0}{C_1-C_0}=\frac{\operatorname{erf}[(\delta-\mu Et)/2(Dt)^{1/2}]-\operatorname{erf}[(x-\mu Et)/2(Dt)^{1/2}]}{\operatorname{erf}[(\delta-\mu Et)/2(Dt)^{1/2}]-\operatorname{erf}[-\mu Et/2(Dt)^{1/2}]}, \tag{A7}$$

and $C(x,t)=C_0$ for $x>\delta$.

By differentiating Eq. (A7) and taking into account that $\operatorname{erfc} z\equiv 1-\operatorname{erf} z$, one obtains

$$\left.\frac{\partial C}{\partial x}\right|_{x=0}=-\frac{C_0-C_1}{(Dt\pi)^{1/2}}$$

$$\times \frac{\exp[-(\mu Et)^2/4Dt]}{\operatorname{erfc}[-\mu Et/2(Dt)^{1/2}] - \operatorname{erfc}[(\delta-\mu Et)/2(Dt)^{1/2}]} \tag{A8}$$

By substituting Eq. (A8) into Eq (A2) and considering that $\operatorname{erfc}\infty = 0$, the expression for the growth velocity is obtained: for $\delta = \infty$ (absence of convection)

$$v = \frac{C_0 - C_l}{C_s - C_l}\left(\frac{D}{\pi t}\right)^{1/2} \frac{\exp[-(\mu Et)^2/4Dt]}{\operatorname{erfc}[-\mu Et/2(Dt)^{1/2}]} - \mu E \frac{C_l}{C_s - C_l}, \tag{A9}$$

and for finite δ (presence of convection)

$$v = \frac{C_0 - C_l}{C_s - C_l}\left(\frac{D}{\pi t}\right)^{1/2} \times \frac{\exp[-(\mu Et)^2/4Dt]}{\operatorname{erfc}[-\mu Et/2(Dt)^{1/2}] - \operatorname{erfc}[(\delta-\mu Et)/2(Dt)^{1/2}]} - \mu E \frac{C_l}{C_s - C_l}. \tag{A10}$$

Equations (3) and (4) can be obtained from Eqs. (A9) and (A10), respectively, taking into account that

$$C_0 - C_l = \left.\frac{dC}{dT}\right|_L^{T_0} \Delta T_p. \tag{A11}$$

APPENDIX B: PELTIER EFFECT AT (GaAs-GaAs) solution interface

As pointed out in this paper, knowledge of the temperature change ΔT_p at the interface, due to the Peltier effect, is essential for assessing the prevailing conditions in electroepitaxial growth. For this reason, the experimental determination of ΔT_p was undertaken for the GaAs system as a function of the type of conduction and carrier concentration in the substrate, thickness of the substrate, and current density.

A standard electroepitaxy apparatus was employed for the measurements. A thermocouple was positioned in the solution about 0.3 mm from the substrate-solution interface. Measurements were carried out with p- and n-type substrates with carrier concentrations from about 10^{16} to $10^{19}/\text{cm}^3$, thickness ranging from 250 to 1500 μm, and under current densities up to 40 A/cm^2 at temperatures of 800 and 900 °C.

The temperature changes ΔT_p were measured by applying dc. The contribution of Joulè heating was determined by applying an equivalent amount of ac power. In most instances, Joule heating of the substrate was negligible in comparison with the Peltier effect, except when the substrates were semi-insulating (Cr doped), and their thickness exceeded 500 μm.

The results are shown in Figs. 12–14. In Fig. 12 ΔT_p is plotted against current density for n-type substrate material of varying thickness; ΔT_p is directly proportional to the cur-

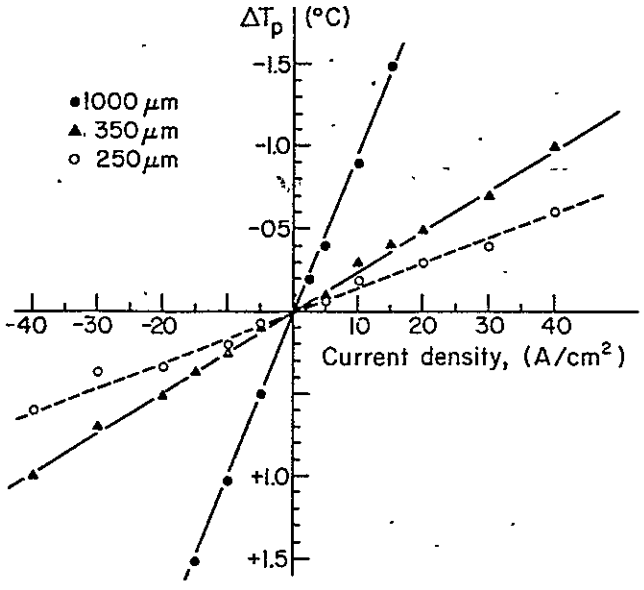

FIG. 12 Changes in temperature at the GaAs-solution interface due to the Peltier effect as a function of current density at 800 °C– substrates were n type $2\times10^{18}/\text{cm}^3$.

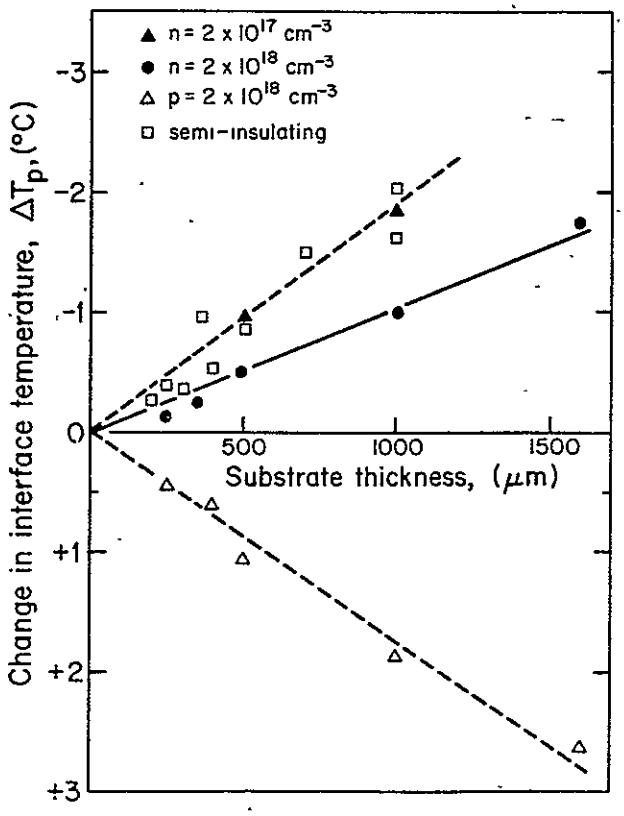

FIG. 13 Changes in temperature at the GaAs-solution interface due to the Peltier effect as a function of substrate thickness of 800 °C under 10 A/cm^2. Substrates were 300 μm thick.

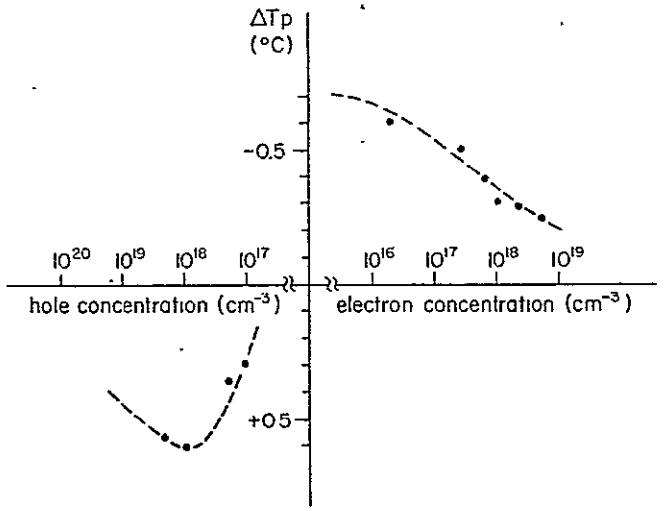

FIG. 14 Changes in temperature at the GaAs-solution interface due to the Peltier effect (800 °C, 10 A/cm²) as a function of substrate-carrier concentration. Substrates were 300 μm thick.

rent density and is negative for positive substrate polarity; for a given current density $|\Delta T_p|$ increases with increasing substrate thickness.

In Fig. 13 the values of ΔT are given as functions of substrate thickness. The polarity of all substrates is positive; note that for the p-type substrates (having an opposite Peltier coefficient to that of the n-type substrates), ΔT_p is positive. It is seen that $|\Delta T_p|$ exhibits approximately linear dependence on substrate thickness [see Eq. (20)]. Similar dependence of ΔT_p on current density and thickness as that in Figs. 12 and 13 has been reported earlier for n-type GaAs material[33]; differences in the absolute values of ΔT_p in the two studies are probably due to differences in the the thermocouple location and/or differences in heat dissipation from the interface.

The values of ΔT_p as a function of carrier concentration are given in Fig. 14 for 300-μm-thick substrates and a current density of 10 A/cm². It should be noted that the dependence seen in Fig. 14 is in qualitative agreement with the expected behavior of the GaAs Peltier coefficient.[35]

Values of ΔT measured at 900 °C were, within 20%, the same as those in Figs. 12–14. Thus, ΔT_p in GaAs electroepitaxy can be estimated for a given carrier concentration, substrate thickness, and current density from Figs. 12–14 and reasonable extrapolations.

[1] A. F. Joffe, Zh. Tekh. Fiz. 26, 478 (1956).
[2] W. G. Pfann, K. E. Benson, and J. H. Wernick, J. Electron. 2, 597 (1957).
[3] J. C. Angus, C. V. Ragone, and E. E. Hucke, Metall. Soc. Conf. (Proc.) 8, 833 (1961).
[4] W. G. Pfann and R. S. Wagner, Trans. Metall. Soc. AIME 224, 1139 (1962).
[5] D. T. J. Hurle, J. B. Mullin, and E. R. Pike Philos. Mag. 9, 423 (1964).
[6] R. S. Wagner, C. E. Miller, and H. Brown, Trans. Metall. Soc. AIME 236, 554 (1966).
[7] J. D. Verhoeven, Trans. Metall. Soc. AIME 239, 694 (1967).
[8] For a review, see J. N. Pratt and R. G. R. Sellors, *Electrotransport in Metals* (Trans. Tech. SA, Riehen, Switzerland, 1973).
[9] M. Kumagawa, A. F. Witt, M. Lichtensteiger, and H. C. Gatos, J. Electrochem. Soc. 120, 583, (1973).
[10] D. J. Lawrence and L. F. Eastman, J. Cryst. Growth. 30, 267 (1975).
[11] D. J. Lawrence and L. F. Eastman, J. Electron. Mater. 6, 1 (1976).
[12] L. Jastrzebski, H. C. Gatos, and A. F. Witt, J. Electrochem. Soc. 123 1121 (1976).
[13] L. Jastrzebski and H. C. Gatos, Inst. Phys. Conf. Ser. B 33, 88 (1976).
[14] L. Jastrzebski and H. C. Gatos, J. Cryst. Growth 42, 309 (1977).
[15] L. Jastrzebski, Y. Imamura, and H. C. Gatos, J. Electrochem. Soc. 125, 1140 (1978).
[16] Y. Imamura, L. Jastrzebski, and H. C. Gatos, J. Electrochem. Soc. 125, 1561 (1978).
[17] Y. Imamura, L. Jastrzebski, and H. C. Gatos (unpublished).
[18] A. Abdul-Fadl and E. K. Stefanakos, J. Cryst. Growth 39, 341 (1977).
[19] J. J. Daniele, Appl. Phys. Lett. 27, 373 (1975).
[20] J. J. Daniele, D. A. Cammack, and P. M. Asbeck, J. Appl. Phys. 48, 914 (1977).
[21] J. J. Daniele, J. Electrochem. Soc. 124, 1143 (1977).
[22] J. J. Daniele, 5th Int. Conf. on Crystal Growth, Boston (1977) (unpublished).
[23] J. J. Daniele and C. Michel, Inst. Phys. Conf. Ser. 24, 155 (1974).
[24] L. Jastrzebski, H. C. Gatos, and A. F. Witt, J. Electrochem. Soc. 124, 633 (1977).
[25] For a Ga-As solution with a height of 1 cm at 800 °C concentration in the vicinity of the susbtrate under 10 A/cm² is estimated from Ref. 4 to be $\Delta C/C_0 \simeq 10\%$, assuming no growth takes place.
[26] M. B. Small and J. F. Barnes, J. Cryst. Growth 5, 9 (1969).
[27] D. L. Rode, J. Cryst. Growth 20, 13 (1973).
[28] R. L. Moon and J. Kinoshita, J. Cryst. Growth 21, 149 (1974).
[29] R. P. Gale, Ph. D. thesis (MIT, 1978) (unpublished).
[30] Recently reported values of D at 800 °C are 7×10^{-5} (Ref. 31) 4 1×10^{-5} cm²/sec (Ref. 27).
[31] M. Mihara, N. Togoda, and T. Hara, Appl. Phys. Lett. 27, 131 (1975).
[32] R. N. Hall, J. Electrochem. Soc. 110, 385 (1963); C. D. Thurmond, J. Phys. Chem. Solids 26, 785 (1965).
[33] E. K. Stefanakos, A. Abdul-Fadl, and M. D. Workman, J. Appl. Phys. 46, 3002 (1975).
[34] J. Crank, *Mathematics of Diffusion* (Oxford U. P. New York, 1955).
[35] R. J. Stirn, in *Semiconductors and Semimetals*, edited by R. K. Willardson and A. C. Beer (Academic, New York, 1972), vol. 8, Chap. 1.

MINORITY CARRIER MOBILITY IN p-TYPE GaAs

W. Walukiewicz,[a] J. Lagowski,[a] L. Jastrzebski,[b] and H. C. Gatos
Department of Materials Science and Engineering
Massachusetts Institute of Technology
Cambridge, Massachusetts 02139

Abstract

Theoretical calculations of electron mobility in p-type GaAs were carried out taking into consideration the screening effects and all major scattering processes. Calculated values of mobility are presented as a function of carrier concentration, compensation ratio and temperature. The basic differences between minority carrier mobility in p-type GaAs and electron mobility in n-type GaAs are pointed out. A practical procedure is also presented for the evaluation of minority carrier mobility from available electron-mobility data.

---

[a] On leave from Institute of Physics, Polish Academy of Sciences, Warsaw Poland.

[b] Present address: RCA Laboratories, Princeton, New Jersey 08540.

Journal of Applied Physics, in press.

Although minority carrier mobility is recognized as a key electronic parameter for device application, theoretical treatments of minority carrier mobility in GaAs and related compounds have thus far been very limited.[1] As a result, it has been a common practice to assume that the electron mobility in p-type GaAs is equal to the electron mobility in n-type GaAs with the same free carrier concentration.[1-3] Such practice ignores the presence of additional scattering centers (heavy holes) in p-type material.[4] Furthermore, it neglects differences in screening effects and electron statistics in n-type and p-type material.

The present mobility calculations utilize the variational method[5,6] of solving the Boltzmann equation without involving the relaxation time approximation. This method has recently been used to evaluate electron mobility in n-type GaAs as a function of carrier concentration and compensation ratio.[7] Comparison of these calculations with experimental values of electron mobility has made possible the determination of the compensation ratio in n-GaAs. It has also been shown[7] that the compensation ratios obtained from mobility measurements are in good agreement with those determined from free carrier absorption measurements. In the present paper the method used in ref. 7 is extended to the calculation of the minority carrier mobility in p-type GaAs. This extension involves some modifications and additional assumptions. First it is assumed that the minority carrier statistics in the conduction band are given by a nondegenerate distribution function described by the crystal lattice temperature. In the case of photoexcited electrons this assumption requires that the electrons become thermalized within the conduction band prior to recombining with holes or being trapped at localized centers. For GaAs, in the temperature range presently considered, this assumption is justified, since the effective relaxation time is few orders of magnitude smaller than the minority carrier lifetime.

In addition to the major scattering mechanisms considered in ref. 7 namely ionized impurity, optical phonon, piezoelectric scattering and acoustical phonon, electron scattering by heavy holes will be taken into account. Because of their large effective mass, heavy holes will be regarded as fixed scattering centers.[8] Thus, the overall concentration of ionized scattering centers is given by $N_i \simeq p_h + N_A^- + N_D^+$, where p_h is the concentration of heavy holes, N_A^- and N_D^+ are the concentrations of ionized acceptors and donors, respectively. Neglecting the contribution from light holes and assuming that the minority carrier concentration is much smaller than p_h one obtains: $p_h + N_A^- \sim N_D^+$ and thus $N_i \simeq 2N_A^-$.

Another modification of the approach of ref. 7 centers about screening effects. For a parabolic heavy hole band, the screening length L_D is given by the following expression:[7]

$$1/L_D^2 = 5.80 \cdot 10^{13} \frac{(m_h/m_o)^{3/2} T^{1/2} F_{-1/2}(\eta_p)}{\varepsilon_o} \qquad (1)$$

where m_h is the heavy hole effective mass, ε_o is the static dielectric constant, $F_n(\eta_p)$ is the n-th order Fermi-Dirac integral, $\eta_p = E_F^{(p)}/k_o T$ is the reduced hole Fermi energy. The reduced screening energy, a, which describes screening of the electron-ionized impurity interaction is given by

$$a = \frac{h^2}{2m_e L_D^2 k_o T} \qquad (2)$$

where m_e is the conduction band electron effective mass. The screening energy of the electron-optical phonon interactions has the following form:[8]

$$a_\infty = a\varepsilon_o/\varepsilon_\infty \qquad (3)$$

where ε_∞ is the high frequency dielectric constant. The screening effects arising from the conduction band electrons and the valence band light holes are negligible as the concentrations of these carriers are much smaller than

the concentration of the heavy holes.

Compensation is included in the present calculations by introducing the compensation ratio, θ_p, defined as $\theta_p = N_D^+/N_A^-$. The hole concentration enters into the calculation through the reduced hole Fermi energy, η_p; the compensation ratio affects the total concentration of ionized impurities as follows:

$$N_i = \frac{2p_h}{1-\theta_p} \qquad (4)$$

The values of GaAs parameters used in ref. 7 have also been adopted in the present case. The hole Fermi energy $E_F^{(p)}$ has been determined from the hole concentration taking the following effective masses[9] for the heavy (m_h) and light holes (m_ℓ): $m_h = 0.54\ m_o$ and $m_\ell = 0.089\ m_o$.

The minority carrier mobility $\mu_e^{(p)}$ as a function of hole concentration is shown in Fig. 1, together with the electron mobility, $\mu_e^{(n)}$, results reported in ref. 7. It is seen that the values for $\mu_e^{(p)}$ are lower than those for $\mu_e^{(n)}$ in n-type material with the same carrier concentration. Furthermore, $\mu_e^{(p)}$ decreases more rapidly with carrier concentration than $\mu_e^{(n)}$. The calculated room temperature mobility ratios $\mu_e^{(p)}/\mu_e^{(n)}$ as a function of carrier concentration is given in Fig. 2. It is seen that for high concentrations this ratio is as low as 0.6, which clearly indicates that the previously reported procedures[1-3] for determining $\mu_e^{(p)}$ from values of $\mu_e^{(n)}$, corresponding to the same free carrier concentration, are not reliable for carrier concentrations exceeding $10^{16}\ cm^{-3}$.

The calculated temperature dependence of $\mu_e^{(p)}$ and $\mu_e^{(n)}$ is given in Fig. 3. For the low concentrations the difference between $\mu_e^{(p)}$ and $\mu_e^{(n)}$ is more significant at low temperatures. This behavior is apparently due to an increased contribution of the electron scattering by heavy holes relative to that by the lattice. For higher carrier concentrations the screening effects become of greater significance and lead to a temperature dependence of $\mu_e^{(p)}$

entirely different from that of $\mu_e^{(n)}$. Actually, for sufficiently low temperatures $\mu_e^{(p)}$ becomes greater than $\mu_e^{(n)}$.

The above behavior of the minority carrier mobility can be understood if one considers the fact that with an increase in the hole concentration, there is: (a) an increase of the total concentration of the scattering centers, and (b) an increase of the heavy hole screening. At room temperature the contribution from (a) is more significant than from (b), and the mobility decreases with increasing concentration. At lower temperatures the mean electron energy in the conduction band becomes much smaller than the screening energy of the valence band holes. Accordingly, screening is strongly enhanced and, consequently, (b) dominates (a). Thus, in contrast to n-type material, in p-type GaAs there is a temperature and hole concentration region in which the electron mobility increases rapidly with decreasing temperature (Fig. 3) and also with increasing carrier concentration.

The effect of compensation on the room-temperature electron mobility in p-type GaAs has been found to be slightly weaker than in n-type material. The computed values of $\mu_e^{(p)}$ with the compensation ratio as a parameter are given in Fig. 1 for hole concentrations ranging from 10^{15}-10^{19}cm^{-3}. A comparison of the present results on $\mu_e^{(p)}$ with those on $\mu_e^{(n)}$ (ref. 7) showed that at room temperature, $\mu_e^{(p)}$ can be approximated with $\mu_e^{(n)}$ as follows:

$$\mu_e^{(p)}(p_h,\theta_p) = \mu_e^{(n)}(n,\theta_n) \qquad (5)$$

taking $n = p_h$ and $\theta_n = (1+\theta_p)/(3-\theta_p)$ where θ_n and θ_p are the compensation ratios in n- and p-type material, respectively. Thus, for example, $\mu_e^{(p)}$ in uncompensated p-type GaAs with a hole concentration p_h is equal to the electron mobility in n-type GaAs with an electron concentration $n = p_h$ and with compensation ratio $\theta_n = 0.33$. This approximation is particularly valid for low carrier concentration material where screening effects are negligible. However, even for the

higher concentrations considered in this study the error associated with this approximation does not exceed 10%.

From a practical point of view it should be noted that the validity of the above procedure is not limited to GaAs. Expression (5) can be applied to any p-type material with GaAs-like energy band structure and scattering properties. For instance, in the case of indium phosphide the electron mobility values reported for n-type material[10,11] can be utilized for obtaining the electron mobility values in p-type material.

In summary, it has been shown that the minority carrier mobility in p-type GaAs is significantly affected by the presence of heavy holes which act as additional scattering centers. The present analysis shows that only at high temperatures and at low carrier concentrations the minority carrier mobility in p-type GaAs equals the electron mobility in n-type material. For higher concentrations the room temperature minority carrier mobility in p-type material can be significantly lower than the electron mobility in n-type material. The minority carrier mobility was found to exhibit an anomalous dependence on temperature and on carrier concentration. A practical procedure was presented which permits the estimation of the minority carrier mobility using available data on electron mobility in n-type material.

ACKNOWLEDGEMENT

The authors are grateful to the National Aeronautics and Space Administration for financial support.

REFERENCES

1. J. Vilims and W. E. Spicer, J. Appl. Phys. 36, 2815 (1965).
2. L. W. Aukerman, M. F. Millea and M. McColl, J. Appl. Phys. 38, 685 (1967).
3. M. Ettenberg, H. Kressel and S. L. Gilbert, J. Appl. Phys. 44, 827 (1973).
4. For early treatments of minority carrier mobility see, for example, T. P. McLean and E. G. S. Paige, J. Phys. Chem. Solids 16, 220 (1960) and references quoted therein.
5. D. Howarth and E. H. Sondheimer, Proc. Phys. Soc. A219, 53 (1953).
6. H. Ehrenreich, J. Appl. Phys. 32, 2155 (1961) and references quoted therein
7. W. Walukiewicz, J. Lagowski, L. Jastrzebski, M. Lichtensteiger and H. C. Gatos, J. Appl. Phys., in press.
8. H. Ehrenreich, J. Phys. Chem. Solids 8, 130 (1959).
9. R. W. Shaw, Phys. Rev. 3, 3283 (1971).
10. D. L. Rode, Phys. Rev. B2, 1012 (1970).
11. W. Walukiewicz, J. Lagowski, L. Jastrzebski, M. Lichtensteiger and H. C. Gatos, to be published.

FIGURE CAPTIONS

Figure 1. Room temperature electron mobility as a function of carrier concentration. Solid curves represent minority carrier mobility in p-type GaAs for different compensation ratios. Dashed curve shows the electron mobility in n-type GaAs.

Figure 2. Ratio of electron mobility in p-type GaAs, $\mu_e^{(p)}$, to the electron mobility in n-type GaAs, $\mu_e^{(n)}$, as a function of free carrier concentration.

Figure 3. Temperature dependence of the electron mobility in p-type (solid curves) and n-type (dashed curves) GaAs for two different carrier concentrations: 10^{16} and $10^{18} cm^{-3}$.

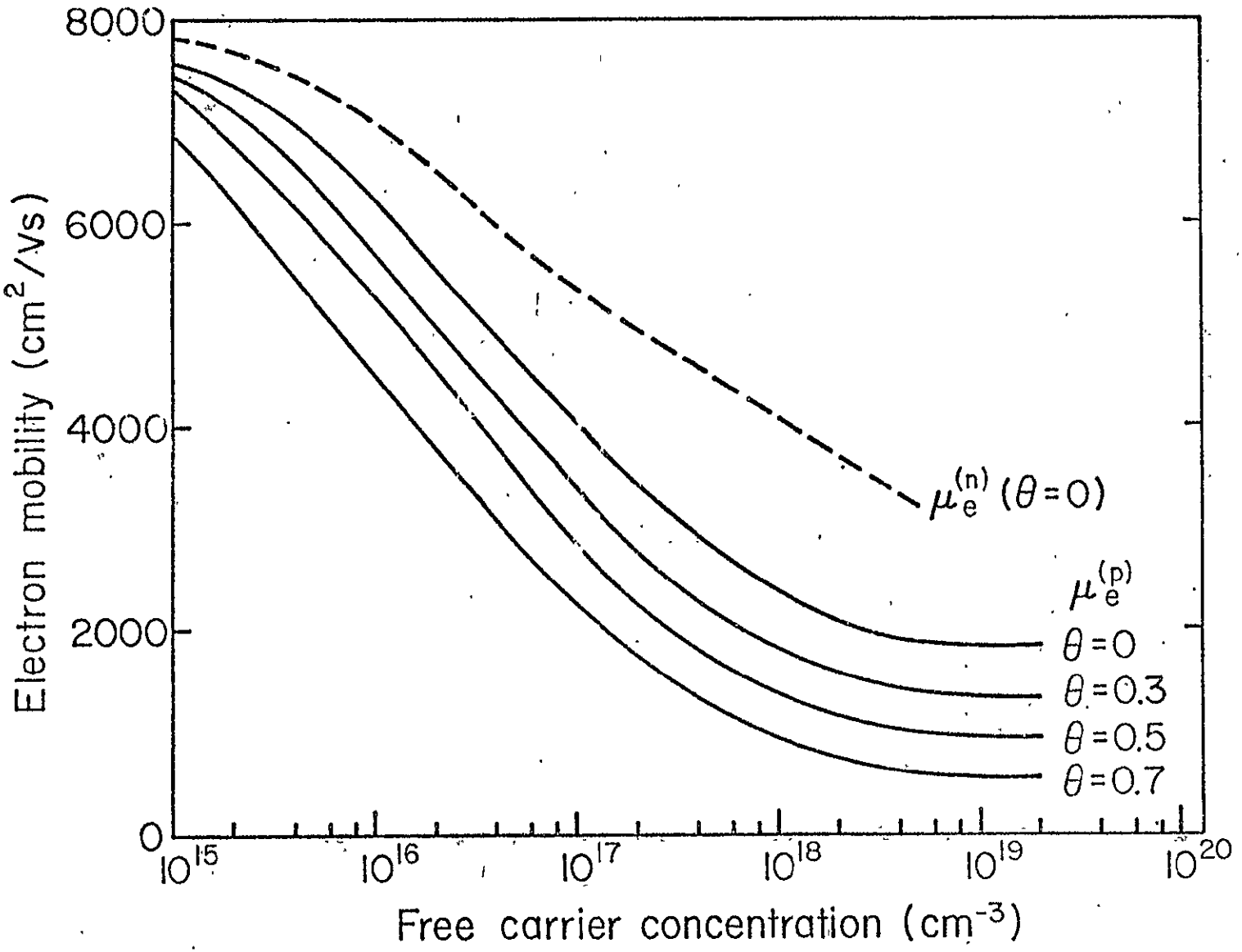
8000
6000
4000
2000
0
Electron mobility (cm²/Vs)
$\mu_e^{(n)}$ (θ=0)
$\mu_e^{(p)}$
θ=0
θ=0.3
θ=0.5
θ=0.7
10^{15}
10^{16}
10^{17}
10^{18}
10^{19}
10^{20}
Free carrier concentration (cm⁻³)

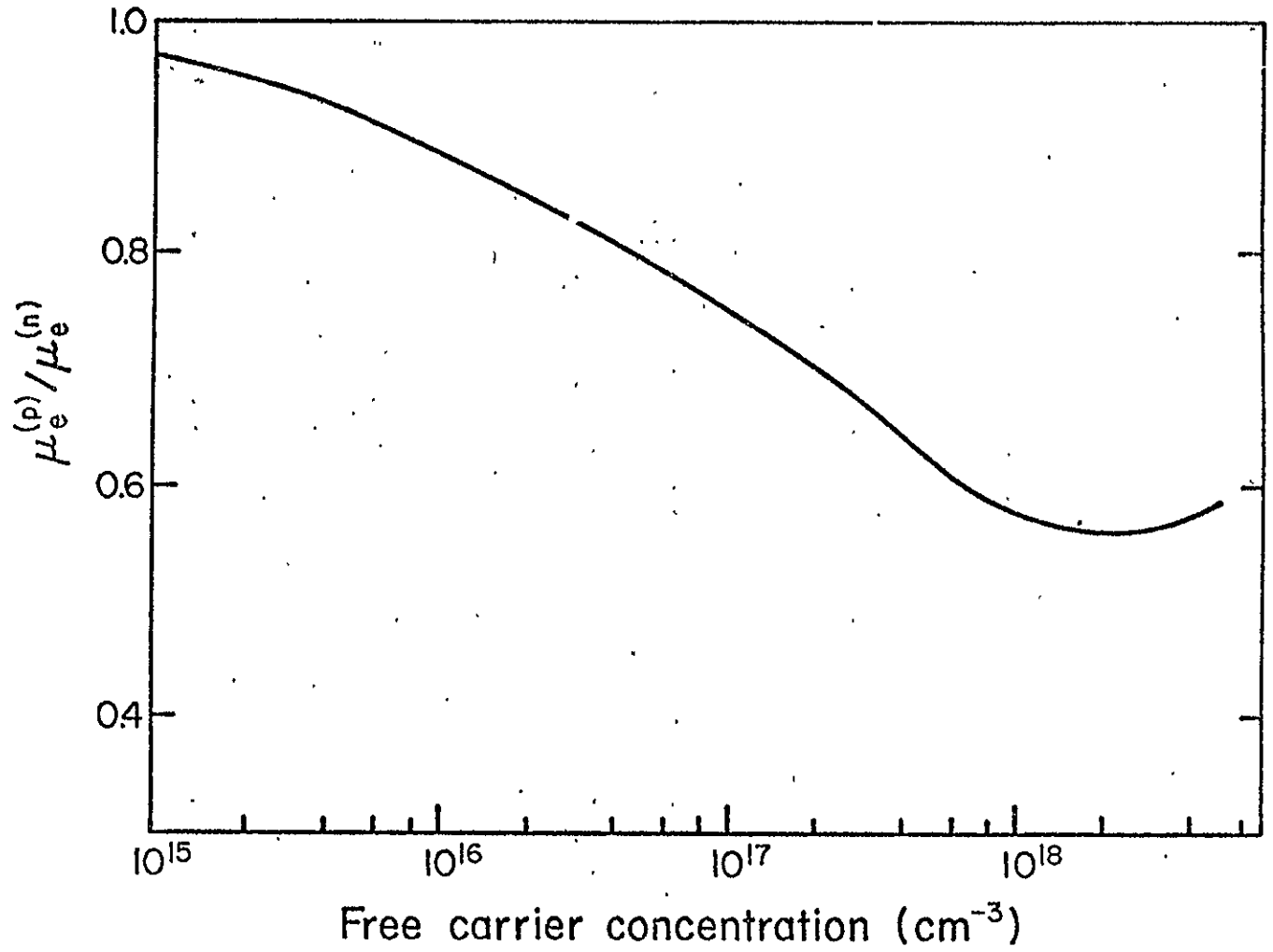
1.0
0.8
0.6
0.4
$\mu_e^{(p)}/\mu_e^{(n)}$
10^{15}
10^{16}
10^{17}
10^{18}
Free carrier concentration (cm^{-3})

Fig 2

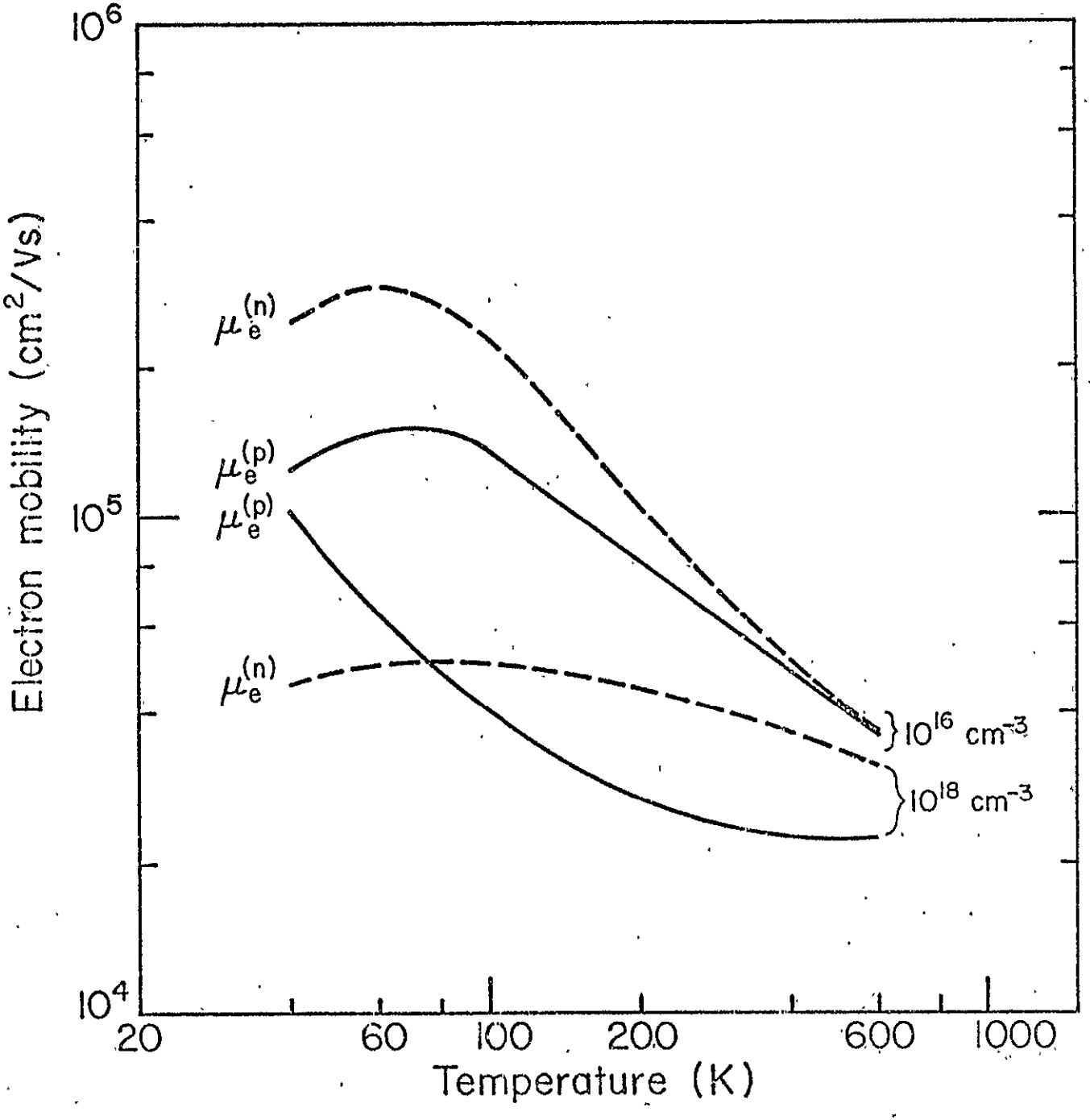
10^6
10^5
10^4
Electron mobility (cm^2/Vs)
$\mu_e^{(n)}$
$\mu_e^{(p)}$
$\mu_e^{(p)}$
$\mu_e^{(n)}$
10^{16} cm^{-3}
10^{18} cm^{-3}
20
60
100
200
600
1000
Temperature (K)

DERIVATIVE SURFACE PHOTOVOLTAGE SPECTROSCOPY; A NEW APPROACH TO THE STUDY OF ABSORPTION IN SEMICONDUCTORS: GaAs

J. Lagowski,* W. Walukiewicz,* M. M. G. Slusarczuk and H. C. Gatos
Department of Materials Science and Engineering
Massachusetts Institute of Technology
Cambridge, Massachusetts 02139

ABSTRACT

Derivative surface photovoltage spectroscopy was achieved with wavelength modulation; it was applied to GaAs and permitted, in a single experiment, the determination of changes in the absorption coefficient over an energy range of 0.5 to 4.3 eV. Photoionization characteristics of deep levels were determined. All known critical point transitions up to 4.3 eV were clearly obtained from second derivative spectra. In addition, previously unresolved transitions were observed at about 2.6 eV. Oscillatory photovoltage in high magnetic fields was observed, and it was used to identify the transitions in the vicinity of the energy gap.

---

*On leave from Institute of Physics, Polish Academy of Sciences, Warsaw, Poland.

Journal of Applied Physics, in press.

This communication reports on the absorption changes in GaAs, over a wide energy range, involving photoionization of deep levels, interface states, transitions in the vicinity of the energy gap and higher energy critical points. Simultaneous determination of these transitions was made possible with a simple experimental approach combining wavelength modulation and surface photovoltage spectroscopy with strikingly enhanced sensitivity through utilization of the MOS structure characteristics.

Surface photovoltage spectroscopy has been employed primarily for surface state studies.(1) Its inherently low sensitivity in all standard experimental configurations does not permit derivative measurements. Wavelength modulation of photovoltaic effects associated with p-n junctions and metal-semiconductor barriers has been reported for indirect gap semiconductors.(2,3) However, p-n junction studies(2) have been limited strictly to the indirect absorption edge. The metal-semiconductor photovoltage spectroscopy has been extended to the vicinity of direct edges.(3) Extension of this approach well above or below the energy gap is not possible because of the high recombination velocity of minority carriers at the metal interface and the appreciable photo-injection of carriers from the metal to the semiconductor. None of the above limitations is encountered in derivative surface photovoltage.

GaAs, n-type, single crystals and epitaxial layers with room temperature carrier concentration 1.0×10^{15} to $3.0 \times 10^{16} cm^{-3}$ and with mobility 6,900 to 3,000 $cm^2/Vsec$ were employed in the present study. The surface photovoltage (illumination-induced change of the surface barrier) was measured with respect to a transparent reference gold electrode, evaporated on an oxide layer (800 to 1000 Å thick) grown anodically(4) on the GaAs. With this insulating layer a sensitivity of 50 nV was achieved in the surface photovoltage measurements

(i.e., 2 to 4 orders of magnitude higher than previously reported) permitting the determination of relative changes in the surface barrier as small as about 10^{-7}.

The illumination system consisted of a quartz halogen light source and a double prism monochromator with a vibrating slit. The illumination intensity and amplitude of the wavelength modulation were experimentally selected at levels (small) not affecting the measured spectra; typically $\Delta\lambda/\lambda_o$ was of the order of 10^{-3}. Precautions were taken to eliminate the interference of spurious signals (arising, for example, from light intensity modulation). The measurements were carried out in the temperature range of 95 to 300 K.

A typical subbandgap derivative surface photovoltage spectrum obtained with a melt-grown GaAs is shown in Fig. 1. The three-peak structure was found to be characteristic of all melt-grown GaAs crystals studied, although the relative amplitude of the peaks was found to vary with the supplying source of the crystals. In high purity LPE layers, only the intermediate energy peak (~ 0.9 eV) was observed, and its amplitude was about two orders of magnitude smaller. Accordingly, the observed transitions are associated with bulk levels rather than with interface states. No photoionization transitions related to interface states were observed. Thus, the surface states in GaAs-oxide interfaces previously reported on the basis of capacitance measurements[5] apparently are not optically active.

By extending the surface photovoltage treatment of surface states[6] to the transitions involving bulk levels (in the surface space charge region) it is shown that the derivative surface photovoltage $(dV)/(dh\nu)$, is directly proportional to the derivative of the photoionization cross section, $(d\sigma)/(dh\nu)$ and thus to the derivative of the absorption coefficient.

The basic features of the deep level absorption characteristics (Fig. 1) coincide with the extensively studied emission characteristics employing photoluminescence.[7] Thus, the sensitivity of the magnitude of the peaks to the crystal growth technique and the doping level are identical in both cases; similarly, in both cases the position of the peaks is not sensitive to the nature of the donor dopant. Furthermore, the position of the minimum (1.02 eV) and that of the zero value of the derivative (1.23 eV) in Fig. 1 are similar to the observed energy positions of photoluminescence maxima. Thus, the two high energy peaks (E_{t1},E_{t2}) correspond to the same deep levels, previously observed by luminescence and attributed to complexes involving gallium vacancies and donor impurities; the similarity of the absorption and emission energies is significant, as it proves directly that there is no measurable Stokes shift associated with these levels, contrary to the literature report on Ge-doped GaAs.[8] In view of the above, the spectrum of Fig. 1 can be analyzed on the basis of the quantum-defect model of an impurity-band photoionization cross section,[9] modified by the introduction of the Lorentzian broadening Γ.

The results calculated from this model are shown in Fig. 1. It is seen that they are in good agreement with experiment; furthermore, the present treatment enables the separation of the individual contributions of the three deep levels and the accurate determination of the binding energies, E_t. It should be pointed out that with the same set of fitting parameters (given in caption of Fig. 1) it was possible to obtain good agreement with experiment for all samples studied in spite of the fact that the relative magnitudes of the experimental peaks were quite different. It is thus concluded that the optically active deep centers in n-type GaAs can be approximated in the quantum defect model as acceptor centers, without invoking configurational changes.

In the region of bandgap transitions second derivative photovoltage spectra can be directly obtained. A typical spectrum is shown in Fig. 2. The photo-generated transition in the vicinity of the energy gap, E_o, the spin-orbit splitting, $E_o + \Delta_o$, and the higher energy structures, E_1 and $E_1 + \Delta_1$, are clearly resolved. The energy positions and temperature dependence of these critical point transitions are in good agreement with those obtained by reflectance measurements.[11,12] It is important to point out that the half-width of photovoltage structures E_o and $E_o + \Delta_o$ at 95 K is comparable to that obtained at 4.2 K in high-resolution electroreflectance spectra.[13]

The structure observed in Fig. 2, designated as E_2'', (2.59 eV at 95 K) coincides in energy with the transition originally reported in ref. 11 but not confirmed in any later study.[12] Since this structure, unlike the others in Fig. 2, is characterized by a minimum-maximum sequence, it can be tentatively identified with the M_2 or M_3 critical point.[14]

In order to establish directly the contribution from Γ_8-Γ_6 transitions to the structure in the vicinity of E_o, derivative surface photovoltage measurements were carried out in high magnetic fields. The results obtained at room temperature are shown in Fig. 3. It is seen that (a) the dominant structure in the vicinity of E_o is essentially unaffected by magnetic fields; accordingly, this structure is not associated with Γ_8-Γ_6 transitions or with free exciton transitions, but rather with residual impurities and/or defects. Thus, the structure at E_o cannot be identified with the energy gap. (b) For higher photon energies magnetic field leads to an oscillatory magnetophotovoltage with the minima and maxima shifting toward higher energies with increasing magnetic field. The quantitative account of the involved Landau levels transitions is complicated in GaAs by the complex nature of its valence band. However

from the convergence of the magnetophotovoltage oscillations at zero magnetic field the energy gap at 300 K of high quality GaAs is precisely obtained as $E_g = 1.440 \pm 0.002$ eV.

In view of the above, it is not surprising that this value is greater than those previously obtained from the derivative spectra in the vicinity of E_o (1.420 to 1.427 eV).[15] Transitions in the vicinity of E_o have been extensively studied in GaAs, as they are important in understanding laser action. However, due to uncertainties in the identification of transitions at room temperature, the energy gap values obtained by various methods range from 1.38 to 1.445.[15]

The present results (figures 2 and 3) clearly show that derivative surface photovoltage is highly sensitive to band-structure optical transitions. This sensitivity can be qualitatively explained by the theory of surface photovoltage arising from trapping of photogenerated holes by surface (interface) states.[16] The spectral response of surface photovoltage is determined by $(\alpha L_p)/(1+\alpha L_p)$ where α is the absorption coefficient. Thus, for small values of the minority carrier diffusion length, L_p, (e.g., 10^{-5}cm) the surface photovoltage is essentially proportional to the absorption coefficient; as L_p increases the sensitivity of photovoltage to absorption coefficient decreases. Consistent with this model the amplitude of the high energy peaks in the spectra (as those shown in Fig. 2) was found to decrease (with respect to the low energy peaks) with increasing L_p. However, the high energy $(E_1+\Delta_1)$ structure could be resolved even for high quality GaAs epitaxial layers ($L_p \simeq 6$ μm and $\alpha L_p >> 1$); this result can be qualitatively explained considering that for high values of α (high energy region) the holes are generated in the space charge region where an electric field (neglected in treatment of ref. 16) as high as 10^3 to 10^4 V/cm opposes their diffusion; accordingly, L_p becomes a much shorter, field-contracted diffusion length.[17]

In summary, it was shown that derivative surface photovoltage spectroscopy constitutes a unique means for derivative absorption spectroscopy studies at energies below and well above the energy gap of GaAs. This technique should be applicable to unipolar semiconductors in general.

ACKNOWLEDGEMENTS

The authors are grateful to the National Aeronautics and Space Administration for financial support. The authors are also grateful to Drs. R. E. Enstrom and D. Richman of RCA Laboratories for providing the high quality epitaxial material and the Francis Bitter National Magnet Laboratory for providing the high magnetic field facilities.

REFERENCES

1. H. C. Gatos and J. Lagowski, J. Vacuum Sci. Technol. 10, 130 (1973).

2. T. Nishino and Y. Hamakawa, Phys. Stat. Sol. (b) 50, 345 (1972).

3. T. Nishino, M. Takeda and Y. Hamakawa, Surface Sci. 37, 404 (1973).

4. H. Hasegawa and H. L. Hartnagel, J. Electrochem. Soc. 123, 713 (1976).

5. L. A. Chesler and G. Y. Robinson, J. Vac. Sci. Technol. 15, 1525 (1978).

6. C. L. Balestra, J. Lagowski and H. C. Gatos, Surface Sci. 64, 457 (1977).

7. G. P. Peka and V. A. Brodovoi, Sov. Phys. Semicond. 7, 1100 (1974); S. Metz and W. Fritz, Inst. Phys. Conf. Ser. B 33a, 66 (1976).

8. E. W. Williams and A. M. White, Solid State Commun. 9, 279 (1971).

9. H. B. Bebb, Phys. Rev. 185, 1116 (1969).

10. N. O. Lipari and A. Baldareschi, Proceedings Eleventh Internat'l. Conf. Phys. Semicond., Warsaw, Polish Scientific Publsihers, Warsaw, 1972, p. 1009.

11. D. L. Greenaway, Phys. Rev. Lett. 9, 97 (1962).

12. D. D. Sell and S. E. Stokowski, Proceedings Tenth Internat'l. Conf. Phys. Semicond., Cambridge, Mass., U.S. Atomic Energy Commission, 1970, p. 417; J. P. Walter, R. R. L. Zucca, M. L. Cohen and Y. R. Shen, Phys. Rev. Lett. 24, 102 (1970); Y. R. Shen, Surface Sci. 37, 522 (1973).

13. D. E. Aspnes and A. A. Studna, Surface Sci. 37, 631 (1973).

14. B. Batz, in Semiconductors and Semimetals, R. K. Willardson and Albert C. Beer, eds., Academic Press, New York, 1972, p. 315.

15. See for example, J. Camassel, D. Auvergne and H. Mathieu, J. Appl. Phys. 46, 2683 (1975) and references quoted therein.

16. N. L. Dimitruk, V. I. Lyashenko, A. K. Tereshenko and S. A. Spektor, Phys. Stat. Sol. (a) 20, 53 (1973).

17. N. J. Harrick, Solid State Electronics 1, 234 (1960).

FIGURE CAPTIONS

Figure 1. First derivative spectrum of subbandgap surface photovoltage of (100) GaAs (melt-grown) with $n = 6 \times 10^{15} cm^{-3}$. The contribution of the individual transitions is shown by dashed lines. Parameters used in fitting procedure: E_t = 1.10; 0.905 and 0.83 eV below conduction band edge; Γ = 40, 15 and 40 meV, respectively; the Bohr radius of the shallow acceptor $a_s = 3.5 \times 10^{-7} cm$; the ionization energy of shallow acceptor E_s = 24.7 meV was adopted from ref. 10.

Figure 2. Second derivative surface photovoltage spectra of (100) GaAs ($n = 6 \times 10^{15} cm^{-3}$, $L_p \simeq 10^{-4} cm$, at room temperature); dashed line 293 K; solid line 95 K. The amplitude of the peaks for $E_o + \Delta_o$, E_2'', E_1 and $E_1 + \Delta_1$ has been multiplied by a factor of 50, 20, 3 and 3, respectively.

Figure 3. Second derivative surface photovoltage of (100) GaAs epitaxial layer ($n = 10^{15} cm^{-3}$) taken in magnetic fields at 300 K. The direction of the magnetic field and that of the light propagation were perpendicular to the surface.

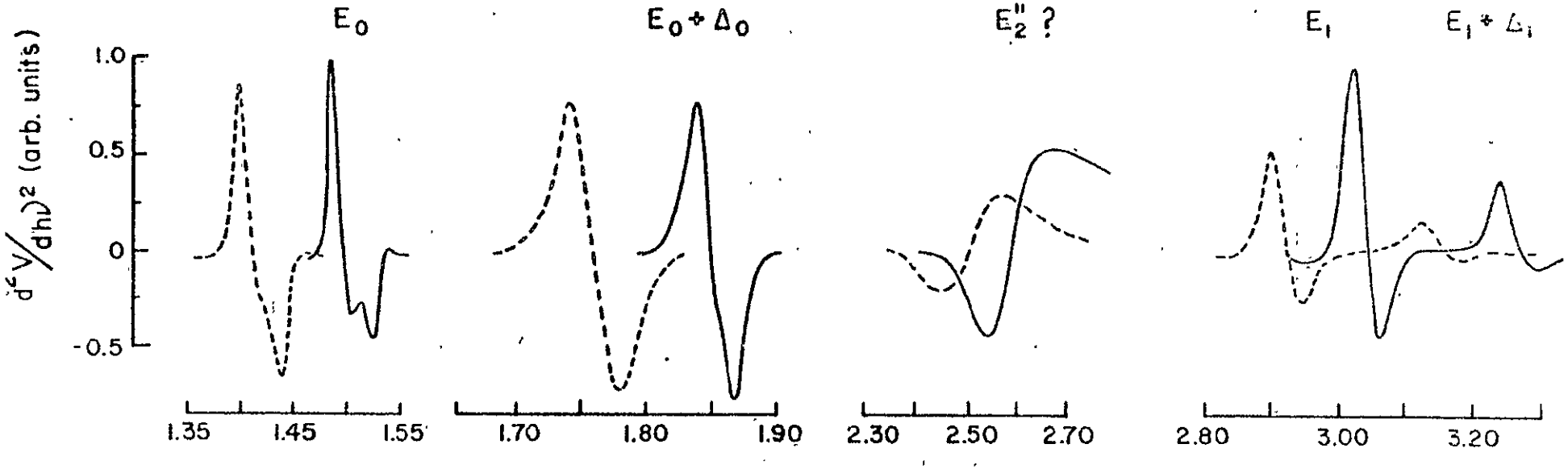

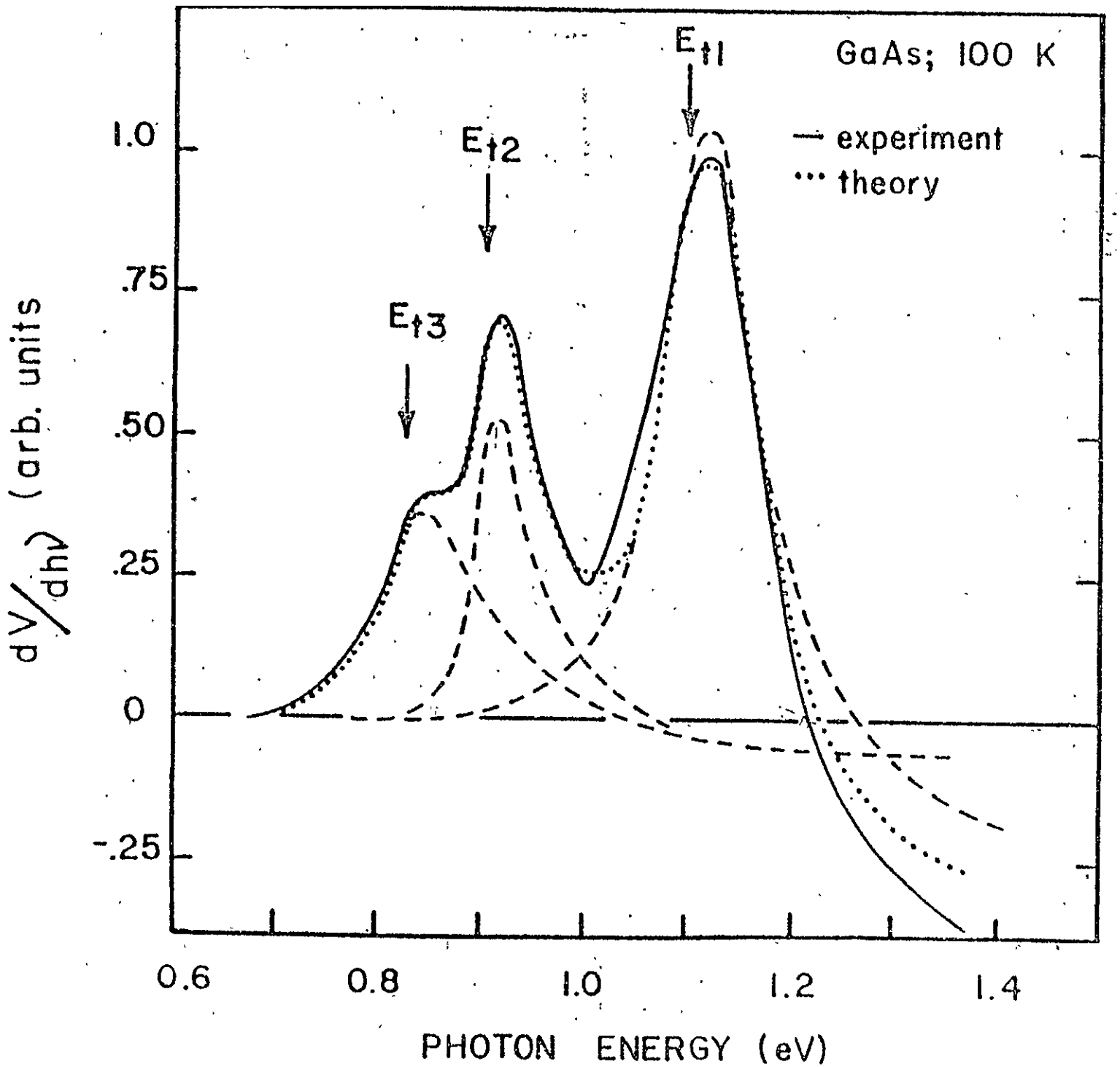
GaAs; 100 K
— experiment
··· theory
E_{t1}
E_{t2}
E_{t3}
1.0
.75
.50
.25
0
-.25
$dV/d(h\nu)$ (arb. units
0.6
0.8
1.0
1.2
1.4
PHOTON ENERGY (eV)

Fig. 2

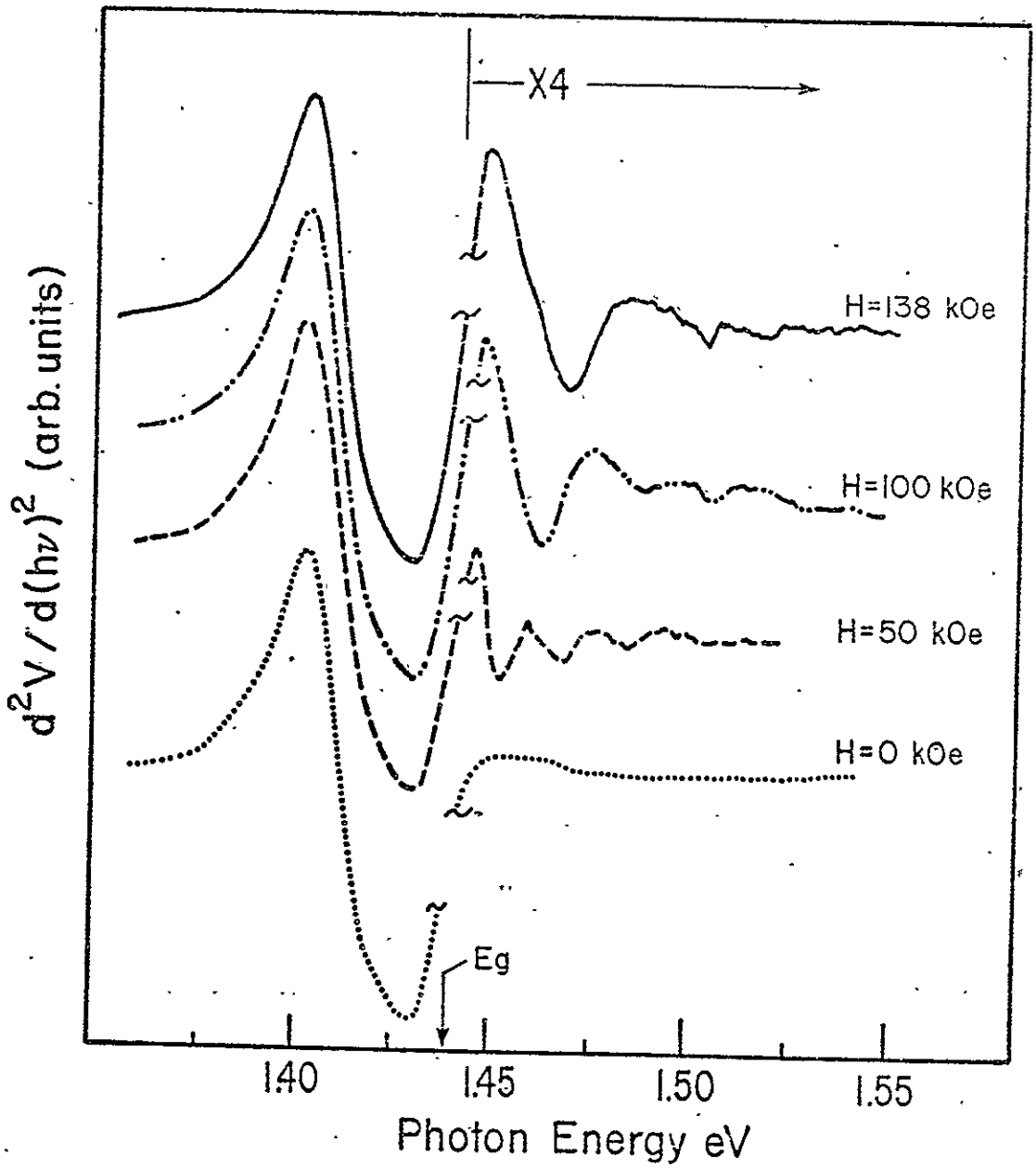

OUTDIFFUSION OF RECOMBINATION CENTERS FROM THE SUBSTRATE TO THE EPITAXIAL LAYER IN LPE GROWTH; GaAs

L. Jastrzebski,* J. Lagowski and H. C. Gatos
Department of Materials Science and Engineering
Massachusetts Institute of Technology
Cambridge, Massachusetts 02139

Abstract

Experimental results are presented showing that outdiffusion of recombination centers from the substrate to the epitaxial layer takes place during growth. Such out-diffusion decreases the carrier lifetime in the epitaxial layer to much lower values than the radiative recombination limit. Furthermore, it introduces a lifetime gradient across the epitaxial layer which depends critically on the growth velocity and thermal treatment. High rates of growth (such as those attainable in electroepitaxy) and high cooling rates can minimize the adverse effects of normally available substrates on the epitaxial layers; however, good quality substrates are essential for the consistent growth of device quality layers.

INTRODUCTION

It has been established that the performance of many semiconductor devices is adversely affected by nonradiative recombination centers. Their presence in the device active region leads to a decrease in the device efficiency (as in the case of solar cells[1]). Furthermore, the recombination-enhanced diffusion of such centers[2] causes a slow degradation of the device performance (as in the case of semiconductor lasers[3]).

The nonradiative recombination centers in GaAs are usually associated with residual impurities such as oxygen,[4] transition metals[5] and nonstoichiometric

---

*Present address: RCA Research Laboratories, David Sarnoff Research Center, Princeton, New Jersey 08540.

Submitted to The Journal of the Electrochemical Society.

point defects.[6] The origin of nonstoichiometric defects is not fully understood, although in GaAs it has been attributed to the solidus of the phase diagram[7] and/or to As depletion of the substrate during the heating cycle prior to epitaxial growth.[8] Growth at low temperatures and backmelting of the substrate prior to growth[9] tend to reduce the concentration of nonstoichiometric defects and improve the quality of the grown epitaxial layer.

Poor quality GaAs substrate material is a source of defects which can diffuse into the epitaxial layer during the growth process. The available melt-grown GaAs substrates are in most instances highly compensated,[10] exhibit large carrier concentration inhomogeneities[11] and contain high concentration of nonradiative recombination centers.[12,13]

The present work is concerned with the outdiffusion of recombination centers from GaAs substrates to GaAs epitaxial layers. Minority carrier diffusion length and lifetime profiling obtained with EBIC-mode (SEM) measurements are employed for the study of such outdiffusion. Growth conditions required to minimize the outdiffusion of recombination centers are pointed out.

EXPERIMENTAL

Epitaxial Growth and Sample Preparation

LPE growth of GaAs was carried out employing classical thermal cooling techniques and electromigration-controlled electroepitaxy.[14,15] Cd-doped ($p \simeq 2 \times 10^{17} cm^{-3}$) 300 μm thick (100) substrates were used. Epitaxial growth was performed in a two-well graphite boat. In one of the wells the substrates were backmelted (about 25 μm) with under-saturated solution to remove the As depleted layer formed during the heating cycle. After backmelting the substrate was positioned in the second well containing 2.5 g of undoped Ga-As solution with a GaAs source at the top. In the electroepitaxy experiments layers ranging

in thickness from 10 to 100 μm were grown at 900°C on an area of 0.5 cm^2 at a rate of about 6 μm/min by passing an electric current of 60 A/cm^2 for a period of 2 to 20 min. Growth was terminated by turning the current off. In the thermal growth experiments the growth was performed from equilibrated solutions by cooling from 910°C to 900°C with a rate of .1°C/min.

In both procedures, after growth was completed, the system was kept at the growth temperature for time periods ranging from 1 minute to 3 hours with the grown layer in contact with the solution. The experiment was terminated by quenching the system to room temperature with an initial cooling rate (from 900°C to 700°C) of about 70°C/min. The solution was left over the epitaxial layer or wiped by the moving slider prior to cooling.

After cooling, if the excess Ga-GaAs mixture was not wiped, it was removed from the epitaxial layer surface by boiling in HCl; the epilayer was cleaved and etched in AB etchant for about 30 sec. Interference contrast microscopy was employed to determine the thickness of the epitaxial layers. Whenever necessary, the part of the epitaxial layer grown during cooling to room temperature (about 5-10 μm in thickness) was etched away in $H_2SO_4H_2O::H_2O_2$. Ohmic contacts were soldered on the substrate and the epilayer employing Sn and In in an H_2 atmosphere.

The epitaxial layers were n-type with a carrier concentration of about $5 \times 10^{16} cm^{-3}$. Schottky barriers required for EBIC-mode measurements were made by evaporating aluminum or gold on the surfaces of the epitaxial layer.

Minority Carrier Diffusion Length and Lifetime

Measurements of the minority carrier diffusion length were performed utilizing electron-beam excitation as shown schematically in Fig. 1. The diffusion length was obtained from the dependence of the electron beam-induced

current (EBIC) on the distance between the generation position and the collecting Schottky barrier or the p-n junction.[16] A 35 keV electron beam energy was used in all experiments to minimize the effect of surface recombination on the measured diffusion length.[17]

The configuration shown in Fig. 1 made possible the determination of the diffusion length, L_p, of the minority carriers in the epitaxial layer near the surface of the epilayer surface (with the electron beam at position 1 and with current circuit I), and near the substrate (with the electron beam in position 2 and with current circuit I); the minority carrier diffusion length was also determined in the p-type substrates (with the electron beam in position 3 and with current circuit II).

Values of lifetime, τ, were estimated from the standard relationship, $L = (\frac{kT}{e} \mu\tau)^{1/2}$, where μ is the minority carrier mobility and kT/e equals 0.026V at 300 K. In p-type GaAs (substrates in the present case) the mobility of electron can be noticeably smaller than the mobility of electrons in n-type material of similar free carrier concentration.[18] Accordingly, in evaluating the electron lifetime in the substrates recently calculated theoretical values of electron mobility in p-type GaAs were used.[18] In these calculations the contribution of electron scattering by heavy holes and the difference in screening energies between holes and electrons have been taken into account. In the case of holes their mobility as majority or minority carriers is expected to be similar at room temperature and for free carrier concentrations below $10^{17} cm^{-3}$ (since screening effects and carrier-carrier scattering are not significant). Accordingly, in evaluating the hole lifetime in epitaxial layers, the hole mobility value of $\mu_p \simeq 300$ $cm^2/V\text{-sec}$ was used, i.e., the hole mobility in p-type GaAs with hole concentration of $5 \times 10^{16} cm^{-3}$,[10]) which is similar to the electron concentration in the epitaxial layers.

RESULTS AND DISCUSSION

Substrate

The minority carrier lifetime in the substrate material was found to be about 10^{-10} sec, i.e., two orders of magnitude smaller than the lifetime value expected from band-to-band radiative recombination.[20] It was also determined that the substrate material is highly inhomogeneous with local lifetime fluctuations exceeding a factor of 4. These findings clearly indicate that the lifetime in the substrates is controlled entirely by nonradiative recombination and thus the substrate must contain a high, nonuniform, concentration of recombination centers.

Outdiffusion of Recombination Centers from the Substrate

The lifetime in the epitaxial layers was measured as a function of position on a given plane parallel to the surface, as a function of distance from the substrate-epitaxial layer interface and as a function of time the layer was kept at the growth temperature.

Typical results of the lifetime measurements as a function of position on a plane parallel to the surface of the epitaxial layer are given in Fig. 2. The lower curve corresponds to positions near the surface of the epitaxial layer. The layer was 40 μm thick; it was grown electroepitaxially and was kept 20 minutes at the growth temperature (from the beginning of growth to the beginning of cooling). It is evident from Fig. 2 that lifetime inhomogeneities of a similar nature are present near the substrate-epitaxial interface and near the surface of the layer; however, near the surface the lifetime values are significantly higher. It should be noted that even the highest values of lifetime are well below the values (of the order of 10^{-7} s) expected from radiative band-to-band recombination.[20]

The above behavior of the minority carrier lifetime can be understood if one considers that the substrate represents a source of recombination centers which diffuse into the epitaxial layer during the growth process and thermal treatment. On this basis, the difference between the lifetime near the epitaxial layer surface and the lifetime near the epitaxial layer-substrate interface should decrease with increasing exposure time of the system to the growth temperature. Similarly, the lifetime in the epitaxial layer should decrease with increasing exposure time to the growth temperature. As is seen from Fig. 3, such behavior is indeed found in electroepitaxially and in thermally grown layers. The lifetime in both electroepitaxially and thermally grown layers behaves similarly upon exposure to high temperature after growth, as it is dominated by recombination at outdiffused centers. Without exposure to high temperature, after growth, the lifetime in electroepitaxial layers is significantly higher than in those grown thermally, as will be discussed below.

The fact that recombination centers outdiffuse from the substrate into the epitaxial layers is further supported by the results shown in Fig. 4. Here the lifetime measured near the epitaxial layer surface is plotted as a function of thickness of the epitaxial layers, all of which have been exposed to a high temperature (growth temperature) for the same period of time (20 minutes). The layers were grown by electroepitaxy and at the same growth rate of about 6 μm/min. It is seen that the lifetime increases by about two orders of magnitude (near the surface) as the distance from the substrate (thickness of the layer) increases from 5 to 90 μm.

If the simplified assumption is made that the lifetime is inversely proportional to the concentration of the recombination centers, the data of Fig. 3 and 4 can be used to estimate the diffusion constant of the recombination centers.

Thus, treating the substrate-epitaxial layer interface as a limited diffusion source,[21] the lifetime becomes

$$\frac{1}{\tau} \sim \frac{1}{\sqrt{Dt}} \exp\left(-\frac{x^2}{4Dt}\right) \qquad (1)$$

where x is the distance from the substrate-epitaxial layer interface, t is the time, and D is the diffusion constant of recombination centers. From this expression the solid line in Fig. 3 is obtained by taking x = constant and the solid line in Fig. 4 by taking t = constant. From these plots a value for the diffusion constant of the recombination centers of approximately $5 \times 10^{-9} cm^2/se$ is obtained (900°C). The same value of $5 \times 10^{-9} cm^2/sec$ has been reported for point defect diffusion in GaAs (gallium vacancies) at 1000°C.[22]

It is important to note that the observed lifetime behavior which is consistent with the above diffusion model, cannot be explained on the basis of impurity segregation effects. A recent experimental and theoretical analysis of impurity segregation in GaAs during electroepitaxy has shown that the maximum changes of dopant segregation coefficient do not exceed 40%, i.e., they are two orders of magnitude smaller than the changes required to account for presently reported lifetime behavior.[23]

Growth Velocity and the Effects of Outdiffusion

The diffusion constant of impurities and point defects decreases exponentially with decreasing temperature, and thus lowering the growth temperature should drastically reduce the effects of outdiffusion from the substrate. However, there are limitations to the lowering of the growth temperature as the attainable growth rate decreases significantly and single crystal growth becomes problematic.

On the other hand, it is evident that the effects of outdiffusion can be reduced if the growth velocity, R, is much greater than the velocity of the dif-

fusion front propagation v_D. In a diffusion process a constant concentration profile can be approximated as $\frac{x^2}{4Dt} = \text{const.}$; consequently, $v_D = \frac{dx}{dt} = \frac{\text{const.}}{\sqrt{Dt}}$. Thus, the condition $R \gg v_D$ can be expressed as:

$$R \gg \left(\frac{D}{t}\right)^{1/2} \qquad (2a)$$

or

$$R \gg \frac{D}{d} \qquad (2b)$$

Expression 2a represents the case where growth is performed for certain time t and 2b represents the case where the growth of a layer of a thickness d is required.

In the present case the outdiffusion constant of recombination centers was found to be $5 \times 10^{-9} cm^2/s$. Thus, according to 2b, for a layer 40 μm thick the growth rate required to reduce significantly the effect of outdiffusion is $R \gg 0.75$ μm/min. Thus, in the present experiments the growth rate was about 6 μm/min, which is high enough to satisfy the above condition for reducing the significant outdiffusion of recombination centers. Accordingly, it is not surprising that, without a post growth heat treatment epitaxial layers 40 μm thick were consistently grown with a lifetime of about 10^{-7} sec.

The growth velocity in thermal LPE is limited by the slow solute transport to the growth interface and by the fact that the relatively small supercooling must be used to prevent spurious nucleation in the solution.[24] These limitations are overcome in electroepitaxy.[15]

Actually employing electroepitaxy a number of GaAs layers were grown at 900°C with rates as high as 20 μm/min. Under such conditions the adverse effects of outdiffusion from the substrate were essentially eliminated.

SUMMARY AND CONCLUSIONS

It was found that outdiffusion of recombination centers from a substrate to the epitaxial layer takes place during liquid phase epitaxial growth. From

the study of the time dependence of the diffusion process a diffusion constant of $5 \times 10^{-9} cm^2/sec$ at 900°C was obtained for the outdiffusion of recombination centers. This value is the same as that reported for the diffusion constant of Ga vacancies in GaAs at 1000°C.

The recombination of minority carriers at the outdiffused defects constitutes the limiting factor for the minority carrier lifetime in the epitaxial layers. It has also been shown that the substrate-epitaxial layer interaction during the growth process can be reduced by increasing the growth velocity. Thus utilizing high growth velocities attainable in electroepitaxy, an improvement of as much as two orders of magnitude in the minority carrier lifetime was observed. In the light of the present results, the improved characteristics (with respect to degradation) of GaAs lasers grown under high growth velocities[25] can be readily understood.

Preliminary experiments performed on substrates obtained from different crystals (and different supplying sources) showed that defects with different diffusion constants outdiffuse from the substrates into the epitaxial layers during growth. Although detailed knowledge of the substrate growth conditions was not available, it seems that factors such as arsenic pressure and growth instabilities due to convection or temperature fluctuations influence the density and type of defect formation in bulk GaAs crystals. Apparently, differences in the type and concentration of recombination centers in Bridgman and Czochralski grown crystals are responsible for the observed differences in quantum efficiency between GaAs diodes fabricated on substrates obtained by these two techniques and the poor characteristics of GaAlAs lasers fabricated on Czochralski grown substrates as compared with those fabricated on Bridgman-grown substrates.

Although high growth rates can minimize the decrease of the lifetime due to the slowly outdiffusing recombination centers (with D of the order of $10^{-9}cm^2/sec$), they cannot influence the effects of fast-diffusing defects (with D of the order of $10^{-5}cm^2/sec$) since the magnitude of the growth rates required are not as yet achievable by any epitaxial technique. These types of defects must be eliminated from the substrates used in epitaxial growth.

ACKNOWLEDGEMENT

The authors are grateful to the National Science Foundation and the National Aeronautics and Space Administration for financial support.

REFERENCES

1. See, for example, J. H. Reynolds and A. Meulenbert, Jr., J. Appl. Phys. 45, 2582 (1974).

2. D. V. Lang and L. C. Kimerling, Phys. Rev. Lett. 33, 489 (1974).

3. P. Petroff, W. D. Johnston, Jr, and R. L. Hartman, Appl. Phys. Lett. 25, 226 (1974), and H. Kressel and H. F. Lockwood, J. Phys. 35, 223 (1974).

4. M. Ishii, H. Kan and W. Susaki, Appl. Phys. Lett. 29, 375 (1976).

5. A. G. Milnes, private communication.

6. J. A. Van Vechten, J. Electron. Mater. 4, 1159 (1975).

7. G. M. Bloom, J. Cryst. Growth 36, 125 (1976).

8. See, for example, R. Zucca, Proc. 6th Int. Symp. on GaAs and Related Compounds, St. Louis, 1976 (Inst. of Physics, London, 1977) p. 228.

9. L. Jastrzebski and H C. Gatos, J. Cryst. Growth 42, 309 (1977).

10. W. Walukiewicz, J. Lagowski, L. Jastrzebski, M. Lichtensteiger and H. C. Gatos, J. Appl. Phys. 50, 899 (1979).

11. P. Rava, L. Jastrzebski, J. Lagowski and H. C. Gatos, to be published.

12. A. M. Sekela, D. L. Feucht and A. G. Milnes, "Proceedings of the Symposium on GaAs and Related Compounds, Deniville, France, 1974 (Inst. of Phys., London and Bristol, 1974), Conf. Ser. 24, p. 245.

13. H. C. Gatos, J. Lagowski and L. Jastrzebski, "Present Status of GaAs", NASA Report 3093, January 1979.

14. L. Jastrzebski, Y. Imamura and H. C. Gatos, J. Electrochem. Soc. 125, 1140 (1978).

15. L. Jastrzebski, J. Lagowski, H. C. Gatos and A. F. Witt, J. Appl. Phys. 49, 5909 (1978)

16. D. B. Wittry and D. F. Kyser, J. Appl. Phys. 36, 1387 (1965).

17. L. Jastrzebski, J. Lagowski and H. C. Gatos, Appl. Phys. Lett. 27, 537 (1975).

18. W. Walukiewicz, J. Lagowski, L. Jastrzebski and H. C. Gatos, J. Appl. Phys., in press.

19. J. D. Wiley, in "Semiconductors and Semimetals", ed. R. K. Willardson and A. C. Beer, Academic Press, N.Y., 1975, vol. 10, ch. 2.

20. See, for example, "Gallium Arsenide, Growth, Properties and Applications", ed. F. P. Kesamanly and D. N. Nasledova, Izdatelstvo Nauka, Moscow, 1973, ch. 5, in Russian.

21. S. M. Sze, "Physics of Semiconductor Devices", Wiley-Interscience, N.Y., p. 82 (1969).

22. J. Blanc, J. Appl. Phys. 45, 1948 (1974).

23. L. Jastrzebski, J. Lagowski, H. C. Gatos and A. F. Witt, presented at ACCG IV, Gaithersburg, Maryland, July 1978.

24. A. Ju. Malinin and O. B. Nevsky, J. Electronic Mat. 7, 757 (1978).

25. M. Ettenberg and H. Kressel, Appl. Phys. Lett. 26, 478 (1975).

Although high growth rates can minimize the decrease of the lifetime due to the slowly outdiffusing recombination centers (with D of the order of $10^{-9}cm^2/sec$), they cannot influence the effects of fast-diffusing defects (with D of the order of $10^{-5}cm^2/sec$) since the magnitude of the growth rates required are not as yet achievable by any epitaxial technique. These types of defects must be eliminated from the substrates used in epitaxial growth.

ACKNOWLEDGEMENT

The authors are grateful to the National Science Foundation and the National Aeronautics and Space Administration for financial support.

REFERENCES

1. See, for example, J. H. Reynolds and A. Meulenbert, Jr., J. Appl. Phys. 45, 2582 (1974).

2. D. V. Lang and L. C. Kimerling, Phys. Rev. Lett. 33, 489 (1974).

3. P. Petroff, W. D. Johnston, Jr, and R. L. Hartman, Appl. Phys. Lett. 25, 226 (1974), and H. Kressel and H. F. Lockwood, J. Phys. 35, 223 (1974).

4. M. Ishii, H. Kan and W. Susaki, Appl. Phys. Lett. 29, 375 (1976).

5. A. G. Milnes, private communication.

6. J. A. Van Vechten, J. Electron. Mater. 4, 1159 (1975).

7. G. M. Bloom, J. Cryst. Growth 36, 125 (1976).

8. See, for example, R. Zucca, Proc. 6th Int. Symp. on GaAs and Related Compounds, St. Louis, 1976 (Inst. of Physics, London, 1977) p. 228.

9. L. Jastrzebski and H. C. Gatos, J. Cryst. Growth 42, 309 (1977).

10. W. Walukiewicz, J. Lagowski, L. Jastrzebski, M. Lichtensteiger and H. C. Gatos, J. Appl. Phys. 50, 899 (1979).

11. P. Rava, L. Jastrzebski, J. Lagowski and H. C. Gatos, to be published.

12. A. M. Sekela, D. L. Feucht and A. G. Milnes, "Proceedings of the Symposium on GaAs and Related Compounds, Deniville, France, 1974 (Inst. of Phys., London and Bristol, 1974), Conf. Ser. 24, p. 245.

13. H. C. Gatos, J. Lagowski and L. Jastrzebski, "Present Status of GaA NASA Report 3093, January 1979.

14. L. Jastrzebski, Y. Imamura and H. C. Gatos, J. Electrochem. Soc. 125, 1140 (1978).

15. L. Jastrzebski, J. Lagowski, H. C. Gatos and A. F. Witt, J. Appl. Phys. 49, 5909 (1978)

16. D. B. Wittry and D. F. Kyser, J. Appl. Phys. 36, 1387 (1965).

17. L. Jastrzebski, J. Lagowski and H. C. Gatos, Appl. Phys. Lett. 27, 537 (1975).

18. W. Walukiewicz, J. Lagowski, L. Jastrzebski and H. C. Gatos, J. Appl. Phys., in press.

19. J. D. Wiley, in "Semiconductors and Semimetals", ed. R. K. Willardson and A. C. Beer, Academic Press, N.Y., 1975, vol. 10, ch. 2.

20. See, for example, "Gallium Arsenide, Growth, Properties and Applications", ed. F. P. Kesamanly and D. N. Nasledova, Izdatelstvo Nauka, Moscow, 1973, ch. 5, in Russian.

21. S. M. Sze, "Physics of Semiconductor Devices", Wiley-Interscience, N.Y., p. 82 (1969).

22. J. Blanc, J. Appl. Phys. 45, 1948 (1974).

23. L. Jastrzebski, J. Lagowski, H. C. Gatos and A. F. Witt, presented at ACCG IV, Gaithersburg, Maryland, July 1978.

24. A. Ju. Malinin and O. B. Nevsky, J. Electronic Mat. 7, 757 (1978).

25. M. Ettenberg and H. Kressel, Appl. Phys. Lett. 26, 478 (1975).

FIGURE CAPTIONS

Figure 1 Schematic representation of the experimental configuration for the determination of the minority carrier diffusion length by the EBIC method; see text.

Figure 2 Minority carrier lifetime profiles along two planes parallel to the growth interface; o - near the original growth interface (position 2 in Fig. 1); ● - near surface of epitaxial layer (position in in Fig. 1).

Figure 3 Minority carrier lifetime as a function of time at the growth temperature (900°C); Δ, o near the original growth interface; ▲, ● - near the surface of the epitaxial layer; triangles correspond to layers grown by electroepitaxy and circles to thermally grown layers; all layers were 40 μm thick.

Figure 4 Minority carrier lifetime near the surface of the layers as a function of the layer thickness.

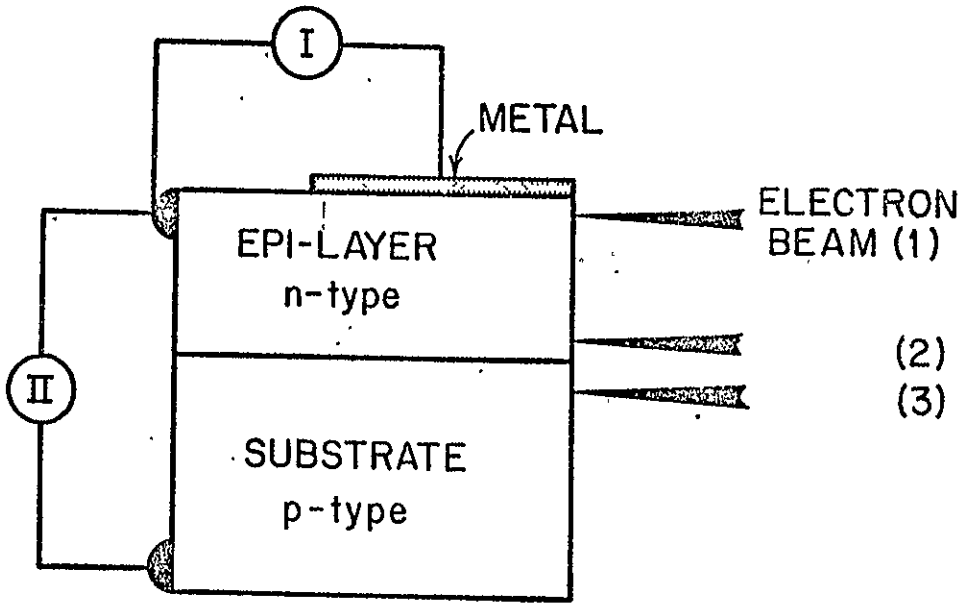
I
METAL
ELECTRON
BEAM (1)
EPI-LAYER
n-type
(2)
II
(3)
SUBSTRATE
p-type

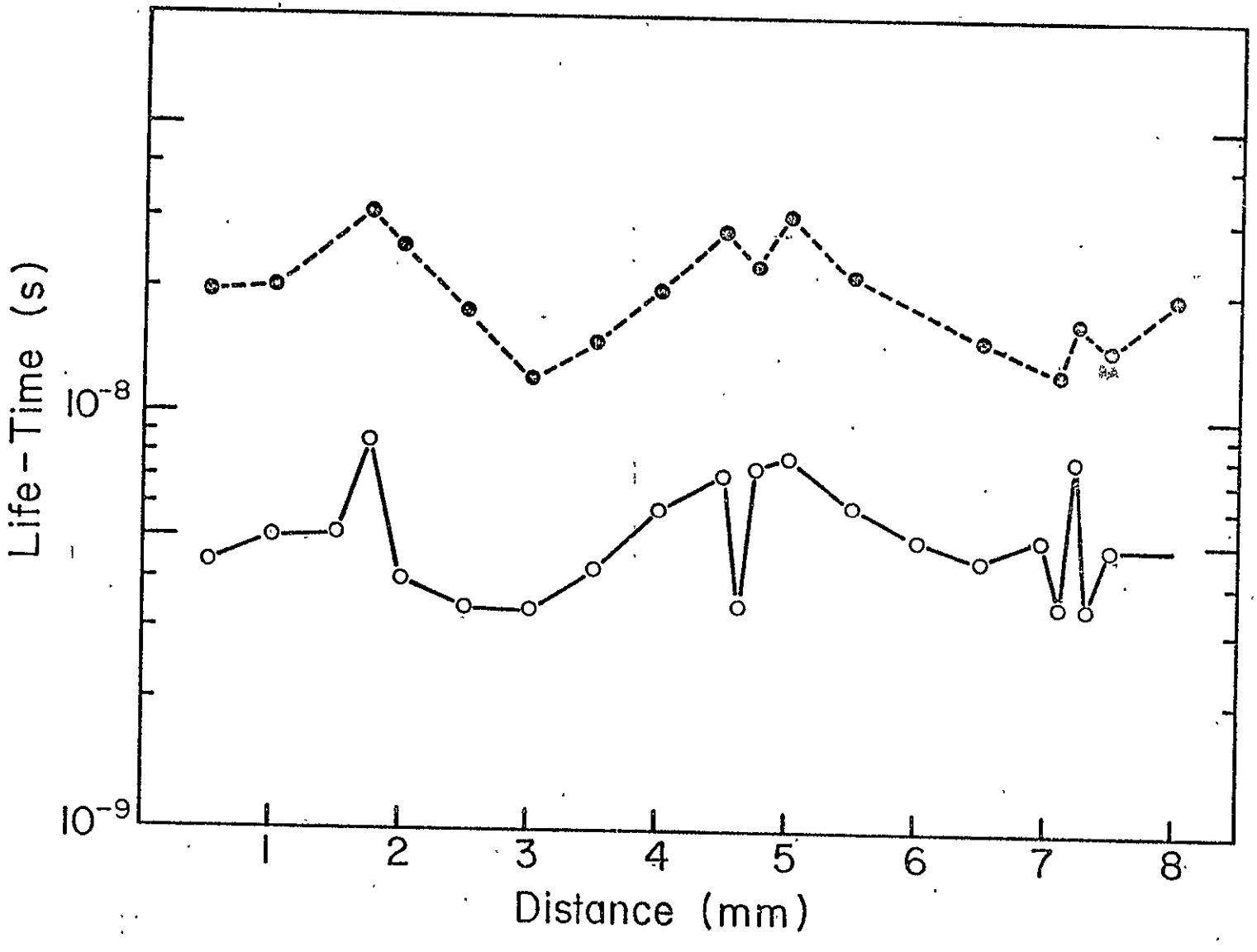
Life-Time (s)
10^{-8}
10^{-9}
1
2
3
4
5
6
7
8
Distance (mm)

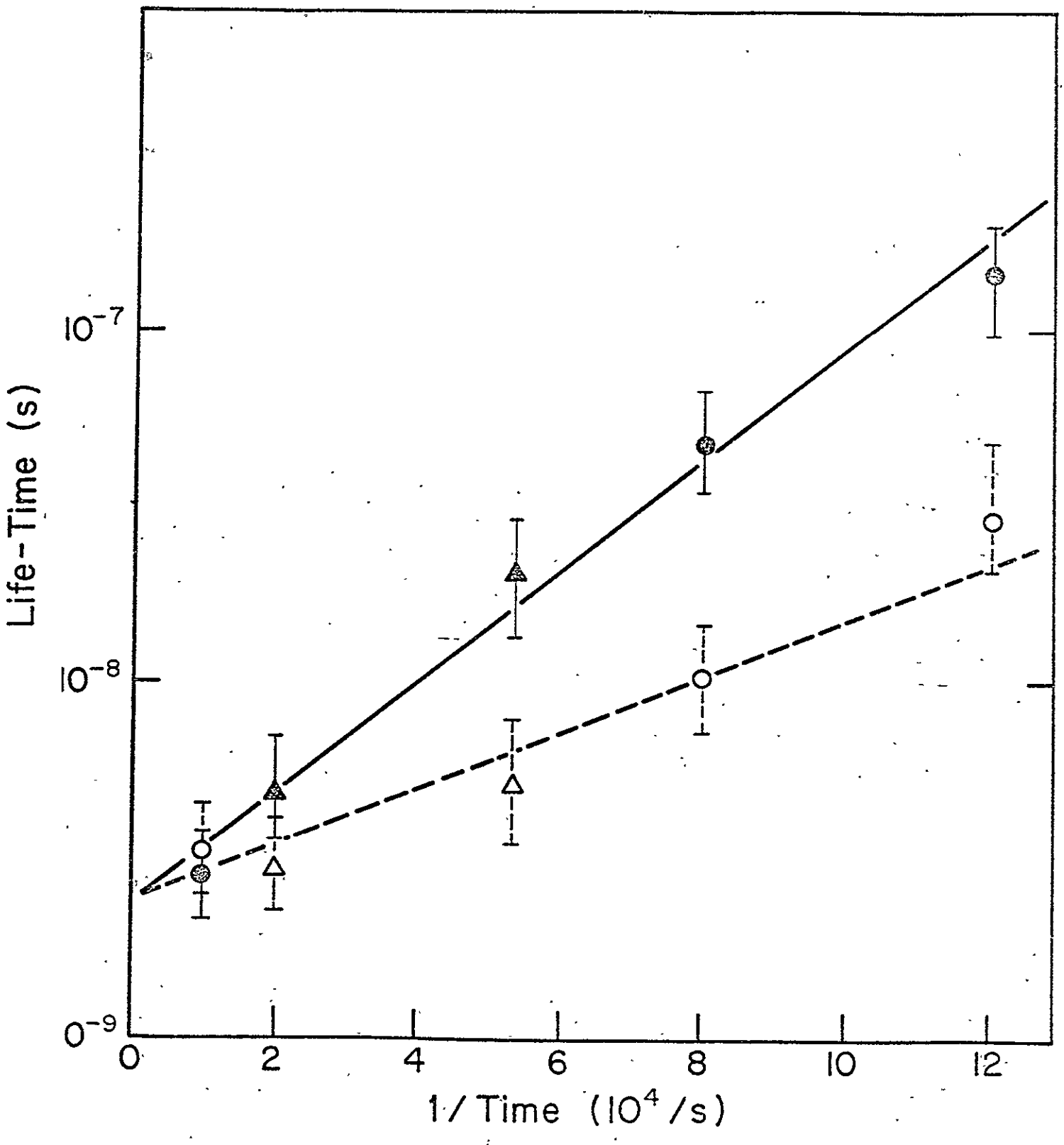
Life-Time (s)
10^-7
10^-8
0^-9
0
2
4
6
8
10
12
1/ Time (10^4 /s)

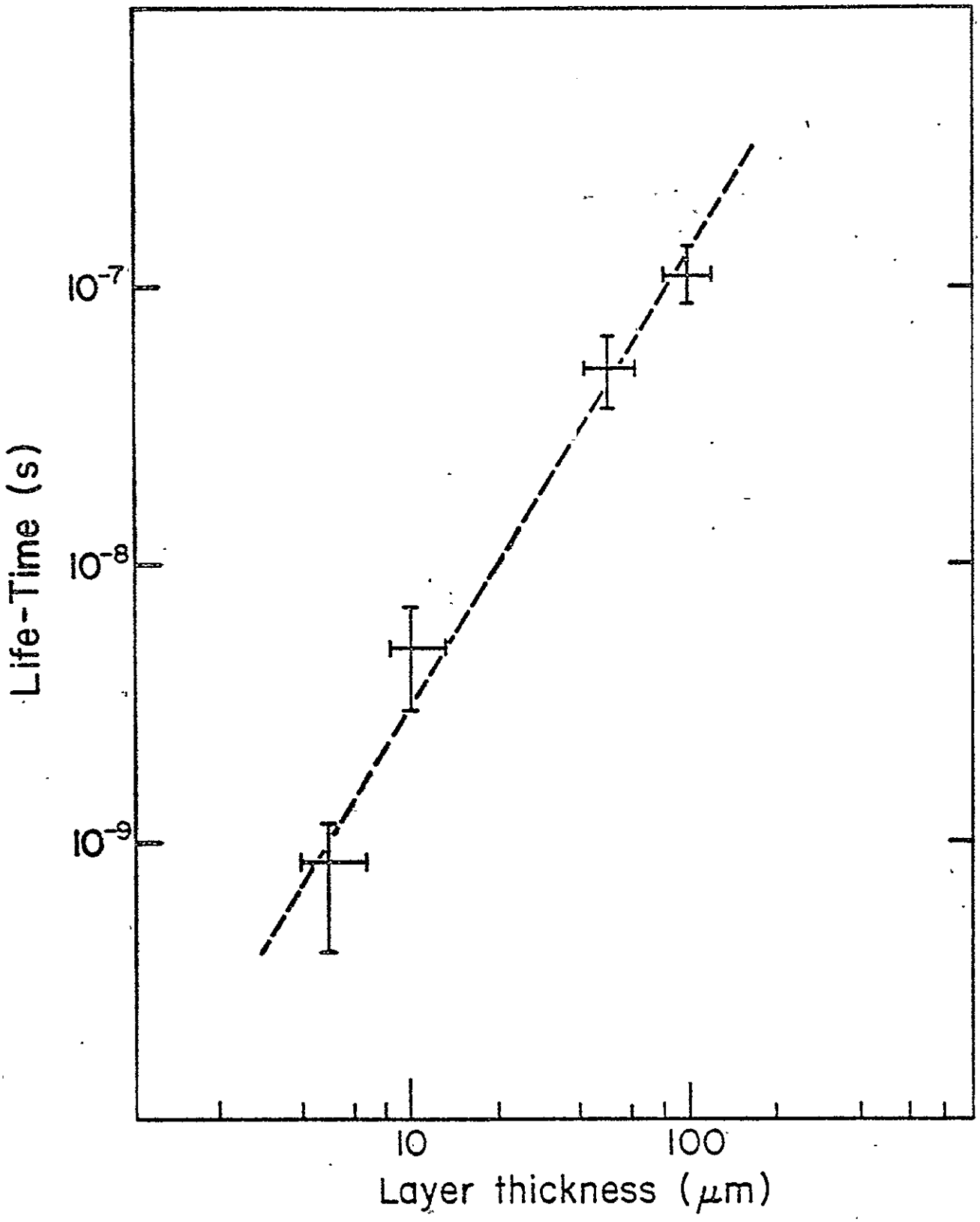

END DATE FIMED, JUNE 11/1979